

LOCKHEED MISSILES & SPACE COMPANY
HUNTSVILLE RESEARCH & ENGINEERING CENTER
HUNTSVILLE RESEARCH PARK
4800 BRADFORD DRIVE, HUNTSVILLE, ALABAMA

SECOND INTERIM REPORT
PRELIMINARY DESIGN STUDY OF
A LUNAR GRAVITY SIMULATOR

9 September 1966

Contract NAS8-20351

Prepared for George C. Marshall Space Flight Center
Huntsville, Alabama

FACILITY FORM 502

N67-30819
(ACCESSION NUMBER)
138
(PAGES)
CR-85583
(NASA CR OR TMX OR AD NUMBER)

(THRU)
0
(CODE)

(CATEGORY)

PREPARED BY:

R. B. Wysor

R. B. Wysor
Systems Engineering

APPROVED BY:

R. S. Paulnock

R. S. Paulnock
Mgr., Systems Engineering

J. S. Farrior

J. S. Farrior
Resident Manager

FOREWORD

This report was prepared by the Lockheed Missiles & Space Company, Huntsville Research & Engineering Center, to document the accomplishments of the second five week study period (ending 26 August) for the Preliminary Design of a Lunar Gravity Simulator, Contract NAS8-20351. The study is being conducted by the Systems Engineering Organization at HREC under the direction of Mr. R. S. Paulnock, Manager, and Mr. R. B. Wysor, Project Engineer. Other contributors to this report and the study efforts during this second reporting period are Dr. Wolfgang Trautwein and Messrs Bob L. Myers, Z. V. Adams, G. P. Gill, E. L. Saenger, G. D. Robinson, W. E. Jones, D. J. Wilson and G. E. Malone. This report was published by the Technical Publications Organization at HREC under the supervision of Mrs. Carolyn Harrell. The study program is sponsored by the Advanced Systems Office of Marshall Space Flight Center under the technical direction of Mr. Herbert Schaefer, Principle COR and Robert Belew, Alternate COR.

Technical data in this report will be delivered to NASA/MSFC technical personnel at an informal presentation scheduled for 12 September 1966.

CONTENTS

Section		Page
	FOREWORD	ii
1	INTRODUCTION	1-1
2	ANALYSES AND SELECTION OF SUSPENSION DEVICE AND DRIVE SYSTEM CONCEPTS	2-1
	2.1 Suspension Force Control System	2-1
	2.2 Trolley Drive System with Displacement Sensor	2-9
	2.3 Trolley Drive System with Angle Sensor	2-19
3	VARIATION OF STATIC ERRORS WITH CABLE LENGTH AND LSV PITCH ANGLES	3-1
	3.1 Non-Vertical Wheel Support Cables for Four- Wheel Vehicle	3-1
	3.2 Roll Angle Variations	3-4
	3.3 Method of Analysis - Four Wheel Vehicle with Pitch Angle Variations	3-4
	3.4 Non-Vertical Chassis Support Cables for Tractor-Trailer Vehicle	3-6
	3.5 Method of Analysis - Tractor-Trailer Vehicle with Pitch Angle Variations	3-7
4	DYNAMIC ANALYSIS OF THE 2-D LUNAR GRAVITY SIMULATOR	4-1
	4.1 Obstacle Simulation	4-1
	4.2 Suspension Device Force Control System Simulation	4-5
	4.3 Trolley Drive System	4-40
5	2-D LGS DESIGN AND COMPONENT SPECIFICATIONS	5-1
	5.1 LGS System Description - 2-D Configuration	5-1

CONTENTS (Continued)

Section		Page
5.2	Structural Analysis of the LGS Suspension Platform	5-7
5.3	Wheel Support System	5-12
5.4	Winch and Motor Systems	5-19
5.5	Trolley Drive System Requirements	5-27
5.6	Hydraulic Power Supply Requirements	5-29
6	2-D LUNAR GRAVITY SIMULATOR COST ANALYSES	6-1
7	CONCLUSIONS AND RECOMMENDATIONS	7-1
8	FUTURE WORK	8-1
9	REFERENCES	9-1

LIST OF ILLUSTRATIONS

Tables

Table	Title	Page
2.1	Summary of Suspension Force Control System Data	2-6
2.2	Preliminary Drive Motor Data for Trolley Drive System	2-15
2.3	Preliminary System Parameters for Trolley Drive System with Displacement Sensing	2-18
3.1	Four Wheel Vehicle Analysis	3-5
3.2	Tractor-Trailer Vehicle Analysis	3-11
4.1	Trolley Drive System Parameters as used for the Simulation	4-41
4.2	Acceleration Disturbances as used during Dynamic Trolley Drive System Simulations	4-42
5.1	Vehicle Suspension Platform Weight Summary	5-4
5.2	Main Support Platform Structure	5-8
5.3	Vertical Displacement of Joints	5-10

FOREWORD

This report was prepared by the Lockheed Missiles & Space Company, Huntsville Research & Engineering Center, to document the accomplishments of the second five week study period (ending 26 August) for the Preliminary Design of a Lunar Gravity Simulator, Contract NAS8-20351. The study is being conducted by the Systems Engineering Organization at HREC under the direction of Mr. R. S. Paulnock, Manager, and Mr. R. B. Wysor, Project Engineer. Other contributors to this report and the study efforts during this second reporting period are Dr. Wolfgang Trautwein and Messrs Bob L. Myers, Z. V. Adams, G. P. Gill, E. L. Saenger, G. D. Robinson, W. E. Jones, D. J. Wilson and G. E. Malone. This report was published by the Technical Publications Organization at HREC under the supervision of Mrs. Carolyn Harrell. The study program is sponsored by the Advanced Systems Office of Marshall Space Flight Center under the technical direction of Mr. Herbert Schaefer, Principle COR and Robert Belew, Alternate COR.

Technical data in this report will be delivered to NASA/MSFC technical personnel at an informal presentation scheduled for 12 September 1966.

LIST OF ILLUSTRATIONS (Continued)

Figure	Title	Page
4.3	Lunar Gravity Simulator Analog Simulation Diagram (Roll Configuration)	4-6
4.4	Lunar Gravity Simulator Analog Simulation Diagram (Pitch Configuration)	4-7
4.5 - 4.8	Force Control System Performance with LSSM Left Wheels Engaging Obstacle (Roll Configuration)	4-16 - 4-19
4.9 - 4.12	Force Control System Performance with LSSM Front and Rear Wheels Engaging Obstacle (Pitch Configuration)	4-20 - 4-23
4.13 - 4.16	Force Control System Performance with MOLAB Left Wheels Engaging Obstacle (Roll Configuration)	4-24 - 4-27
4.17 - 4.20	Force Control System Performance with MOLAB Front and Rear Wheels Engaging Obstacle (Pitch Configuration)	4-28 - 4-31
4.21	Lunar Gravity Error vs Obstacle Height - LSSM Vehicle in Roll Configuration	4-32
4.22	Lunar Gravity Error vs Obstacle Height - MOLAB Vehicle in Roll Configuration	4-33
4.23	Lunar Gravity Error vs Obstacle Height - LSSM Vehicle in Pitch Configuration	4-34
4.24	Lunar Gravity Error vs Obstacle Height - MOLAB Vehicle in Pitch Configuration	4-35
4.25	Peak Wheel Accelerations vs Obstacle Height, LSSM and MOLAB	4-36
4.26	LSSM Rear Wheel Displacement and Lunar Gravity Error	4-37
4.27	LSSM Chassis c.g. Displacement and Lunar Gravity Error	4-38
4.28	Lunar Gravity Error vs Cable Length for LSSM in Pitch Configuration	4-39
4.29	Trolley Drive System Response Characteristics (LSSM Vehicle)	4-44
4.30	Trolley Drive System Response Characteristics (MOLAB Vehicle)	4-45
4.31	Trolley/LSV Force Diagram	4-46

LIST OF ILLUSTRATIONS (Continued)

Table	Title	Page
5.4	Preliminary LGS Motor/Winch Specifications	5-20
6.1	Cost Analyses Summary	6-2

Figures

Figure	Title	Page
1.1	Lunar Gravity Simulator System Configuration	1-3
1.2	Program Plan	1-4
2.1	Block Diagram of Constant Force Control System	2-2
2.2	Derivation of the Open-Loop Transfer Function from the Block Diagram	2-1
2.3	Basic Configuration of Trolley Positioning Control System	2-10
2.4	Signal Flow Chart of Trolley Drive System with Displacement Sensing	2-12
2.5	Notation	2-16
2.6	Transverse Wave at LSV Attachment	2-16
2.7	Cable Angle Sensing by Potentiometer	2-20
2.8	Effects of Upward and Downward Type Transverse Cable Waves on the Trolley Drive with Angle Sensor	2-23
2.9	Approximate Signal Flow Chart of Trolley Positioning Control System with Cable Angle Sensing	2-24
2.10	Multiplier Phototube Diagrams	2-27
3.1	Four-Wheel Vehicle Suspension System	3-2
3.2	Vehicle Static Longitudinal Error from Wheel Suspension System	3-3
3.3	Tractor-Trailer Chassis Support System	3-8
3.4	Vehicle Static Longitudinal Error for Tractor-Trailer Chassis Suspension System	3-9
4.1	Rolling Wheel Obstacle Simulation	4-2
4.2	Simplified Obstacle Simulation	4-4

LIST OF ILLUSTRATIONS (Continued)

Figure	Title	Page
4.32	Effect of Cable Length on the Horizontal Acceleration Error for Various Decelerations	4-48
4.33	Effect of Cable Length on the Horizontal Acceleration Error for Various Decelerations	4-49
5.1	Lunar Gravity Simulator, Two-Dimensional Configuration	5-2
5.2	Joint-Member Orientation	5-11
5.3	Comparison of Wheel Suspension Systems	5-13
5.4	LGS Wheel Support Frame	5-14
5.5	Support Frame Weight vs Vehicle Wheel Diameter	5-17
5.6	Winch Assembly for Chassis Suspension System	5-21
5.7	Winch Assembly for Wheel Suspension System	5-22
5.8	Vickers, Inc. Typical Motors	5-25
5.9	Vickers, Inc. Typical Motors	5-26
5.10	Total Hydraulic Fluid Flow vs Terrain Slope	5-31
6.1	Design and Fabrication Schedule for Two-Dimensional Lunar Gravity Simulator	6-3

Section 1 INTRODUCTION

The Lunar Gravity Simulator (LGS) is a system planned for the evaluation of full scale Lunar Surface Vehicles (LSV) over simulated Lunar terrain in an Earth's gravity environment. The purpose of such a system will be to:

- Substantiate the LSV mobility system performance parameters under simulated loading conditions as may occur from the $1/6$ g environment and the anticipated obstacle, slope and velocity combination.
- Establish the confidence level of the ability to design the mobility systems for various LSV configurations.
- Determine the effect of the vehicle dynamic behavior on the vehicle operator and the man-machine relationship in a $1/6$ g environment.
- Train astronauts in handling LSV's in a $1/6$ g environment.

With these objectives in mind, LMSC has been conducting a Preliminary Design Study of a Lunar Gravity Simulator System under contract to the Marshall Space Flight Center. The concept under study is illustrated in Figure 1.1. This study effort will encompass a 15 week period which will be subdivided into three five-week intervals. This report describes the tasks and accomplishments of the second five-week period ending 26 August 1966, and the tasks and approaches planned for subsequent study efforts.

Figure 1.2 depicts the overall LGS study program plan (Task, Schedule and Manloading). The first ten-week period is devoted to a study of the two-dimensional LGS and the results of the first portion of this study were described in the First Interim Report (Reference 1). The completion of the two-dimensional study is described in this document. Efforts during this reporting period were devoted to the following tasks:

<u>Task</u>	<u>Study Efforts</u>
1.2	Refine 2-D math model of 2-D LGS/LSV to include wheel dynamic input, derive a math model for the trolley drive system.
1.3	Continued analysis and selection of suspension device and drive system concepts
1.4	Conduct dynamic analysis of 2-D LGS to determine LGS/LSV interaction and Lunar g error.
1.5	Conduct tradeoff study of rail height versus pertinent LGS system parameters.
1.6	Conduct cost analysis of 2-D LGS system.
1.7	Continue design, layout and component specification analysis of 2-D system.

The following sections discuss the accomplishments on these tasks and the work planned on subsequent tasks for the remainder of the program.

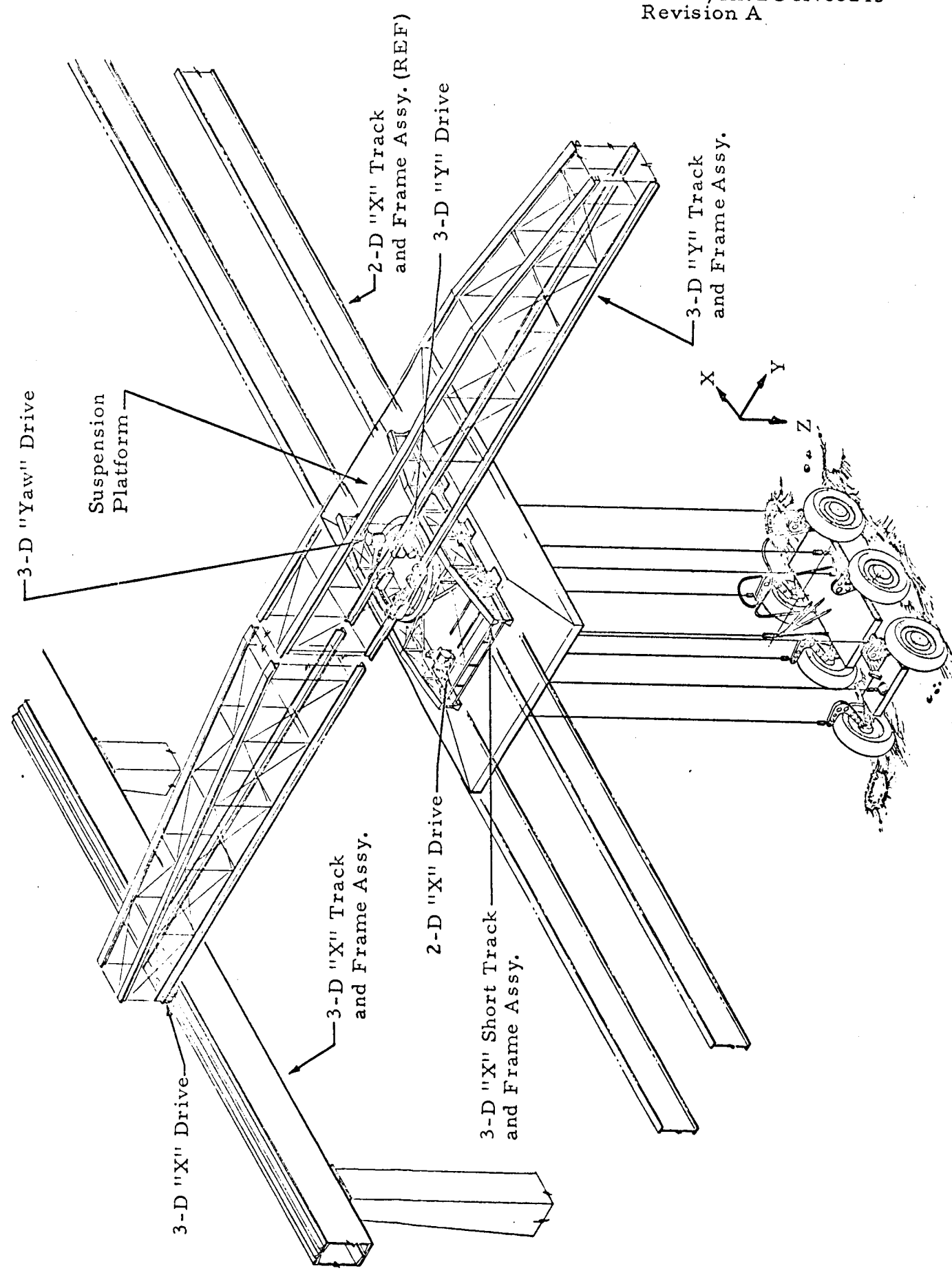


Figure 1.1 - Lunar Gravity Simulator System Configuration

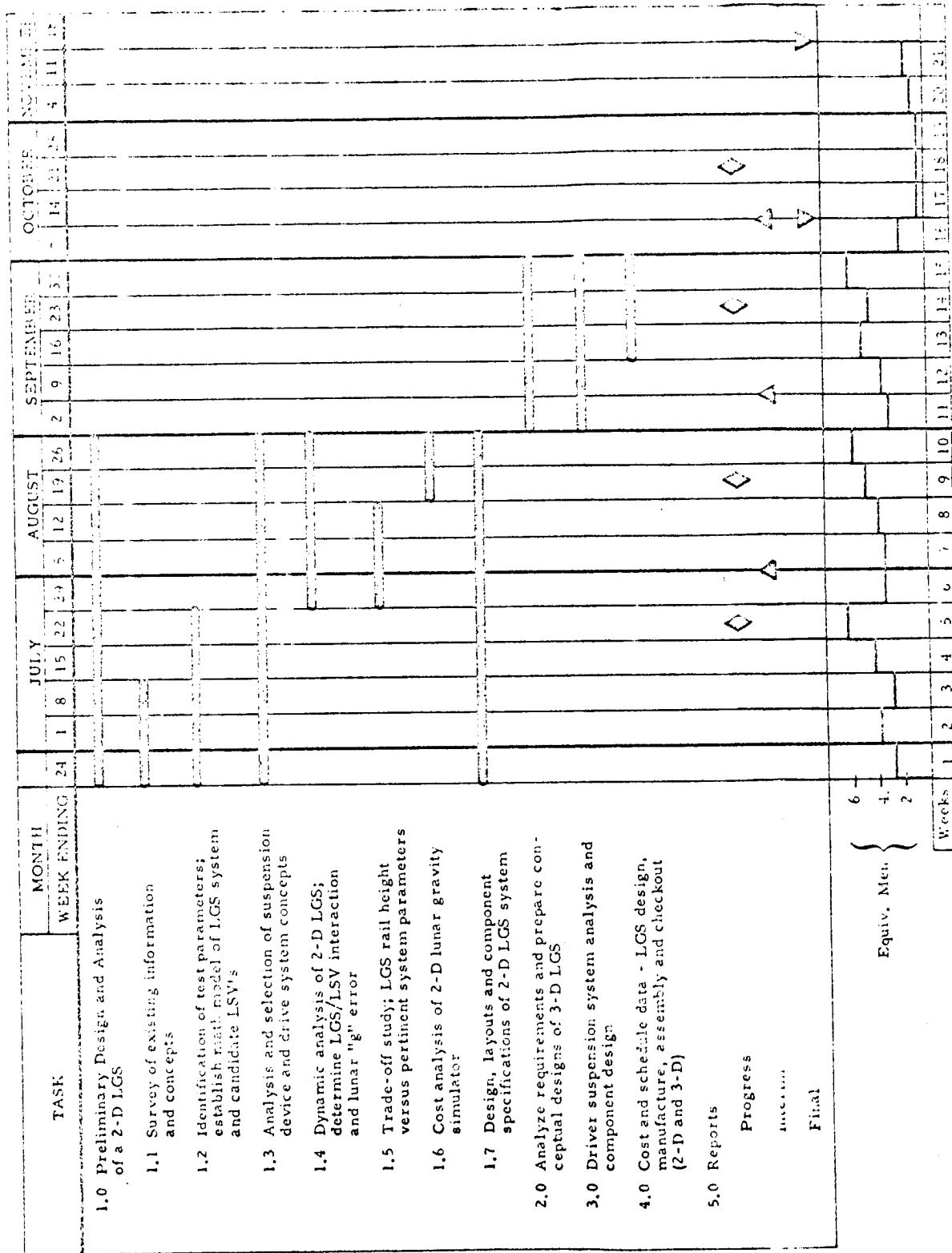


Figure 1.2 - Program Plan

Section 2

ANALYSES AND SELECTION OF SUSPENSION DEVICE AND DRIVE
SYSTEM CONCEPTS

2.1 SUSPENSION FORCE CONTROL SYSTEM

During this reporting period, the electrohydraulic force control system as described in the previous report (Figures 9 and 10 of Reference 1) has been further refined to reduce suspension force deviations from the nominal values of $5/6$ times the earth weight of the suspended parts. A new set of coefficients was calculated that accounted for all changes in the system parameters made after the first approach.

Precise control of the LSSM wheel cable forces was found to be the most critical task. The uncompensated control system had a very poor damping of 7% of critical damping. Therefore, tandem-type compensating networks were designed via the root-locus method in an effort to increase damping in all force control loops to about 70% of critical damping.

The analysis was based on the configuration given in Figure 2.1 (from Figure 10 of Reference 1) and redrawn in lumped form in Figure 2.2. Vertical

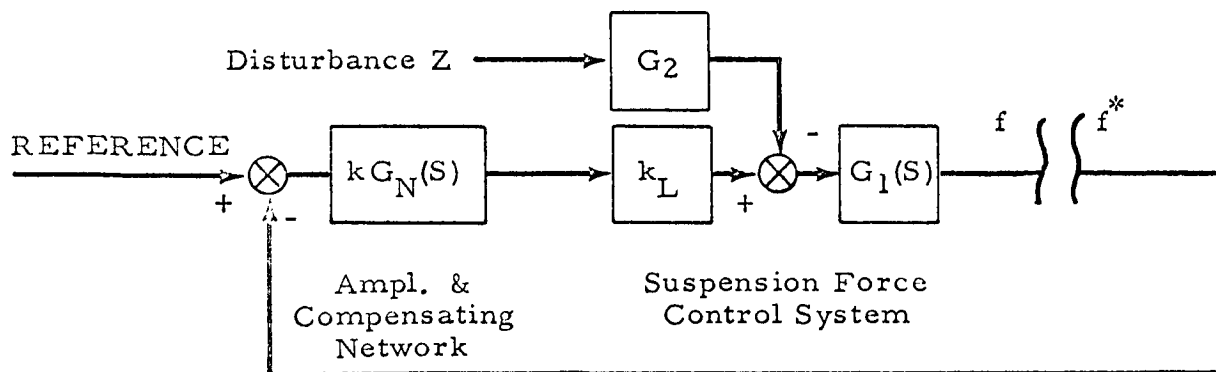


Figure 2.2 - Derivation of the Open-Loop Transfer Function from the Block Diagram

$$\frac{f(s)}{Z(s)} = -\frac{K_c}{F_o} \frac{A_1 s^3 + A_2 s^2 + B_3 s + B_4}{A_1 s^4 + A_2 s^3 + A_3 s^2 + A_4 s + A_5}$$

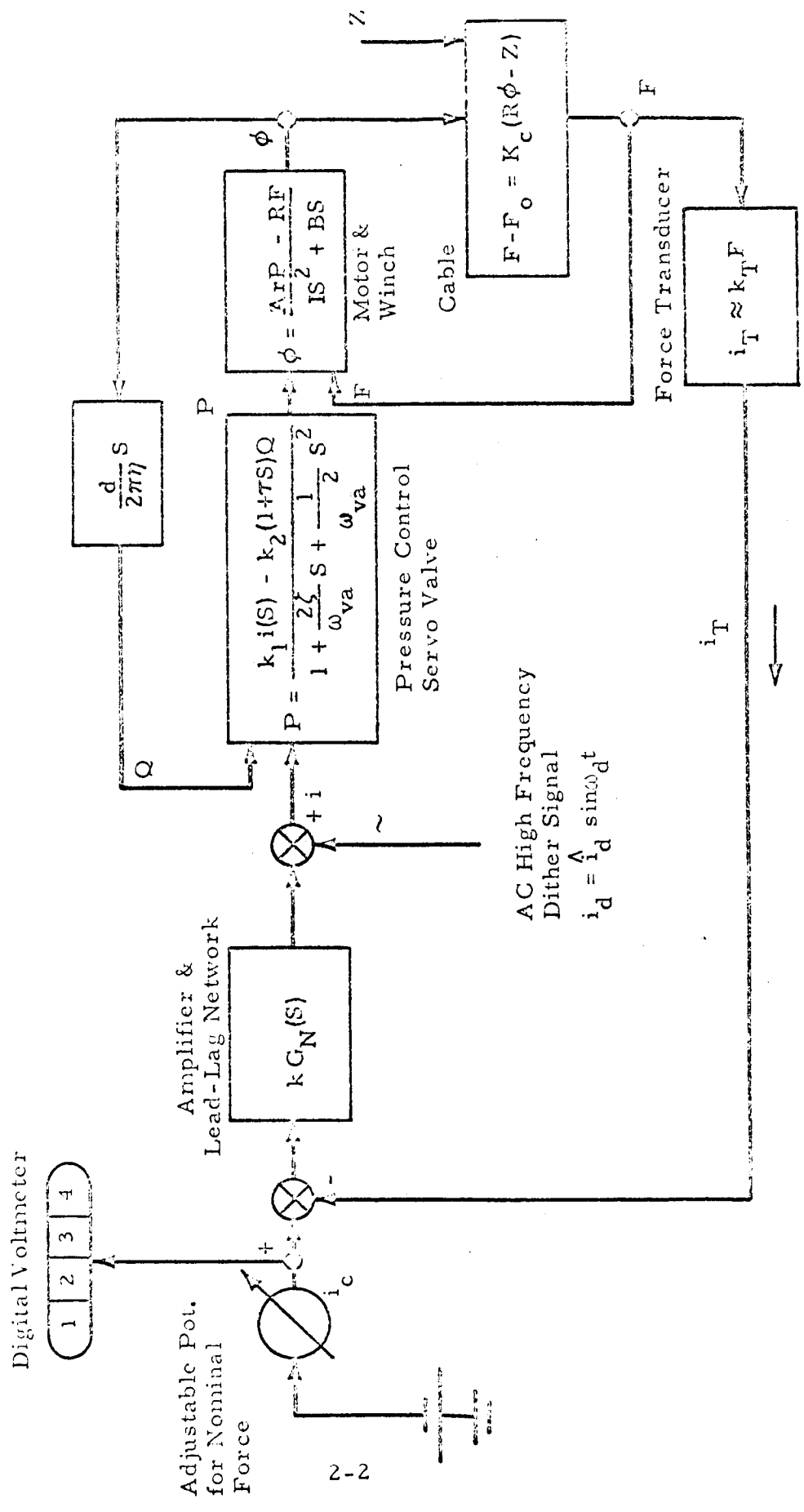


Figure 2.1 - Block Diagram of Constant Force Control System

displacements Z in this formulation are considered as external disturbances.
The open-loop transfer function is

$$f(S) = -G_1(S) \left[k k_L G_N(S) f^*(S) + G_2(S) Z(S) \right]$$

where

$$G_1(S) = \frac{K_c}{A_1 S^4 + A_2 S^3 + A_3 S^2 + A_4 S + A_5}$$

$$G_2(S) = \frac{S}{F_o} (A_1 S^3 + A_2 S^2 + B_3 S + B_4)$$

$$k_L = k k_1 k_T R$$

and the optimum compensating filter

$$G_N(S) = \frac{cd}{a^2 + b^2} \frac{S^2 + 2aS + a^2 + b^2}{(S + c)(S + d)}$$

The coefficients

$$A_1 = \frac{IP_o}{T_o \omega_v^2} \left[\frac{\text{lb sec}^4}{\text{ft}^2} \right]$$

$$A_2 = \frac{P_o}{T_o \omega_v} \left(2\zeta I + \frac{B}{\omega_v} \right) \left[\frac{\text{lb sec}^3}{\text{ft}^2} \right]$$

$$A_3 = \frac{P_o}{T_o} \left(I + \frac{2B\zeta}{\omega_v} + \frac{K_c R^2}{\omega_v^2} \right) + \frac{k_2 \tau d}{2\pi\eta} \left[\frac{\text{lb sec}^2}{\text{ft}^2} \right]$$

$$B_3 = \frac{P_o}{T_o} \left(I + \frac{2B\zeta}{\omega_v} \right) + \frac{k_2 \tau d}{2\pi\eta} \left[\frac{\text{lb sec}^2}{\text{ft}^2} \right]$$

$$A_4 = \frac{P_o}{T_o} \left(B + \frac{2\zeta K_c R^2}{\omega_v} \right) + \frac{k_2 d}{2\pi\eta} \left[\frac{\text{lb sec}}{\text{ft}^2} \right]$$

$$B_4 = \frac{B P_o}{T_o} + \frac{k_2 d}{2\pi\eta} \left[\frac{\text{lb sec}}{\text{ft}^2} \right]$$

$$A_5 = K_c R \left(\frac{P_o}{F_o} + k k_1 k_T \right) = k_3 K_c R \left[\frac{\text{lb}}{\text{ft}^2} \right]$$

are defined in Reference 1, pages 24 and 25, where the parameters are:

- I = the moment of inertia of motor and winch and cable
- P_o = the nominal hydraulic pressure
- T_o = the nominal hydraulic motor torque
- F_o = the nominal cable force
- ω_v = valve natural frequency
- ζ_v = the valve damping constant
- B = the viscous damping in the motor
- K_c = EA_c/L_c the cable spring constant, where E is Young's modulus, A_c is the cross sectional area of cable, and L_c is the cable length
- R = the effective winch radius
- τ = the valve droop time constant
- d = the volumetric displacement of motor per revolution
- η = the volumetric efficiency of motor
- k_T = the force transducer constant
- k₁ = valve constant
- k₂ = the valve static droop constant
- k₃ = P_o/F_o + k k₁ k_T, is the adjustable loop gain

The selected system components and their parameters are listed in Table 2.1 with the optimum filter coefficients found for the four typical force control systems. The loop gains and filter data are given for five different rail heights.

Each filter can be mechanized by a circuit with four operational amplifiers and a module of passive RC components that can be mounted in racks of the control console. While the same amplifiers may be used for all LSV's, exchangeable RC modules of the plug-in type may be used to adapt the filter data to the specific vehicle to be tested.

Results of analog simulations are given in Section 4.2. The poorly damped mode of the uncompensated system is completely eliminated by the compensation.

Table 2.1
SUMMARY OF SUSPENSION FORCE CONTROL SYSTEM DATA

Description	Dimen- sion	Suspended Part			
		Chassis LSSM	Chassis MOLAB	Wheel LSSM	Wheel MOLAB
CABLE: Type	-	7×7 1/8	7×7 1/4	7×7 3/64	7×7 1/16
Diameter	in.				
Cross-section Area A_c	ft ²	$.497 \times 10^{-4}$	1.88×10^{-4}	$.0745 \times 10^{-4}$	$.133 \times 10^{-4}$
Nominal tension F_o	lb	785	2500	67	167
Spring Constant K_c for 50 ft cable	lb/ft	1809	6843	271	484
MOTOR: Vickers Type		MF-3921-30	M-3921-30	MF-3918-25	
No. of motors		1	2	1	
Moment of inertia I (motor(s) & winch)	slug ft ²	.0522	.0867 (total)	.00595	
Viscous damping B		≈ 0	≈ 0	≈ 0	
Max. stall torque T_o	lb-ft	458	917	79	
System pressure P_o	lb/ft ²	4.32×10^5			
Displacement/Rev d	ft ³	6.66×10^{-3}			
Volumetric efficiency η	-	0.95			
Weight	lb	32.6	65.2	22.1	22.1
WINCH:					
Gear ratio	-	3.14:1	3.14:1	1:1	1:1
Winch radius R	ft	0.25			

Table 2.1 (Continued)

Description	Dimension	Suspended Part			
		Chassis LSSM	Chassis MOLAB	Wheel LSSM	Wheel MOLAB
VALVE: Moog					
Pressure control servo valve		Model 15-010			→
No. of valves		1	2	1	1
Natural frequency ω_v	sec^{-1}	1256			→
Damping ζ_v	-	0.5			→
Droop constant k_2	lb sec/ft^5	5×10^6			→
Droop time const. τ	sec	0.016			→
AMPLIFIERS FORCE TRANSDUCER, COMPEN- SATING FILTER:					
Overall loop gain $kk_1 k_t$	ft^{-2}				
for rail height 30'		597		1970	
50'		121		4230	
90'		188		2910	
130'		214		2454	
170'		224		4230	980
Filter Parameter a	sec^{-1}				
for rail height 30'		22.08			
50'		↓		7.30	
90'				8.44	
130'				9.19	
170'				9.48	
			23.98	9.63	9.76

Table 2.1 (Continued)

Description	Dimension	Suspended Part			
		Chassis LSSM	Chassis MOLAB	Wheel LSSM	Wheel MOLAB
Filter Parameter b for rail height 30' 50' 90' 130' 170'	sec ⁻¹	59.0	43.9	123.8	80.7
		45.5		95.6	
		28.9		70.9	
		20.7		58.7	
		14.6		51.1	
Filter Parameter c	sec ⁻¹	5	for all rail heights		→
Filter Parameter d	sec ⁻¹	15			→

2.2 TROLLEY DRIVE SYSTEM WITH DISPLACEMENT SENSOR

Two basic methods have been proposed in the previous report to maintain a constant relative position between the LSV and the trolley supporting the suspension cables:

1. Detect horizontal displacement between a point on the trolley and the c.g. of the LSV and compensate accordingly (Displacement Sensing).
2. Detect variations of the cables from the vertical and drive the trolley to compensate (Cable Angle Sensing).

During this reporting period, the dynamic equations for both control concepts have been derived and analyzed. The analysis was based on the configuration shown schematically in Figure 2.3.

A comparison of several drive motor types revealed that best performance in terms of high torques and low inertias, together with minimum weight, is obtained with a hydraulic drive. A rotary-type hydraulic motor may be directly coupled to a drive wheel or capstan if a cable is used to ensure zero slippage.

The equations for the displacement sensing concept were derived under the following simplifying assumptions.

- Changes of the cable forces (due to imperfections in the constant force control systems) have negligible effects on the trolley dynamics.
- The transversal cable dynamics are dominated by the first oscillatory mode.
- After an initial disturbance such as a sudden acceleration $\ddot{X}(0)$ or velocity change $\Delta\dot{X}(0)$ of the LSV, both cables suspending the main LSV chassis oscillate with identical phase and amplitude.
- The periodic components of the cables suspending the wheels have negligible effect on the trolley dynamics. This assumption is justified because of the small

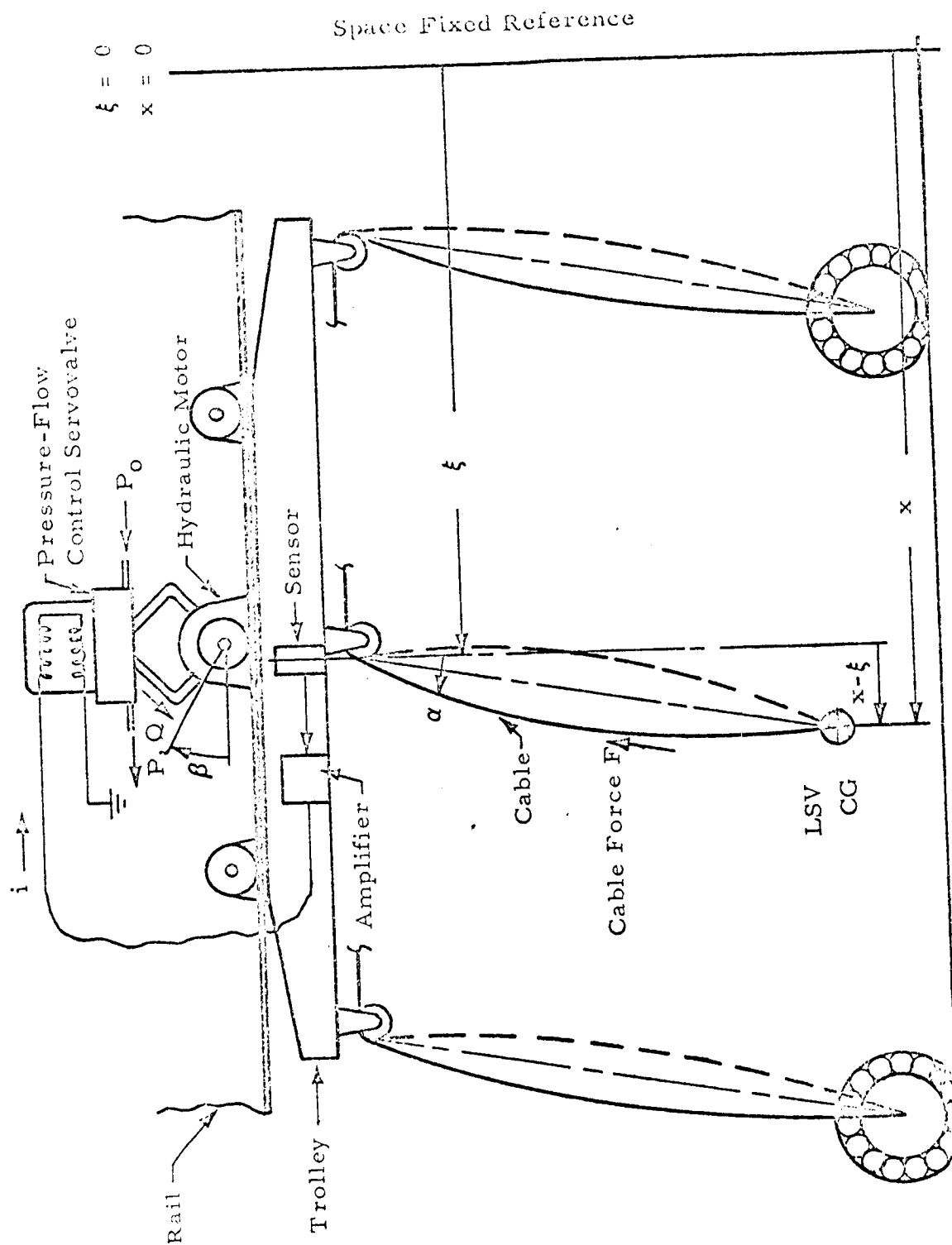


Figure 2.3 - Basic Configuration of Trolley Positioning Control System

amount of the wheel-cable force compared with the total chassis cable forces (about 1:20) and due to the fact that in the general case, not all four or six wheel cables will oscillate in phase. Hence, some of the periodic horizontal force components will at least partially cancel.

- The time-delay between a sudden horizontal displacement $X - \xi$ at the lower end of the cable and the resulting change in the upper mean cable angle $\bar{\alpha}$ (due to the finite transversal wave propagation velocity) may be represented by a first-order lag term

$$\alpha(S) = \frac{1}{L} \frac{1}{T_{\alpha} S + 1} (X - \xi)$$

Initial investigations of control systems for the drive system indicated that displacement sensing only would not be adequate for the accuracy requirements. Rate sensing, or $(\dot{X} - \dot{\xi})$, was found necessary. This did not present a particular problem in either of the sensing techniques considered. The optical method required differentiating the voltage output. The angle sensing potentiometer method would require the addition of a tachometer for the rate signal.

The transfer functions resulting from these assumptions and corresponding signal flow diagrams are shown in Figure 2.4 for the Displacement Sensing Concept. The dynamic equations are listed in Section 4.3.

For a first approximate evaluation of the control loop performance, the valve spool natural frequency ($\omega_v \approx 600 \text{ sec}^{-1}$) and the frequency of the first transverse mode of the cable ($\omega_T \approx 70 \text{ sec}^{-1}$) were considered much larger than the control frequencies to be expected. Neglecting these high frequency modes, the following closed-loop transfer function is obtained for the displacement sensing configuration:

$$\frac{\xi(S)}{X(S)} = \frac{E_5 S^2 + E_4 S + E_3}{E_0 S^3 + E_1 S^2 + E_2 S + E_3} \quad (2.1)$$

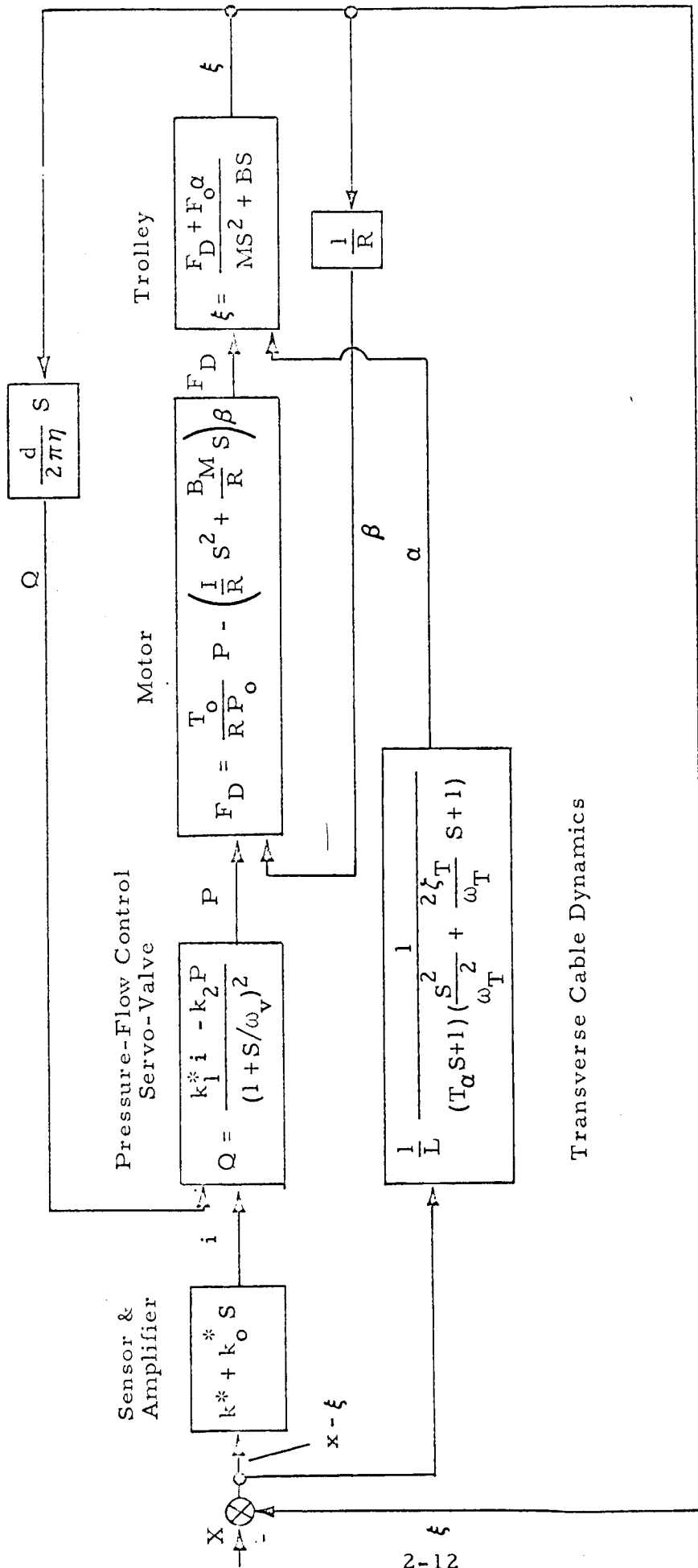


Figure 2.4 - Signal Flow Chart of Trolley Drive System with Displacement Sensing

where¹

$$E_0 = \frac{k_2^* P_o T_\alpha}{T_o} \left(RM + \frac{I}{R} \right) \left[ft^2 \sec^2 \right]$$

$$E_1 = \frac{k_2^* P_o}{T_o} \left(RM + \frac{I}{R} \right) + q T_\alpha + k_o^* k_1^* T_\alpha \left[ft^2 \sec \right]$$

$$E_2 = k_1^* (k_o^* + k^* T_\alpha) + q \left[ft^2 \right]$$

$$E_3 = k^* k_1^* + \frac{k_2^* P_o F_o R}{T_o L} \left[ft^2 \sec^{-1} \right]$$

$$E_4 = k_1^* (k_o^* + k^* T_\alpha) \left[ft^2 \right]$$

$$E_5 = k_o^* k_1^* T_\alpha \left[ft^2 \sec \right]$$

For a stability analysis, the complete transfer function with the high-frequency modes included was derived. The characteristic equation is

$$\Delta = G_0 S^6 + G_1 S^5 + G_2 S^4 + G_3 S^3 + G_4 S^2 + G_5 S + G_6 \quad (2.2)$$

where

$$G_0 = \frac{T_\alpha q}{\omega_T^2 \omega_v^2}$$

$$G_1 = \frac{q}{\omega_v^2} a + \frac{T_\alpha}{\omega_T^2} b$$

$$G_2 = \frac{q}{\omega_v^2} c + \frac{T_\alpha}{\omega_T^2} d + ab$$

¹ See Table 2.3 for definition of terms.

$$G_3 = \frac{q}{\omega_v} + \frac{k^* k_1^* T_\alpha}{\omega_T} + ab + bc$$

$$G_4 = k^* k_1^* a + b + cd$$

$$G_5 = k^* k_1^* c + d$$

$$G_6 = k^* k_1^* + \frac{k_2^* P_o R F_o}{L T_o}$$

$$a = \frac{1}{\omega_T} \left(2 \zeta_T T_\alpha + \frac{1}{\omega_T} \right)$$

$$b = \frac{T_\alpha}{\omega_T} \left[\frac{2q}{\omega_v} + \frac{k_2^* P_o}{T_o} \left(R_M + \frac{1}{R} \right) \right]$$

$$c = T_\alpha + \frac{2 \zeta_T}{\omega_T}$$

$$d = q + k_0^* k_1^* + \frac{k_2^* P_o}{T_o} \left(\frac{B_M}{R} + R_B \right)$$

2.2.1 Selection of Components

Drive Motors - The power and speed requirements for the trolley in the most severe cases (v_{\max} for MOLAB, 2g horizontal decelerations) dictated the choice of hydraulic drive motors. Data for possible motor candidates are given in Table 2.2. The optimization and analog simulation were based on these motor and transmission data.

Table 2.2

PRELIMINARY DRIVE MOTOR DATA FOR TROLLEY
DRIVE SYSTEM

Type of Motor:	Vickers MF-3924-30
No. of Motors Required for X-Drive:	2
Torque at 3000 psi:	476 lb-ft (total)
Gear Ratio Motor to Drive Shaft:	2.78:1
Drive Wheel Radius:	$R = 0.26 \text{ ft}$
Moment of Inertia (motors & gears):	0.129 slug ft^2

Servo Valves - Electro-Hydraulic Servo Valves of the Pressure-Flow Control type were found to best meet the requirements.

According to manufacturer's data (Moog Bulletin No. 103), typical data for the natural valve frequency and the sensitivity to load pressure for this type of valves are

$$\omega_v \text{ typical} = 630 \text{ sec}^{-1} \qquad k_2^* \text{ typical} = 8.2 \times 10^{-8} \frac{\text{ft}^5}{\text{lb-sec}}$$

As a wide variation in k_2^* is said to be possible, a value

$$k_2^* = \frac{1}{4} k_2^* \text{ typical}$$

was assumed for the control system synthesis.

2.2.2 Transverse Cable Dynamics

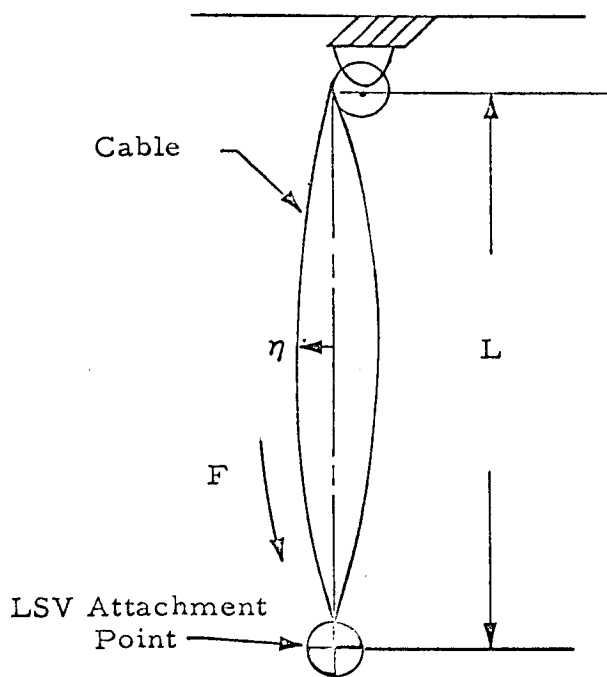


Figure 2.5 - Notation

The first transversal mode of a cable with tension F and a distributed mass of μ slugs/ft may be described by the equation

$$\frac{\mu L}{3} \ddot{\eta} + B \dot{\eta} + \frac{4F_o}{L} \eta = 0$$

with a natural frequency

$$\omega_T = \frac{1}{L} \sqrt{\frac{12F}{\mu}}$$

The time constant accounting for the time-delay between a displacement $(X - \xi)$ of the lower attachment point and a change in the upper cable angle α is

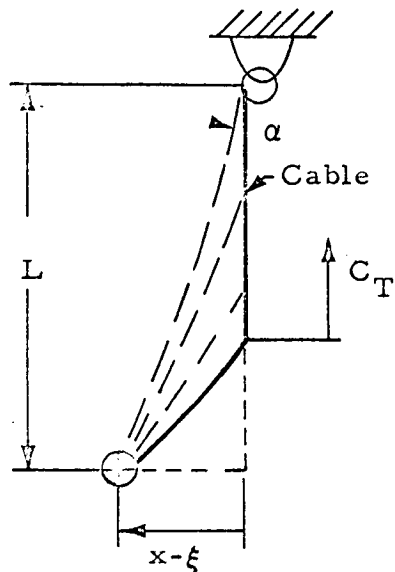


Figure 2.6 - Transverse Wave at LSV Attachment

$$T_\alpha \approx \frac{L}{C_T}$$

where $C_T = \sqrt{\frac{F}{\mu}}$ is the transversal wave propagation velocity.

In Table 2.3, all the fixed trolley drive system parameters are listed. (Motor data are reduced to the drive wheel station.) It is assumed that the LSV chassis is suspended by two cables.

2.2.3 Optimal Gain Adjustment

The gain factors, k^* and k_0^* , for the position and rate feedback were selected in order to minimize the ITAE-performance criterion (integral of time multiplied by absolute value of error)

$$I = \int_0^{\infty} |X - \xi| t dt \rightarrow \text{Min}$$

after a step-type displacement, $X(0) - \xi(0)$, with the additional specification that the error $X - \xi$ during constant velocity inputs \dot{X} be also a minimum. The standard forms of optimum transfer functions as developed by Graham and Lathrop (Reference 2) were used to determine optimum gains. For both the LSSM and MOLAB as test articles, these gains were found to be

$$\begin{aligned} k^* k_1^* &= 1.35 \text{ ft}^2 \text{ sec}^{-1} \\ k_0^* k_1^* &= 0.0046 \text{ ft}^2 \end{aligned} \quad (2.3)$$

For the displacement sensing concept, these values are virtually independent of rail height.

Table 2.3
PRELIMINARY SYSTEM PARAMETERS FOR TROLLEY DRIVE SYSTEM
WITH DISPLACEMENT SENSING

Parameter	Test Article	
	MOLAB	LSSM
Trolley Mass	68.4 slugs	68.4 slugs
Viscous Damping (Trolley)	≈ 0	≈ 0
Total Cable Forces (for Trolley Equation)	5 660 lbs	1830 lbs
I/R	0.5 slug ft	0.5 slug ft
Viscous Damping (Motors)	≈ 0	≈ 0
Drive Wheel Radius	0.26 ft	0.26 ft
Torque-Pressure	0.003 ft^3	0.003 ft^3
Flow/Trolley Displacement		
$q = \frac{d}{2\pi R \eta}$	0.0061 ft^2	0.0061 ft^2
(η = volumetric efficiency of motors)		
Valve Natural Frequency	628 sec^{-1}	628 sec^{-1}
Valve Pressure Sensitivity	$2.07 \times 10^{-7} \text{ ft}^5/\text{lb sec}$	$2.07 \times 10^{-7} \text{ ft}^5/\text{lb sec}$
Cable Length	45 ft	45 ft
Transv. Wave Time Constant for Cable Diameter	0.052 sec $1/4''$	0.047 sec $1/16''$
Transversal Mode Frequency	67 sec^{-1}	73 sec^{-1}
Transv. Mode Dampg. (estimated)	0.1	0.1

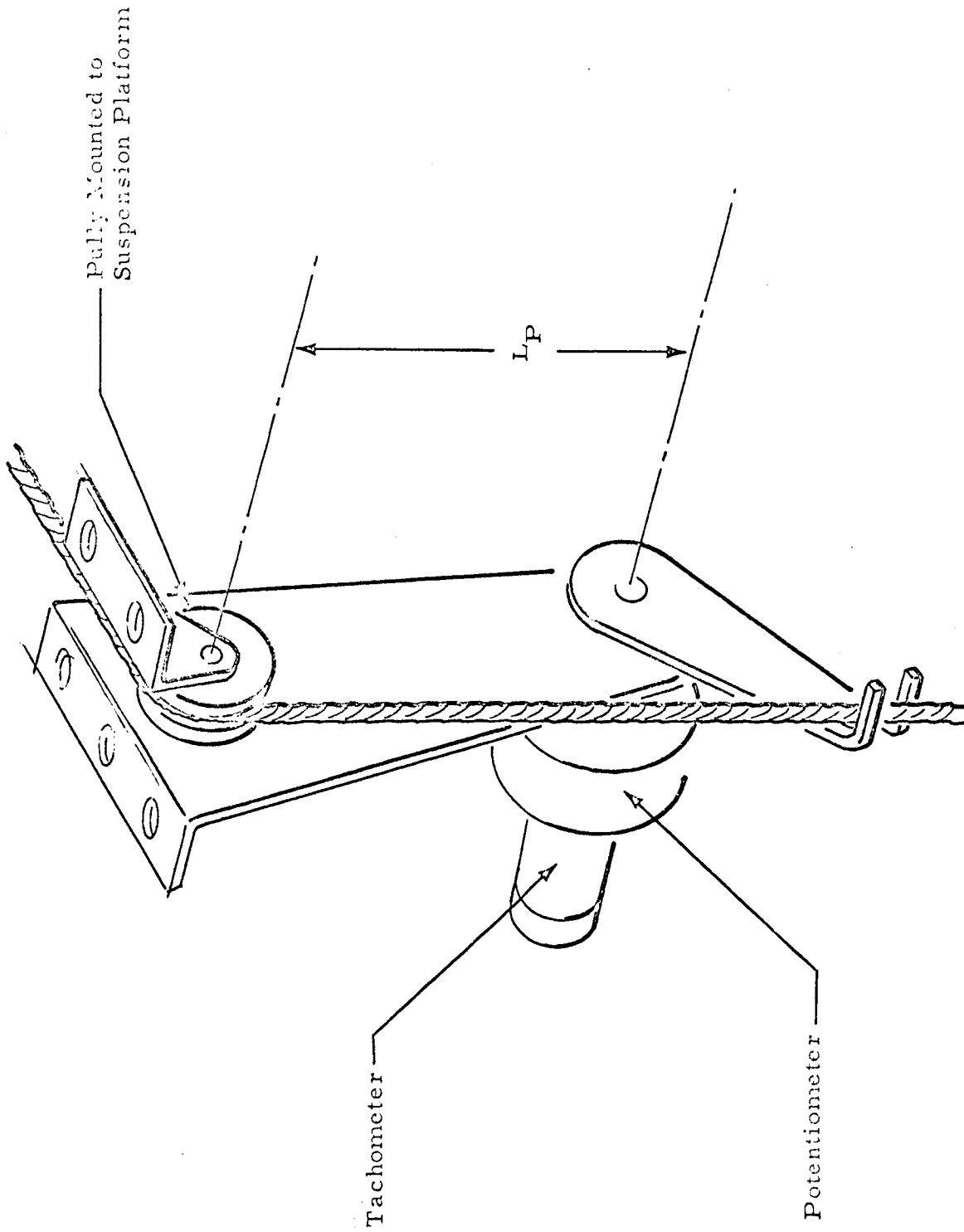


Figure 2.7 - Cable Angle Sensing by Potentiometer

2.3 TROLLEY DRIVE SYSTEM WITH ANGLE SENSOR

Sensing the angular deviations of the suspension cables from the vertical is the most straightforward and least expensive approach from the implementation point of view.

One potentiometer in the 2D configuration or a pair of perpendicular potentiometers in the 3D configuration would be sufficient to sense cable misalignments as sketched in Figure 2.7. Tachometers mounted on the Pot-shafts could provide the rate signals required. Angular resolution of the pots can be considerably increased by lowering the pot mount by a distance L_p below the pulley.

For a meaningful dynamic analysis of a trolley drive system with such a sensing device the cable motions close to the upper pulley have to be studied carefully.

A more complete representation of the transverse cable dynamics is therefore made while the equations describing valve, motor and trolley dynamics are the same as in the preceeding section.

2.3.1 Transverse Cable Dynamics

Two cases are considered:

- Upward Wave Propagation. - This occurs when there are LSV accelerations $\ddot{X} \neq 0$. The angular cable motion can then be approximately described as in Section 2.2. The time-delay due to the finite wave velocity C_T is precisely accounted for here by the equation

$$\alpha_x(s) = \frac{e^{-T_\alpha s}}{L \left(\frac{s^2}{\omega_T^2} + \frac{2}{\omega_T} s + 1 \right)} \quad (2.4)$$

where $T_\alpha = \frac{L}{C_T}$, $\omega_T = \frac{1}{L} \sqrt{\frac{12F}{\mu}}$, and α_x denotes the cable angle due to LSV motion.

The upper cable angle α is affected by another type of transient dynamics, however, which can be neglected in the displacement sensing concept but should be considered here.

- Downward Wave Propagation - Transversal waves of this type are generated whenever the trolley is accelerated ($\ddot{\xi} \neq 0$). Their effect on α can be expressed as

$$\alpha = \alpha_x + \alpha_\xi \quad (2.5)$$

where α_ξ is the contribution due to trolley motions. For a trolley accelerated at time t_0 we obtain for the time interval $t_0 < t < t_0 + T_\alpha$

$$\alpha_\xi(t) = - \frac{\int_{t_0}^t \ddot{\xi} dt}{C_T(t - t_0)} \quad (2.6)$$

Assuming $\ddot{\xi} \approx \text{constant}$ during T_α seconds, Equation (2.6) reduces to

$$\text{Max. } \alpha_\xi \approx - \frac{\ddot{\xi}}{2C_T} T_\alpha \quad (2.7)$$

During the time interval Equation (2.7) is valid, α_ξ can rise to values between 0.12° for 50 ft rail height to 0.4° for 170 ft rail height.

In order to clarify the effects of the cable dynamics on the overall trolley drive system response, a typical test case shall be considered in subsequent intervals.

LSV Step Disturbance $\ddot{X}(0)$

$$0 < t < T_\alpha :$$

During this first time interval Equation (2.4) applies. Due to the time delay T_α , α is zero as shown in Figure 2.8a. At time T_α (Figure 2.8b) there is a sudden feedback signal due to $\dot{\alpha} > 0$ and $\alpha > 0$ which results in a trolley acceleration $\ddot{\xi} > 0$ and a downward type transverse cable wave. The upper cable angle at time T_α is

$$\alpha(T_\alpha) = \alpha_x = \frac{x - \xi}{L}$$

and after T_α reduces according to Equations (2.5) and (2.6) to

$$\alpha(T_\alpha + \Delta t) = \alpha_x - \left| \alpha_\xi \right| .$$

The α and $\dot{\alpha}$ feedback signals reduce the trolley acceleration between the time T_α and $2T_\alpha$. After $2T_\alpha$ the cable motion may be approximated by a decaying α -oscillation of the transverse mode. This indicates that the downward type of transverse cable waves have a very unfavorable effect on the servosystem as they help in exciting the transverse mode of cable oscillations and further increase the effective time-delay in addition to the delay of T_α caused by the upward type of wave.

For an approximate evaluation of the overall system, however, the downward wave dynamics may be neglected. This results in the Signal-Flow Chart of Figure 2.9.

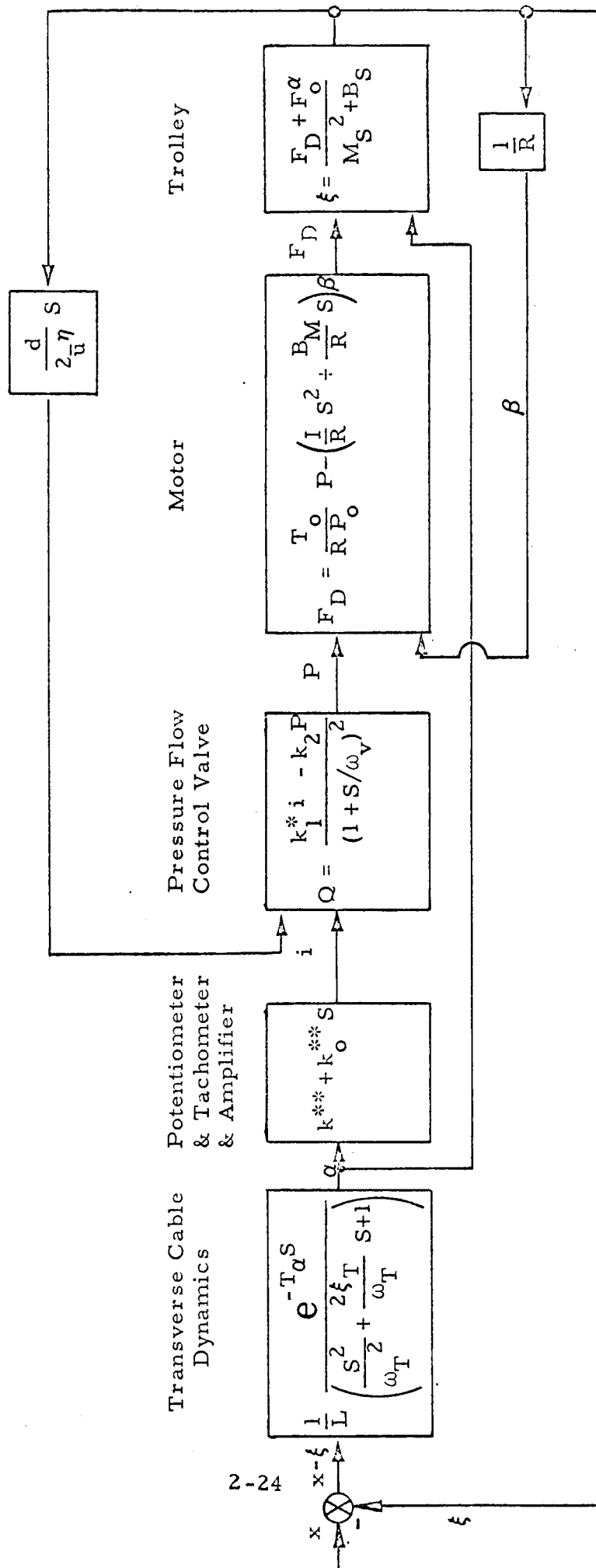


Figure 2.9 - Approximate Signal Flow Chart of Trolley Positioning Control System with Cable Angle Sensing

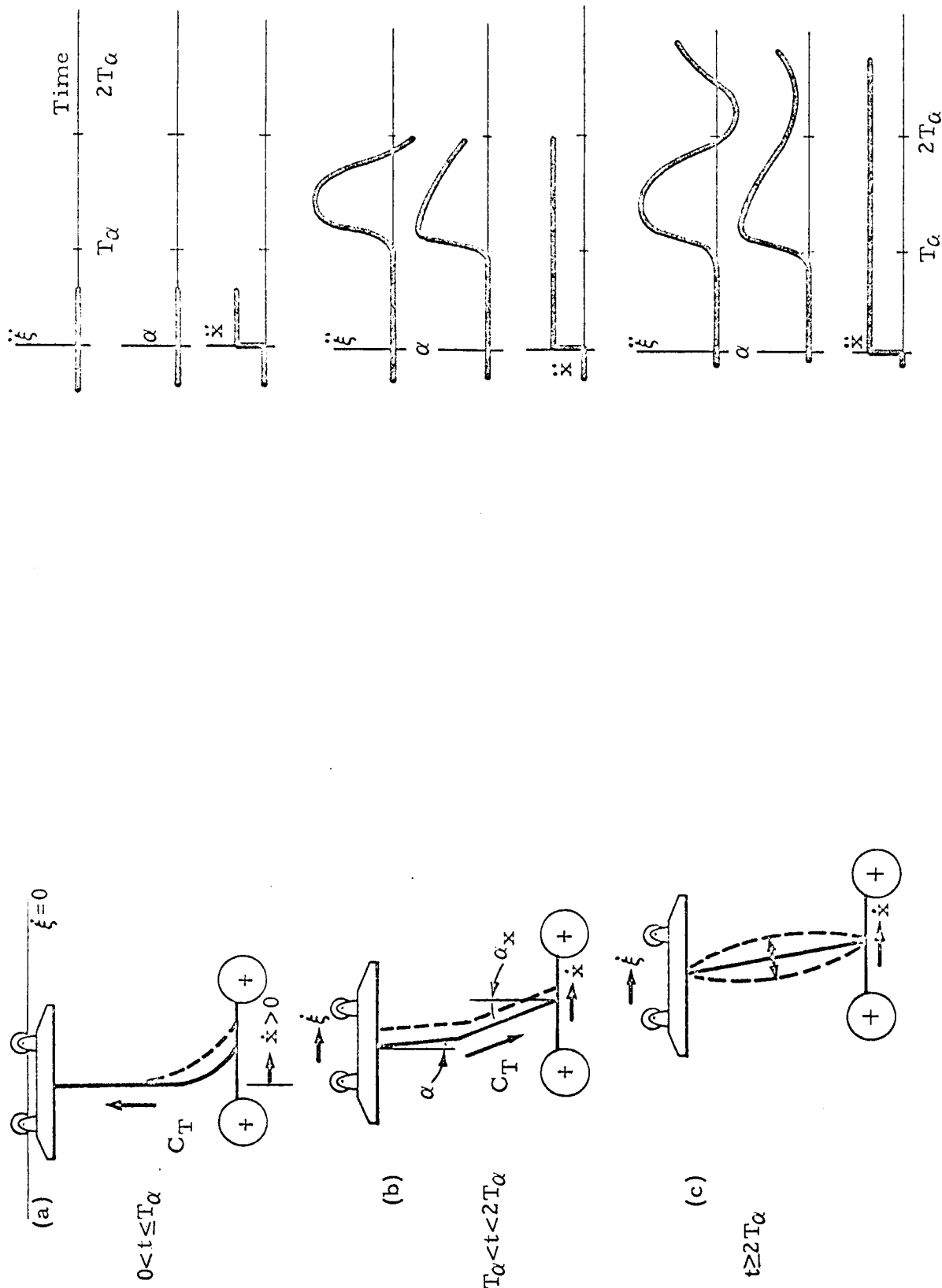


Figure 2.8 - Effects of Upward and Downward Type Transverse Cable Waves on the Trolley Drive with Angle Sensor

2.3.2 Comparison: Angle Sensing vs Displacement Sensing Concept

Comparing the flow charts of the two concepts (Figures 2.4 and 2.9) reveals that virtually all feedback signals are delayed by at least T_Q seconds in the angle sensing concept and contaminated by a certain amount of noise due to transverse cable oscillations. The time delay can be as high as 0.18 seconds for 170 ft rail height.

Considering the additional deterioration of performance due to the downward type cable waves discussed earlier the cable sensing concept was excluded from a further dynamic analysis. The cost advantage over the displacement sensing configuration was not considered large enough to justify the appreciable deterioration in performance predicted.

2.3.3 Optical Displacement Sensor

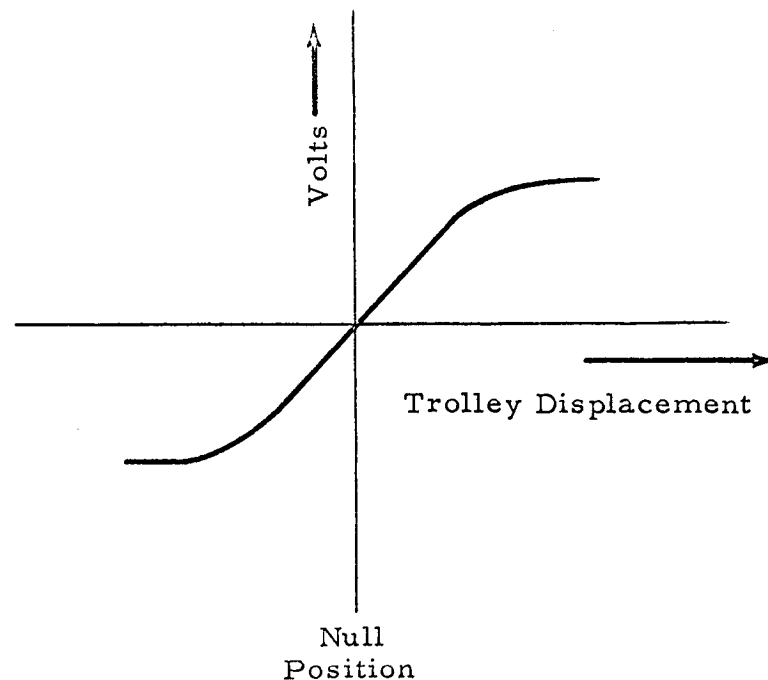
Optical determination of the position of the trolley relative to the LSV has been examined. Electro-Mechanical Research, Inc. and Perkin Elmer Corp. were consulted. The following is a summary of the investigation of optical tracking for the two-dimensional LGS:

A multiplier phototube type star tracking instrument mounted on the trolley will be used to track a hemispherical diffuse light source mounted along the LSV pitch axis. The tracker and associated trolley drive system will be designed to maintain the trolley mounted instrument directly above (within $2/3^\circ$ fore or aft from the vertical) the LSV mounted light source. The instrument will have a field of view of approximately 4° to allow for:

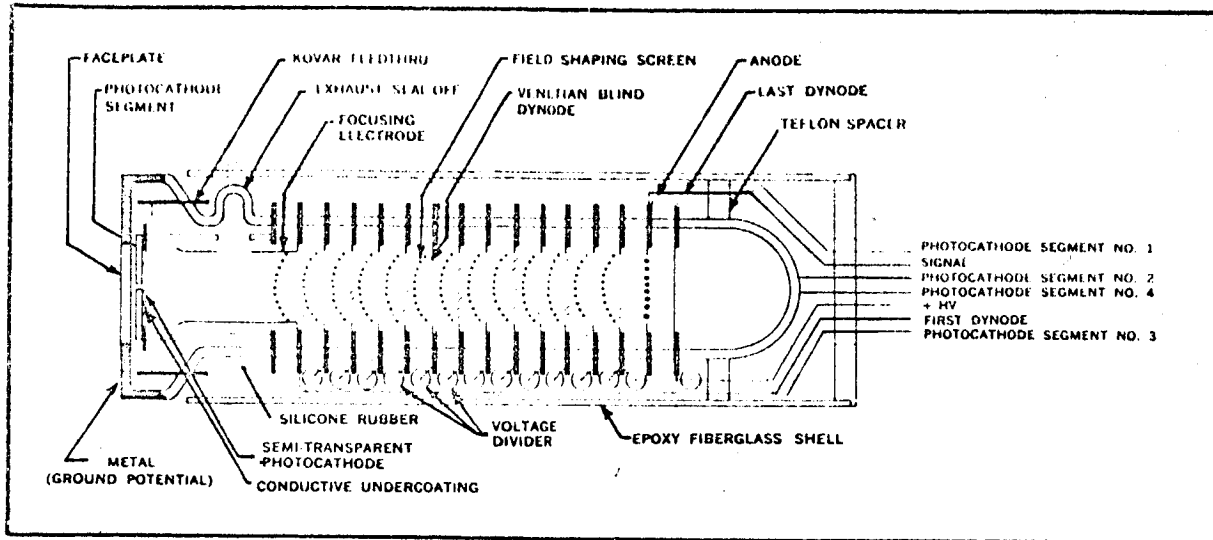
- a. initial acquisition of LSV light source
- b. larger than expected transient displacements
- c. lateral displacement due to roll motion.

The star tracker will be able to respond to a LSV frequency as great as 10 hertz. It will provide measurements of rate of relative displacement as well as relative displacement between the LSV and trolley. Automatic gain control is required to provide a constant gain which is independent of vertical separation between light source and light sensor.

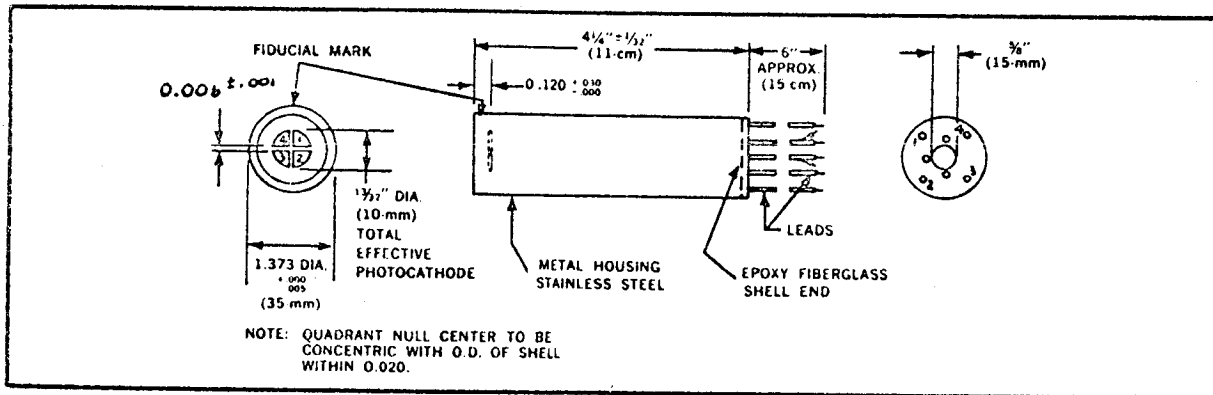
Figure 2.10 illustrates a typical multiplier phototube which can be employed as a tracking instrument. The cathode of the tube has been physically cut into four quadrants to provide null information along two axes. For two-dimensional simulation, a cathode which has been halved instead of quartered will provide sufficient tracking information along the one axis of translational motion. The output of the tracking instrument will be of the following form:



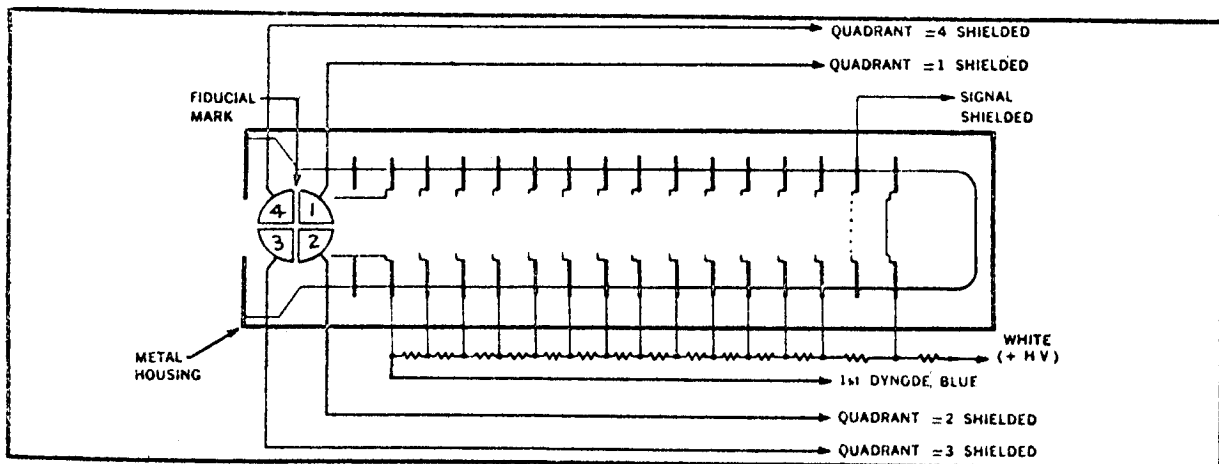
This displacement voltage can be differentiated to provide rate of displacement information.



FUNCTIONAL DIAGRAM



OUTLINE DRAWING



SCHEMATIC DRAWING

Resistor values are equal throughout.

Figure 2.10 - Multiplier Phototube Diagrams (Reference Electro-Mechanical Research, Inc., MODEL 571A-01-14, Specification April 1966)

If the LSV is allowed to roll about its wheels, the LSV mounted light source will be displaced laterally out of the star tracker field of view. Therefore, the LSV must be restricted to roll only about its c.g. This can be accomplished by proper design of the two-dimensional terrain such that the lateral LSV c.g. displacement is limited to the field of view of the tracker unit.

Section 3

VARIATION OF STATIC ERRORS
WITH CABLE LENGTH AND LSV PITCH ANGLES

If the points of attachment between the LSV support cables and trolley are fixed and the distance between these points and the LSV is less than approximately 30 to 50 feet, static longitudinal force errors become significant when the LSV goes through pitch and roll modes. In this study both four wheel and tractor-trailer LSV/trolley configurations are examined in order to quantitatively determine force errors for different cable lengths and various pitch angles.

3.1 NON-VERTICAL WHEEL SUPPORT CABLES FOR FOUR-WHEEL
VEHICLE

In order to minimize force errors due to pitch, the chassis of four-wheel vehicles (example: Bendix MOLAB) should be supported by a single cable at the vehicle c.g. or by two cables along the pitch axis equidistant from the c.g. (see Figure 3.1). If relative trolley movement with respect to the LSV c.g. is minimized, the chassis support cable(s) will remain vertical independently of the LSV pitch angle. Therefore, zero static force error will be exerted on the LSV through the main chassis support cable(s). However, errors will arise due to the non-vertical wheel support cables.

If the main chassis support cable(s) are maintained vertical, fixed trolley attachment points ensure non-vertical wheel support cables (see Figure 3.1) as the LSV goes through pitch movements. Parametric curves for several pitch angles comparing longitudinal error to cable length (distance from trolley attachment point to LSV attachment point) are provided in Figure 3.2. Vertical errors, $(1.0 - \cos\eta) \times \text{wheel weight/vehicle}$

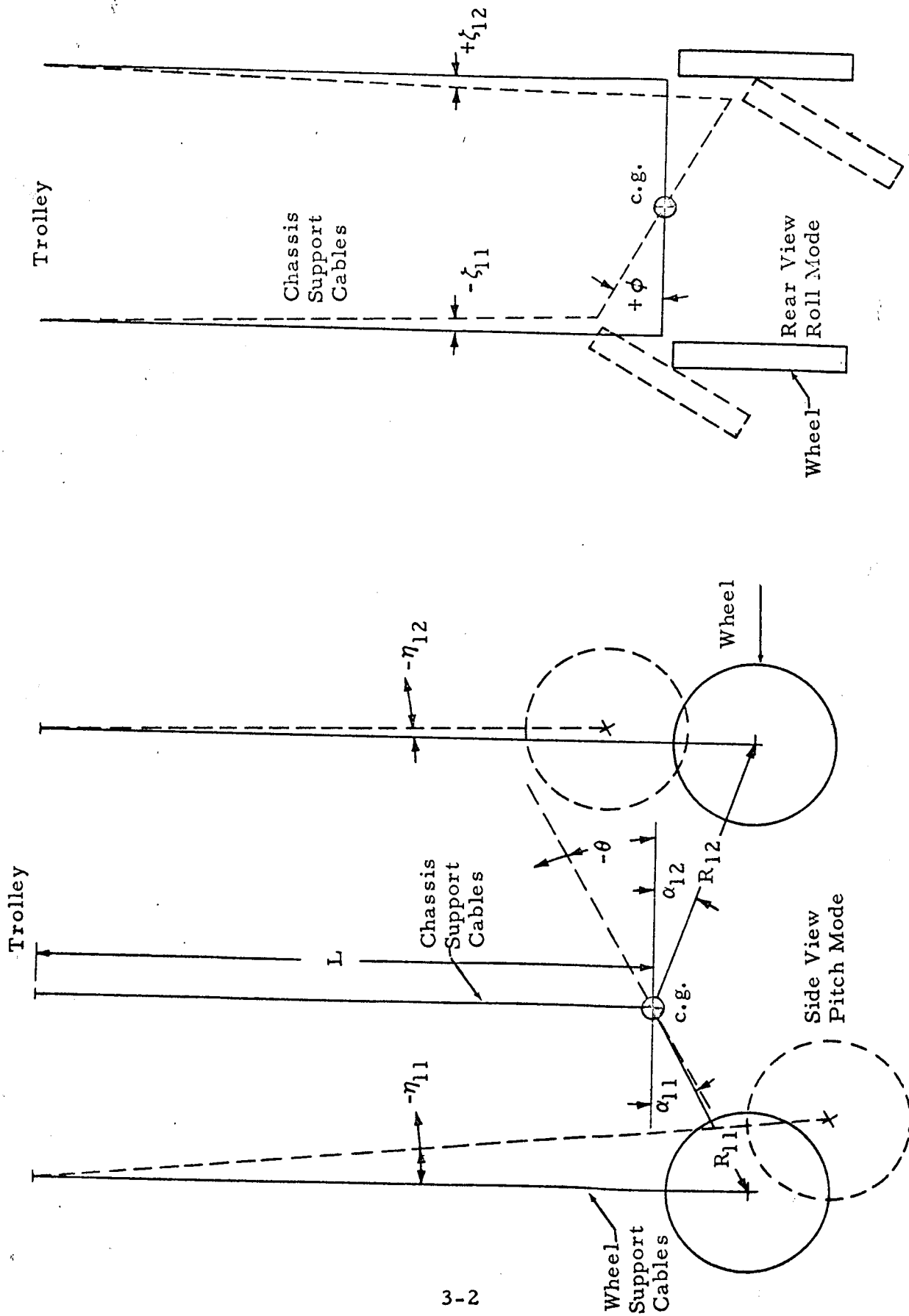


Figure 3.1 - Four-Wheel Vehicle Suspension System

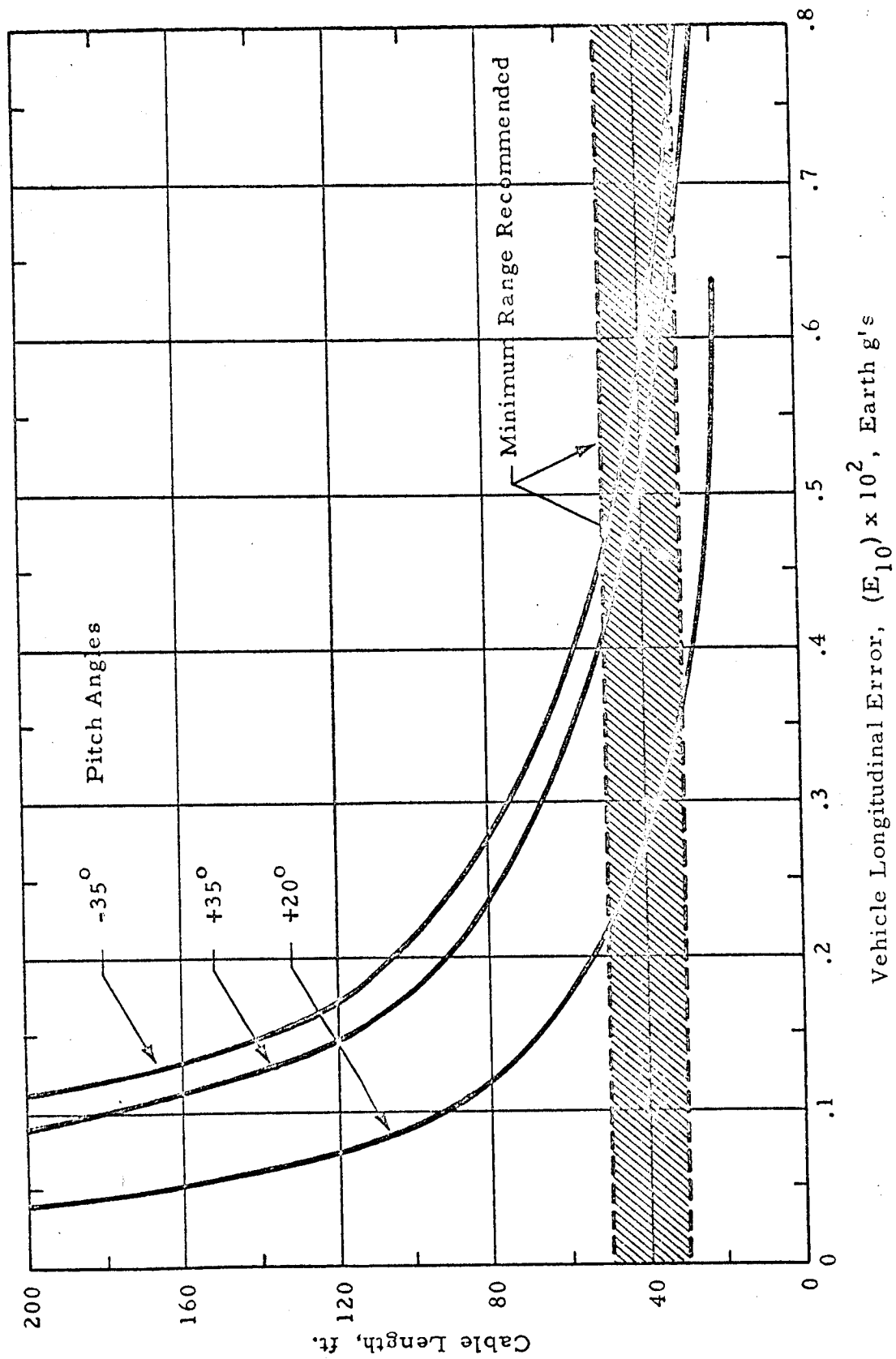


Figure 3.2 - Vehicle Static Longitudinal Error from Wheel Suspension System

weight, are insignificant in comparison with the vehicle longitudinal errors. Analysis of these curves indicates cable length should not be less than 30 to 50 feet for acceptable error.

3.2 ROLL ANGLE VARIATIONS

Error present because of non-vertical chassis support cables in the roll mode (assuming 2 cables used) is depicted in Figure 3.2. Since the two support cables are attached along the pitch axis equidistant from the LSV c.g. and trolley motion relative to the LSV c.g. is minimized, the horizontal static force errors in the chassis support cables due to roll motion are of opposite signs and the net error is negligible. A worst-case of 35° roll angle and 40 foot cable length was calculated to be approximately .001 g (Earth) net longitudinal error. The wheel support cable longitudinal error in the roll mode is even less significant since the nominal forces in these cables are much less than in the main chassis support cables.

If the LSV rolls with its pivot point at the wheels instead of at its c.g., the angular displacement of the cables becomes large and the corresponding lateral force error becomes intolerable in the two dimensional LGS. All roll motions should therefore be made with the LSV pivoting about its c.g. This can be accomplished by proper design of the terrain along the LSV path.

3.3 METHOD OF ANALYSIS - FOUR WHEEL VEHICLE WITH PITCH ANGLE VARIATIONS

The vehicle static longitudinal error due to the wheel suspension system, E_{10} is found by summing the static cable force errors parallel to the terrain, F_{51} and F_{52}^* , and dividing by the total LSV weight. The nomenclature for this analysis is defined in Table 3.1.

$$E_{10} = \frac{2F_{51} + 2F_{52}}{\text{total LSV weight}}$$

*The Bendix MOLAB, a four-wheel vehicle, was used in this example. If a six-wheel vehicle were used, F_{33} would be present also.

Table 3.1
FOUR WHEEL VEHICLE ANALYSIS
Nomenclature

L , ft (m)	length of cable from trolley to LSV
θ , deg	pitch angle
R_{11}, α_{11} , ft(m), deg R_{12}, α_{12} , ft(m), deg	} coordinates of wheels referenced to LSV c.g.*
η_{11}, η_{12} deg	
$F_{11\omega}, F_{12\omega}$ lb (newton)	nominal tension in wheel support cables
F_{21}, F_{22} lb (newton)	static vertical error in cable tension
F_{31}, F_{32} lb (newton)	nominal cable force directed parallel to the terrain (i.e., in direction of θ)
F_{41}, F_{42} lb (newton)	actual cable force directed parallel to the terrain
F_{51}, F_{52} lb (newton)	static error in cable force parallel to the terrain
E_{10} earth g's	net static error in cable force parallel to the terrain divided by LSV weight
ζ_{11}, ζ_{12} deg	wheel support cable angles referenced to the vertical (roll mode)
ϕ	roll angle

* Second subscript refers to front (1) or rear (2) of LSV

The individual static errors in cable forces parallel to the terrain, F_{51} and F_{52} , are the differences between the nominal cable forces directed parallel to the terrain, F_{31} and F_{32} , and the actual cable forces directed parallel to the terrain, F_{41} and F_{42} .

$$F_{51} = F_{31} - F_{41}, \quad F_{52} = F_{32} - F_{42}$$

where F_{31} , F_{32} , F_{41} and F_{42} are functions of LSV pitch, θ , cable angles η_{11} and η_{12} , and nominal cable tensions, $F_{11\omega}$ and $F_{12\omega}$.

$$\begin{aligned} F_{31} &= F_{11\omega} \sin \theta, & F_{32} &= F_{12\omega} \sin \theta \\ F_{41} &= F_{11\omega} \sin(\theta - \eta_{11}), & F_{42} &= F_{12\omega} \sin(\theta - \eta_{12}) \end{aligned}$$

$F_{11\omega}$ and $F_{12\omega}$ are simply the wheel masses multiplied by the fraction of the vehicles weight supported by the LGS, i.e.,

$$\begin{aligned} F_{11\omega} &= \text{front wheel mass} \times 5/6 \text{ g} \\ F_{12\omega} &= \text{rear wheel mass} \times 5/6 \text{ g} \end{aligned}$$

The cable angles, η_{11} and η_{12} , are geometric functions of LSV pitch, θ , cable length L , and cable attachment point coordinates, R_{11} , R_{12} , α_{11} , and α_{12} ,

$$\begin{aligned} \eta_{11} &= \arctan \left\{ \frac{-\cos \alpha_{11} + \cos \alpha_{11} \cos \theta + \sin \alpha_{11} \sin \theta}{L/R_{11} + \sin \alpha_{11} \cos \theta - \cos \alpha_{11} \sin \theta} \right\} \\ \eta_{12} &= \arctan \left\{ \frac{\cos \alpha_{12} - \cos \alpha_{12} \cos \theta + \sin \alpha_{12} \sin \theta}{L/R_{12} + \sin \alpha_{12} \cos \theta + \cos \alpha_{12} \sin \theta} \right\} \end{aligned}$$

3.4 NON-VERTICAL CHASSIS SUPPORT CABLES FOR TRACTOR-TRAILER VEHICLE

Since the tractor and trailer chassis of vehicles such as the Boeing MOLAB are supported by separate cables, it is impossible to pick a single

relative position between the trolley and LSV which will maintain all chassis support cables vertical through all LSV pitch angles. On first try it was assumed that the relative position between the trolley and tractor-trailer pivot point would be fixed. The parallel errors were analyzed and found to be intolerable.

A trade-off study was made to determine the best point on the LSV to hold fixed relative to the trolley. This point was found to be located near the composite c.g. of the LSV (Figure 3.3). If the movement of this point relative to the trolley is minimized, the tractor and trailer support cable errors due to LSV pitch subtract from each other such that the net error is relatively small. Figure 3.4 depicts parametric curves with tractor-trailer pivot neglected. Again the minimum cable length can be chosen for acceptable longitudinal errors.

Further study is proposed for deeper analysis of tractor-trailer LSV/trolley configurations. The errors due to wheel support cable angles, although less significant than chassis support cable errors, should be analyzed. Roll errors should also be considered, and errors involved with pivoting between trailer and tractor should be examined.

3.5 METHOD OF ANALYSIS - TRACTOR-TRAILER VEHICLE WITH PITCH ANGLE VARIATIONS

Assume that two cables under equal tension support the tractor along its pitch axis and two more equal tension cables support the trailer* along its pitch axis. Under this assumption equations derived for the four-wheel LSV wheel suspension system can be easily converted to determine the static longitudinal error for the tractor-trailer chassis suspension system. The second subscript now refers to the tractor (1) or the trailer (2) rather than to front wheels (1) or rear wheels (2). The following additions and

*Actually only one cable is planned to support the trailer chassis but this assumption will not effect the results of this analysis.

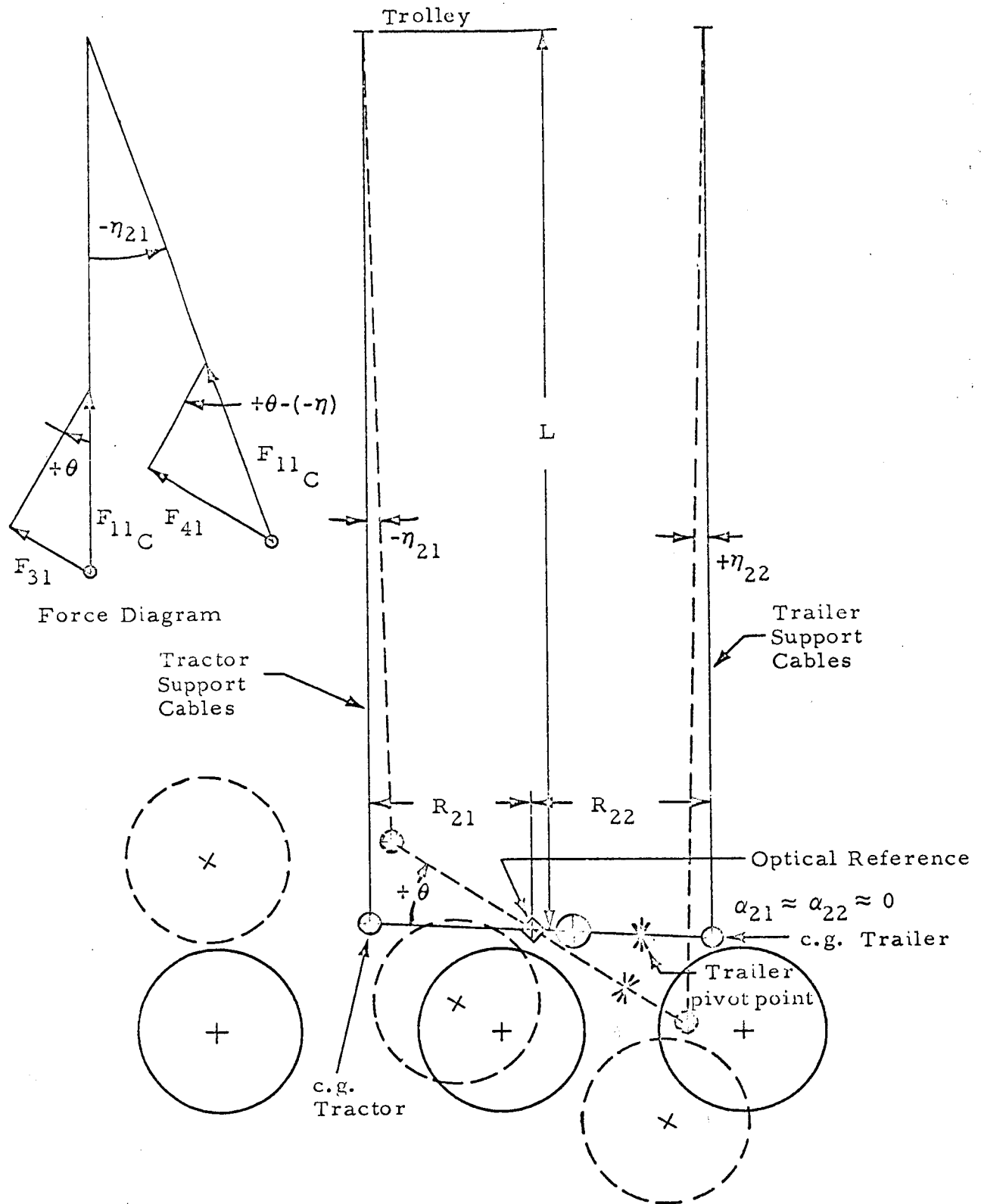


Figure 3.3 - Tractor-Trailer Chassis Support System

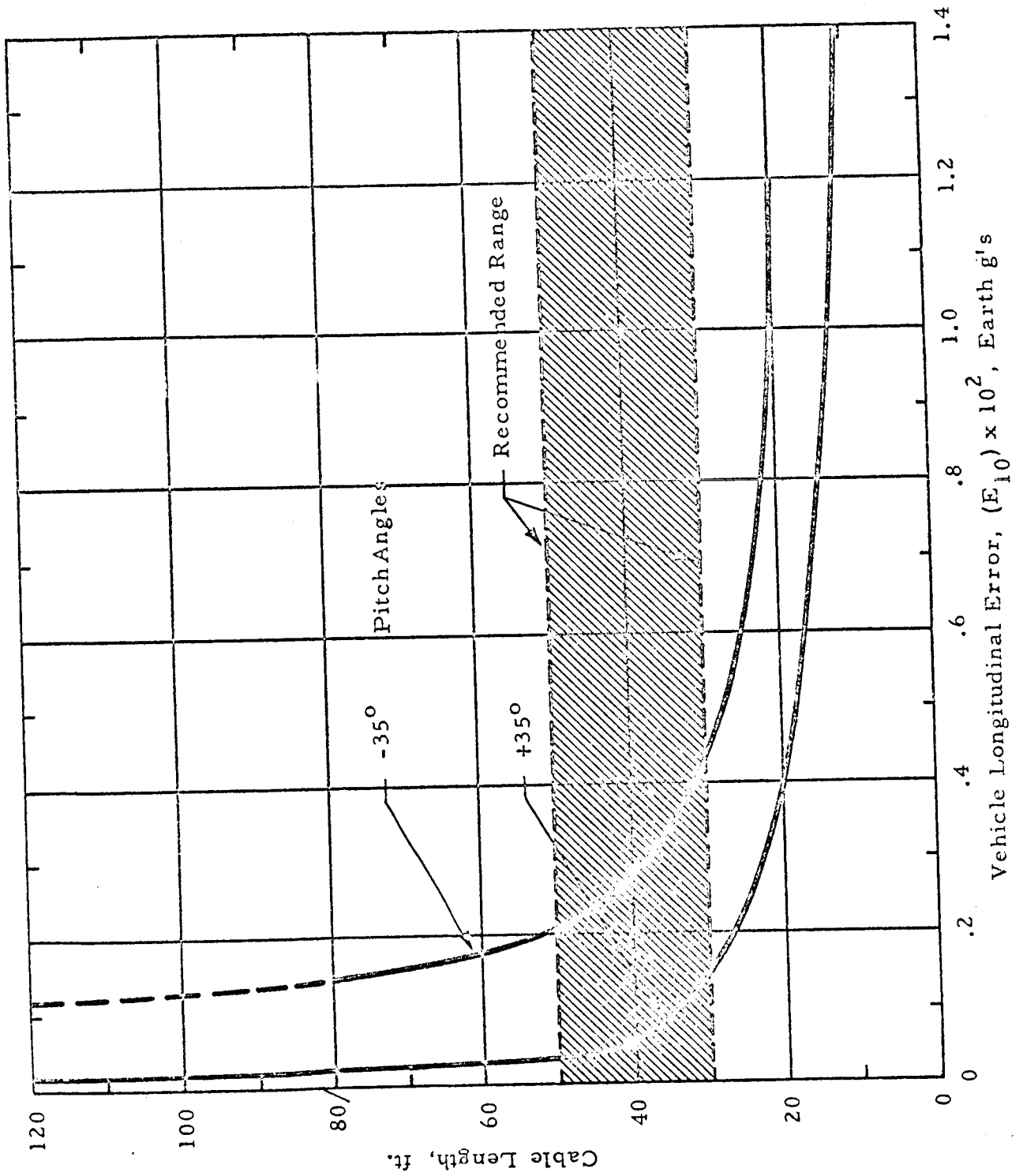


Figure 3.4 - Vehicle Static Longitudinal Error for Tractor-Trailer Chassis Suspension System

modifications are made to the original equations:

Vehicle static longitudinal errors, E_{21} , E_{22} , can be found individually for the tractor or trailer chassis support.

$$E_{21} = (2 F_{51} \div \text{total LSV weight})$$

$$E_{22} = (2 F_{52} \div \text{total LSV weight})$$

The static compression or tension, F_{60} , in the joint between the tractor and trailer is found by:

- Taking the smaller of F_{51} and F_{52} if their signs are different.
- Taking the difference of F_{51} and F_{52} if their signs are the same.

Nominal tensions in chassis support cables, F_{11C} and F_{12C} , replace $F_{11\omega}$ and $F_{12\omega}$ where

$$F_{11C} = \frac{\text{tractor mass}}{2} \times 5/6 \text{ g}$$

$$F_{12C} = \frac{\text{trailer mass}}{2} \times 5/6 \text{ g}$$

Cable angles, η_{21} and η_{22} , replace η_{11} and η_{12} where:

$$\eta_{21} = \arctan \left\{ \frac{-\cos\alpha_{21} + \cos\alpha_{21} \cos\theta - \sin\alpha_{21} \sin\theta}{L/R_{21} - \sin\alpha_{21} \cos\theta - \cos\alpha_{21} \sin\theta} \right\}$$

$$\eta_{22} = \arctan \left\{ \frac{\cos\alpha_{22} - \cos\alpha_{22} \cos\theta - \sin\alpha_{22} \sin\theta}{L/R_{22} - \sin\alpha_{22} \cos\theta + \cos\alpha_{22} \sin\theta} \right\}$$

The nomenclature for the above terms are defined in Table 3.2 and the configuration is illustrated in Figure 3.3.

Table 3.2
TRACTOR-TRAILER VEHICLE ANALYSIS

Nomenclature

$\theta, F_{21}, F_{22}, F_{31}, F_{32}, F_{41},$ $F_{42}, F_{51}, F_{52}, E_{10},$	same as for Bendix Configuration except: second subscript refers to tractor (1) or trailer (2) of LSV
R_{21}, α_{21} ft (m), deg } R_{22}, α_{22} ft (m), deg }	coordinates of main tractor and trailer cable supports with respect to mounting point of optical reference
η_{21}, η_{22} deg	main support cable angles referenced to the vertical
F_{11_C}, F_{12_C} lb (newton)	nominal tension in chassis support cables
F_{60} lb (newton)	static compression or tension between tractor and trailer
E_{21}, E_{22} earth g's	static error in cable force parallel to the terrain divided by LSV weight

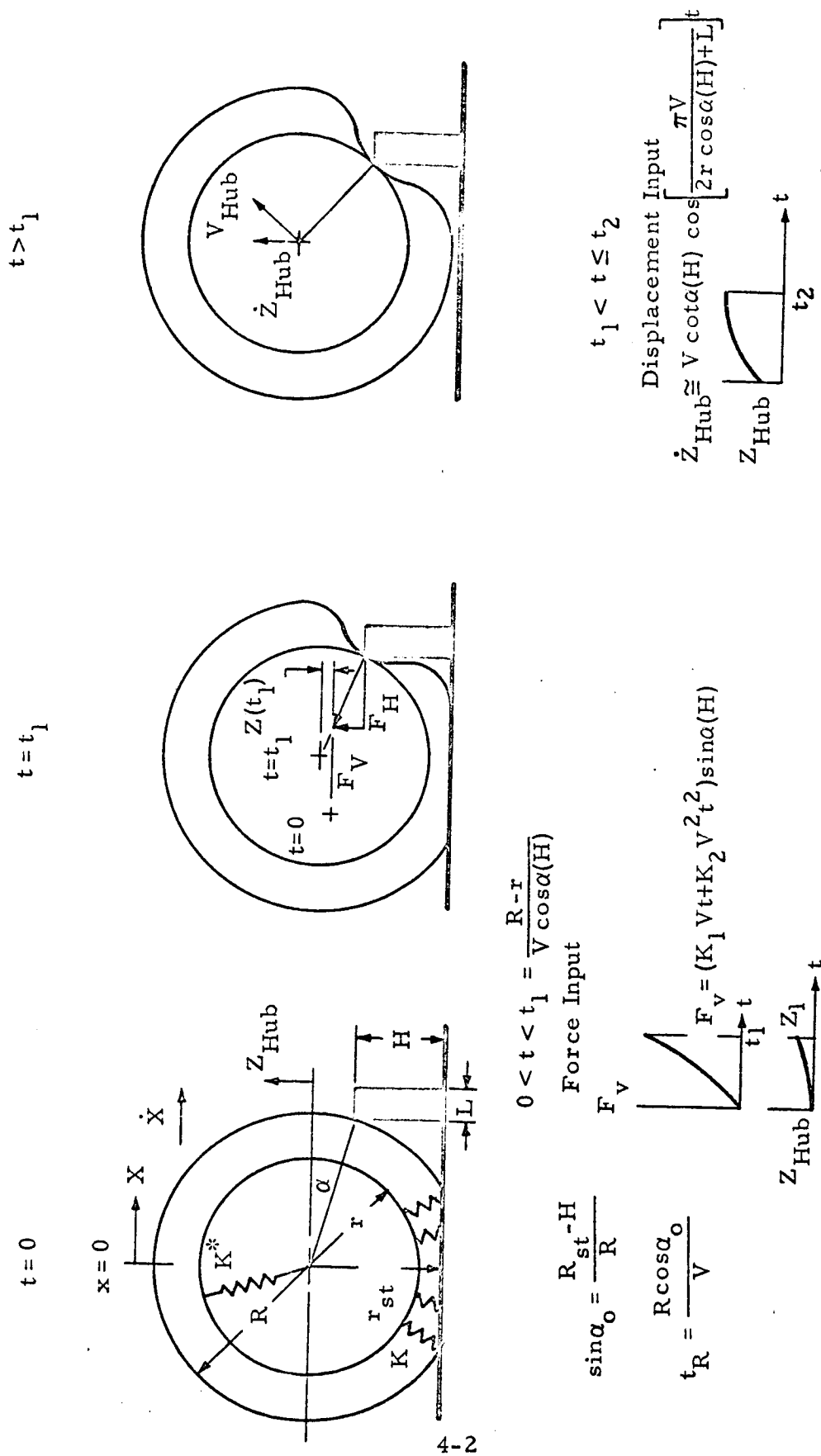


Figure 4.1 - Rolling Wheel Obstacle Simulation

Section 4

DYNAMIC ANALYSIS OF THE 2-D LUNAR GRAVITY SIMULATOR

4.1 OBSTACLE SIMULATION

Wheel input disturbances occurring from the LSV transversing a simulated lunar terrain produce the major dynamic problems for the 1/6g simulation. Thus, a realistic appraisal of these disturbances has been an important part of the dynamic analysis of the 2-D LGS system. Previous recommendations for obstacle simulations were described in the First Interim Report (Reference 1), and this simulation method was investigated further during this reporting period. The two phases involved in this simulation are illustrated in Figure 4.1 (repeated from Reference 1). These phases are:

Phase 1 ($0 < t < t_1$) - A force input from touching the obstacle at $t = 0$ until the outer wheel springs or the tire bottoms on the inner wheel frame.

Phase 2 ($t > t_1$) - Sinusoidal wheel hub displacement after bottoming of tire.

From further study of this simulation it was found that this method resulted in a complex input for the analog simulation and would have compromised the amount of data which could be developed in the time allotted. Further, it was felt that this simulation represented a worst case situation (sharp edge obstacle) and may not be representative of the normal obstacles anticipated (round or oval shaped objects). Accordingly a more simplified obstacle simulation was derived to be used in the analog simulation.

The simplified obstacle simulation considered a constant vertical velocity input to the bottom of the tire at the ground line. Displacement of the ground line point would proceed until a given obstacle height (H) is

reached, or until the wheel breaks ground due to the forces produced in this time interval. The time interval was determined from the vehicle forward velocity (\dot{X}), the wheel radius, and the obstacle height. Thus, from Figure 4.1, the obstacle time interval may be

$$t_{ob} = \frac{R \cos \alpha_o}{\dot{X}}$$

where:

α_o = obstacle/wheel contact angle at $t = 0$.

$$= \sin^{-1} \frac{r_{st} - H}{R}$$

Additionally, the simplified obstacle may be extended at a constant height for a time interval L_{ob}/\dot{X} and then return to the original ground line height at a rate corresponding to the rise rate ($-H/t_{ob}$). Typical groundline displacement-time characteristics for the simplified obstacle simulation are illustrated in Figure 4.2. The obstacle shown is for the LSSM at maximum velocity (9.0 km/hr) and a 1.0 ft obstacle. Also, a comparison of resulting wheel hub displacement and velocity characteristics is illustrated for the LSSM. Note that the peak wheel hub velocity and displacement for the rolling obstacle is slightly over twice that for the simplified obstacle. The simplified obstacle was considered to more nearly approximate the average obstacle condition and was used in the analog simulations described in the following sections.

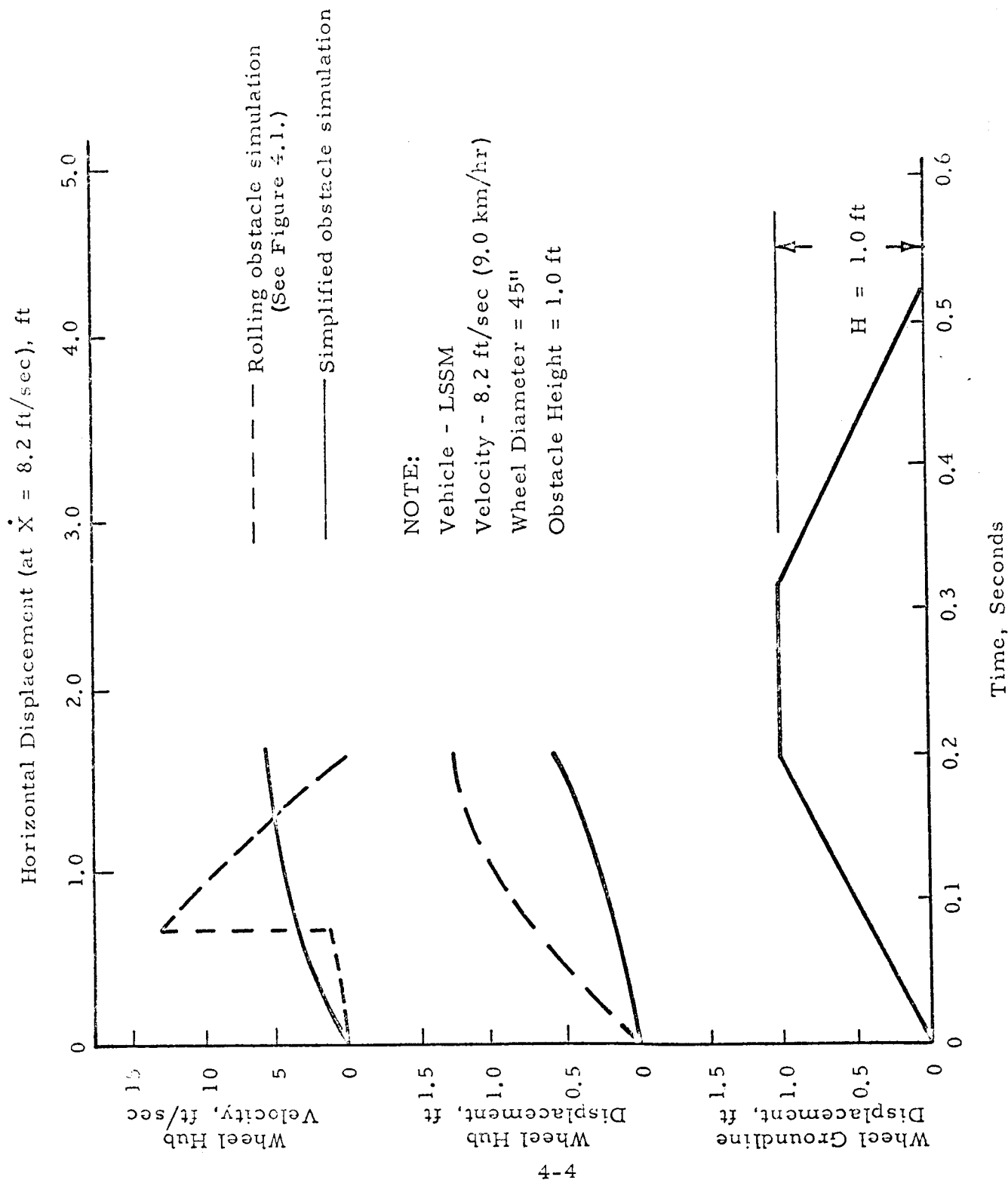


Figure 4.2 - Simplified Obstacle Simulation

4.2 SUSPENSION DEVICE FORCE CONTROL SYSTEM SIMULATION

4.2.1 Analog Simulation

The analog computer mathematical model for the LGS/LSV system were two-dimensional planar models for the roll and pitch directions. Typical model diagrams are shown in Figure 4.3 and 4.4. Note the provisions for a two-stage spring constant in each wheel and the viscous damped suspensions take into consideration a free flight ballistic trajectory if the wheels leave the ground. Also, note the sign conventions for the dimensions Z , ϕ and θ .

From Figure 4.3 the differential equations representing the vertical displacement time histories for each mass and the effects of roll and cable dynamics can be derived giving results as follows.

$$\ddot{Z}_1 = \frac{D_6}{M_1} (\dot{Z}_8 - \dot{Z}_1) + \frac{K_6}{M_1} (Z_8 - Z_1) - \frac{(K_1 + K_{11})}{M_1} (Z_1 - Z_{01}) - g_L \\ + \frac{F_{018}}{M_1} f_{18}$$

where

$$\text{Constraint: } |Z_8 - Z_1| \leq S$$

$$-S < (Z_1 - Z_{01}) < 0$$

$$K_1 = > 0 \quad K_{11} = 0$$

$$(Z_1 - Z_{01}) \leq -S_1$$

$$K_1 = > 0 \quad K_{11} = > 0$$

$$(Z_1 - Z_{01}) > 0$$

$$K_1 = 0 \quad K_{11} = 0$$

$$\ddot{Z}_2 = \frac{D_3}{M_2} (\dot{Z}_9 - \dot{Z}_2) + \frac{K_3}{M_2} (Z_9 - Z_2) - \left(\frac{K_2 + K_{22}}{M_2} \right) (Z_2 - Z_{02}) - g_L \\ + \frac{F_{019}}{M_2} f_{19}$$

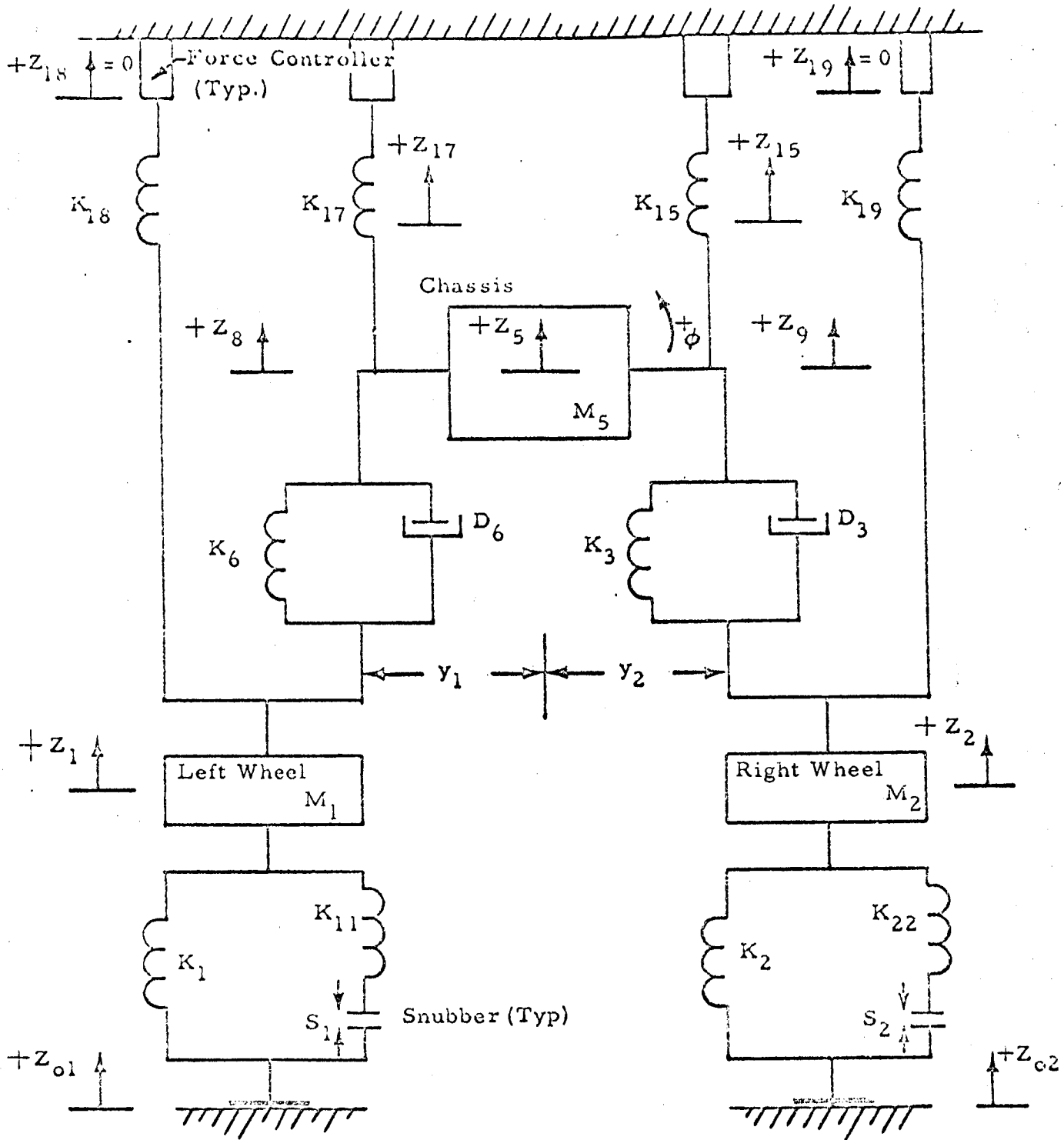


Figure 4.3 - Lunar Gravity Simulator Analog Simulation Diagram (Roll Configuration)

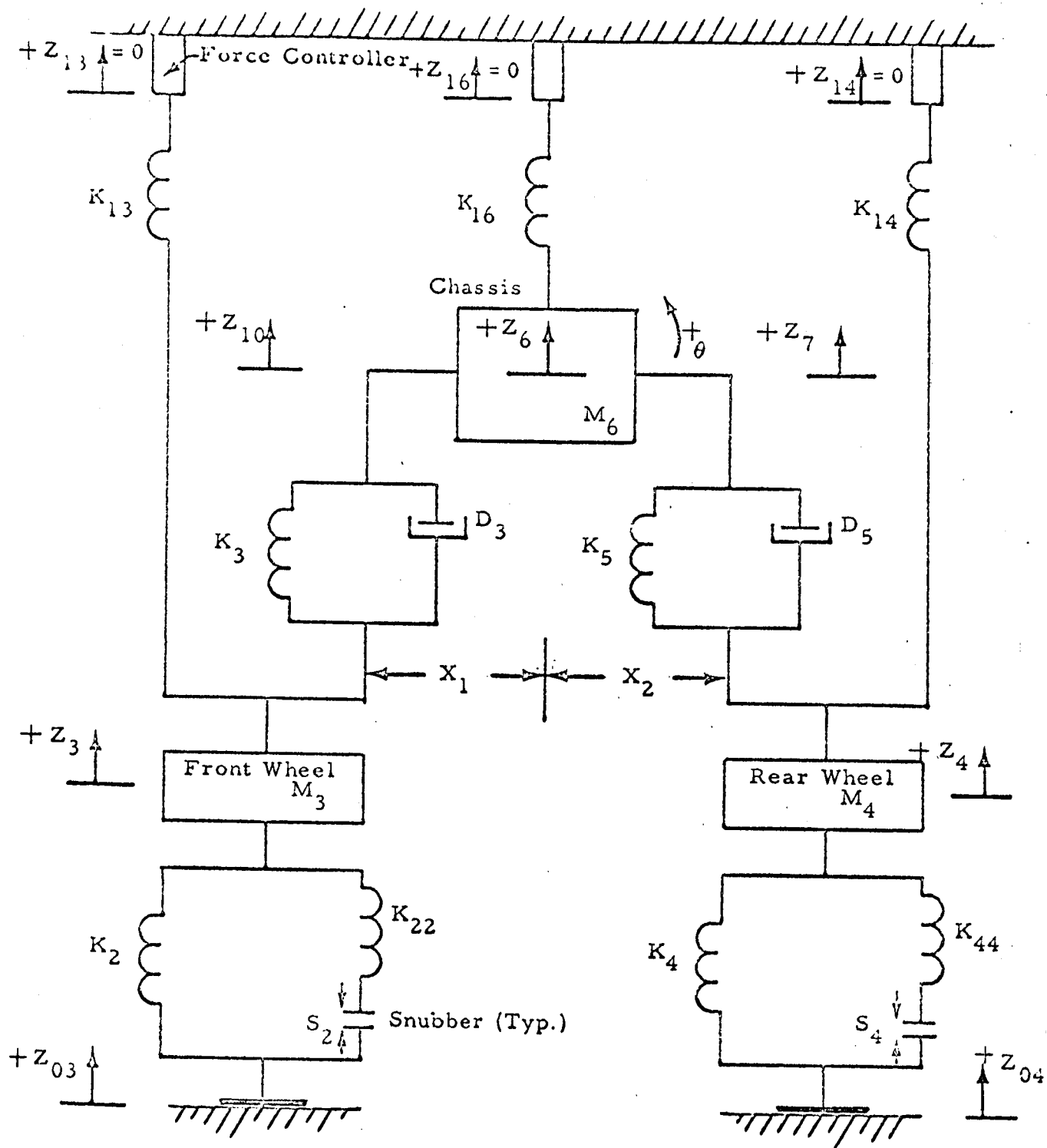


Figure 4.4 - Lunar Gravity Simulator Analog Simulation Diagram (Pitch Configuration)

where

$$\text{Constraint: } |Z_9 - Z_2| \leq S$$

$$-S_2 < (Z_2 - Z_{02}) < 0$$

$$K_2 = > 0$$

$$K_{22} = 0$$

$$(Z_2 - Z_{02}) \leq -S_2$$

$$K_2 = > 0$$

$$K_{22} = > 0$$

$$(Z_2 - Z_{02}) > 0$$

$$K_2 = 0$$

$$K_{22} = 0$$

$$\begin{aligned} \ddot{Z}_5 = & -\frac{D_6}{M_5} (\dot{Z}_8 - \dot{Z}_1) - \frac{K_6}{M_5} (Z_8 - Z_1) - \frac{D_3}{M_5} (\dot{Z}_9 - \dot{Z}_2) - \frac{K_3}{M_5} (Z_9 - Z_2) - g_L \\ & + \frac{F_{015}}{M_5} f_{15} + \frac{F_{017}}{M_5} f_{17} \end{aligned}$$

where:

$$\text{Constraints: } |Z_9 - Z_2| \leq S$$

$$|Z_8 - Z_1| \leq S$$

$$\begin{aligned} \ddot{\phi} = & \frac{y_1}{I_X} \left[K_6 (\dot{Z}_8 - \dot{Z}_1) + D_6 (Z_8 - Z_1) \right] - \frac{y_2}{I_X} \left[K_3 (Z_9 - Z_2) + D_3 (\dot{Z}_9 - \dot{Z}_2) \right] \\ & + \frac{F_{015}}{I_X} f_{15} - \frac{F_{017} y_3}{I_X} f_{17} \end{aligned}$$

$$Z_8 = Z_5 - y_1 \phi$$

$$\dot{Z}_8 = \dot{Z}_5 - y_1 \dot{\phi}$$

$$Z_9 = Z_5 + y_2 \phi$$

$$\dot{Z}_9 = \dot{Z}_5 + y_2 \dot{\phi}$$

$$\dot{Z}_{15} = \dot{Z}_5 + y_4 \dot{\phi}$$

$$\dot{Z}_{17} = \dot{Z}_5 - y_3 \dot{\phi}$$

$$F_{o18} = 5/6 M_1 g_E$$

$$F_{o19} = 5/6 M_2 g_E$$

$$F_{o15} = 5/12 M_5 g_E$$

$$F_{o17} = 5/12 M_5 g_E$$

$$f_{18} = -\frac{K_{18}}{F_{o18}} \left[\frac{A_1 S^3 + A_2 S^2 + B_3 S + B_4}{A_1 S^4 + A_2 S^3 + A_3 S^2 + A_4 S + A_5} \right] \dot{Z}_1$$

$$f_{19} = -\frac{K_{19}}{F_{o19}} \left[\frac{A_1 S^3 + A_2 S^2 + B_3 S + B_4}{A_1 S^4 + A_2 S^3 + A_3 S^2 + A_4 S + A_5} \right] \dot{Z}_2$$

$$f_{15} = -\frac{K_{15}}{F_{o15}} \left[\frac{C_1 S^3 + C_2 S^2 + D_3 S + D_4}{C_1 S^4 + C_2 S^3 + C_3 S^2 + C_4 S + C_5} \right] \dot{Z}_{15}$$

$$f_{17} = -\frac{K_{17}}{F_{o17}} \left[\frac{C_1 S^3 + C_2 S^2 + D_3 S + D_4}{C_1 S^4 + C_2 S^3 + C_3 S^2 + C_4 S + C_5} \right] \dot{Z}_{17}$$

$$K_{18} = \frac{E \cdot A_{C19}}{L_{C18}}$$

$$E = 17.3 \times 10^8 \text{ lb/ft}^2$$

$$K_{19} = \frac{E \cdot A_{C19}}{L_{C19}}$$

A_C = Cable cross sectional area

L_C = Cable length

$$K_{15} = \frac{E \cdot A_{C15}}{L_{C15}}$$

$$K_{17} = \frac{E \cdot A_{C17}}{L_{C15}}$$

From Figure 4.4 the differential equation representing the vertical displacement time histories for each mass and the effects of pitch and cable dynamics can be derived giving results as follows:

$$\ddot{Z}_3 = \frac{D_3}{M_3} (\dot{Z}_{10} - \dot{Z}_3) + \frac{K_3}{M_3} (Z_{10} - Z_3) - \frac{(K_2 + K_{22})}{M_3} (Z_3 - Z_{03}) - g_L + \frac{F_{ol3}}{M_3} f_{13}$$

where:

$$\text{Constraint: } |Z_{10} - Z_3| \leq S$$

$$\begin{array}{lll} S_2 < (Z_3 - Z_{03}) < 0 & K_2 = > 0 & K_{22} = 0 \\ (Z_3 - Z_{03}) \leq S_2 & K_2 = > 0 & K_{22} = > 0 \\ (Z_3 - Z_{03}) > 0 & K_2 = 0 & K_{22} = 0 \end{array}$$

$$\ddot{Z}_4 = \frac{D_5}{M_4} (\dot{Z}_7 - \dot{Z}_4) + \frac{K_5}{M_4} (Z_7 - Z_4) - \frac{(K_4 + K_{44})}{M_4} (Z_4 - Z_{04}) - g_L + \frac{F_{ol4}}{M_4} f_{14}$$

where:

$$\text{Constraint: } |Z_7 - Z_4| \leq S$$

$$\begin{array}{lll} S_4 < (Z_4 - Z_{04}) < 0 & K_4 = > 0 & K_{44} = 0 \\ (Z_4 - Z_{04}) \leq S_4 & K_4 = > 0 & K_{44} = > 0 \\ (Z_4 - Z_{04}) > 0 & K_4 = 0 & K_{22} = 0 \end{array}$$

$$\ddot{Z}_6 = -\frac{D_5}{M_6} (\dot{Z}_7 - \dot{Z}_4) - \frac{K_5}{M_6} (Z_7 - Z_4) - \frac{D_3}{M_6} (\dot{Z}_{10} - \dot{Z}_3) - \frac{K_3}{M_6} (Z_{10} - Z_3)$$

$$- g_L + \frac{F_{ol6}}{M_6} f_{16}$$

$$\text{where: } |Z_7 - Z_4| \leq S \\ |Z_{10} - Z_3| \leq S$$

$$\ddot{\theta} = \frac{X_1}{I_y} \left[D_3 (\dot{Z}_{10} - \dot{Z}_3) + K_3 (Z_{10} - Z_3) \right] - \frac{X_2}{I_y} \left[D_5 (\dot{Z}_7 - \dot{Z}_4) + K_5 (Z_7 - Z_4) \right]$$

$$Z_7 = Z_6 + X_2 \theta$$

$$\dot{Z}_7 = \dot{Z}_6 + X_2 \dot{\theta}$$

$$Z_{10} = Z_6 + X_1 \theta$$

$$\dot{Z}_{10} = \dot{Z}_6 + X_1 \dot{\theta}$$

$$F_{o13} = 5/6 M_3 g_E$$

$$F_{o14} = 5/6 M_4 g_E$$

$$F_{o16} = 5/6 M_6 g_E$$

$$f_{13} = - \frac{K_{13}}{F_{o13}} \left[\frac{A_1 S^3 + A_2 S^2 + B_3 S + B_4}{A_1 S^4 + A_2 S^3 + A_3 S^2 + A_4 S + A_5} \right] \dot{Z}_3$$

$$f_{14} = - \frac{K_{14}}{F_{o14}} \left[\frac{A_1 S^3 + A_2 S^2 + B_3 S + B_4}{A_1 S^4 + A_2 S^3 + A_3 S^2 + A_4 S + A_5} \right] \dot{Z}_4$$

$$f_{16} = - \frac{K_{16}}{F_{o16}} \left[\frac{C_1 S^3 + C_2 S^2 + D_3 S + D_4}{C_1 S^4 + C_2 S^3 + C_3 S^2 + C_4 S + C_5} \right] \dot{Z}_6$$

$$K_{13} = \frac{E \cdot A_{C13}}{L_{C13}}$$

$$K_{14} = \frac{E \cdot A_{C14}}{L_{C14}}$$

$$K_{16} = \frac{E \cdot A_{C14}}{L_{C14}}$$

The previous equations for the LGS/LSV mathematical model have been programmed on the Lockheed/HREC analog computers. Reduced data are discussed in the following paragraphs of this report.

4.2.2 Force Control System Analog Simulation Results

Evaluation of the wheel and chassis force control system for the 2-D LGS was accomplished by perturbing simulated LSSM and MOLAB LSV's with a range of obstacle heights at the maximum horizontal velocity for the respective vehicle. Also, the force control system was evaluated with the LSSM vehicle for suspension cable length ranging from 30 ft to 170 ft and a 1.0 ft obstacle height. The majority of the data for the LSSM and MOLAB vehicles was obtained with a constant cable length of 50 ft and obstacle heights ranging from 0.5 ft to 1.5 ft for the LSSM. MOLAB obstacle heights ranged from 1.0 ft to 3.0 ft. Vehicle velocities were 8.2 ft/sec (9.0 km/hr) for the LSSM and 18.25 ft/sec (20 km/hr) for the MOLAB. Both roll and pitch configurations were considered for both vehicles. In all cases in the analog simulations the Bendix vehicle configurations were used for both LSSM and MOLAB vehicles.

◦ Typical Data

Typical analog output data is shown in Figures 4.5 through 4.20. LSSM roll and pitch data is presented in Figures 4.5 through 4.12. MOLAB roll and pitch data is presented in Figures 4.13 through 4.20. Maximum vehicle vehicle

velocities, an obstacle height of 1.0 ft, and a cable length of 50 ft was used in all cases shown.

o Lunar Gravity Error vs Obstacle Height

Maximum lunar gravity error for a given obstacle height was computed from the analog data by measuring the peak percentage force error and applying a factor of 5.0*. Maximum lunar g error versus obstacle height for the LSSM and MOLAB vehicles is shown in Figures 4.21 through 4.24 for both roll and pitch configurations. The following paragraphs discuss these cases.

Lunar gravity errors are shown in Figures 4.21 and 4.22 for the roll case. Figure 4.21 is for the LSSM vehicle moving 8.2 ft/sec, 50 ft length cables and the obstacle on the left wheel. Note that the lunar gravity error of the left chassis ranges from +11.5% to -19% and for the left wheel from +9% to -19.5% where the lunar gravity error for the right wheel (+1.5 to -2.0) and right chassis (+3.0 to -5.0) are considerably less. Figure 4.22 gives the lunar gravity error of the MOLAB vehicle with a velocity of 18.25 ft/sec and a 50 ft cable length. The lunar gravity error ranges from +8% to -50%. The additional mass of the MOLAB results in the large negative errors. The small plus error is understandable since the cables tend to buckle under compression forces.

The lunar gravity error for the pitch case is shown in Figures 4.23 and 4.24. The LSSM vehicle with a velocity of 8.2 ft/sec and a cable length of 50 ft gives errors of +10% to -23% which is in the same order of magnitude as the roll condition. The MOLAB vehicle with a velocity of 18.25 ft/sec and a cable length of 50 ft gives errors of +40% to -77%. Note that there is an additional +13% error and an additional -27% error on the rear wheels due to adverse conditions at the time the rear wheels hits the obstacle.

*The force control system is controlling a force of 5/6 earth g while lunar gravity is only 1/6 g. Thus, percentage gravity error is 5 x the force error.

• Peak Wheel Accelerations

Peak wheel accelerations versus obstacle height relations are shown in Figure 4.25 for the LSSM and MOLAB vehicles. Peak values for both roll and pitch configurations are shown. All values shown disregarded points in which discontinuities appeared from wheel bottoming. Note that the peak wheel acceleration is linear with obstacle height for all conditions shown. Also, the acceleration levels for the MOLAB are almost twice the LSSM values. This is probably due to the higher MOLAB velocity. Wheel accelerations for the roll configurations and the front wheel in the pitch configuration were found to be coincident. A plus acceleration in this figure tends to accelerate the wheel hub away from the ground plane.

The rear wheel accelerations for the MOLAB pitch case indicated considerably increased plus values and decreased negative values. This is caused by the pitch dynamics resulting from the front wheel perturbation. Peak decelerations for the maximum obstacle heights considered for each vehicle are

<u>Vehicle</u>	<u>Obstacle ht, ft</u>	<u>Peak Acceleration</u>	
		<u>ft/sec²</u>	<u>Earth g's</u>
MOLAB	3.0	+247	+7.66
		-272	-8.45
LSSM	1.5	+ 68	+2.11
		- 75	-2.33

Figures 4.26 and 4.27 show the LSSM at 8.2 ft/sec with an obstacle 1.0 ft high on the lunar surface and then in the LGS. The force error is shown along with the displacement difference. There is a phase shift due to the LGS cable dynamics. When force error is quite large there is a large displacement error about 0.6 seconds later. These variations return to zero after sufficient time has lapsed.

◦ Cable Length Effects

Figure 4.28 shows the lunar gravity error as a function of cable length for the LSSM vehicle at 8.2 ft/sec over a 1.0 foot obstacle. In general the error increases with cable length. The gravity error is most sensitive for the wheels than the chassis due to their faster vertical movements. This is illustrated in Figure 4.28. The importance of minimizing cable length is depicted by this graph. It is anticipated that the MOLAB type vehicle with higher velocity capability (20 km/hr) would result in higher gravity error with cable length variation than the LSSM. More simulation analysis in this area is recommended. The peak error for the rear wheel was less than that shown for the front wheel.

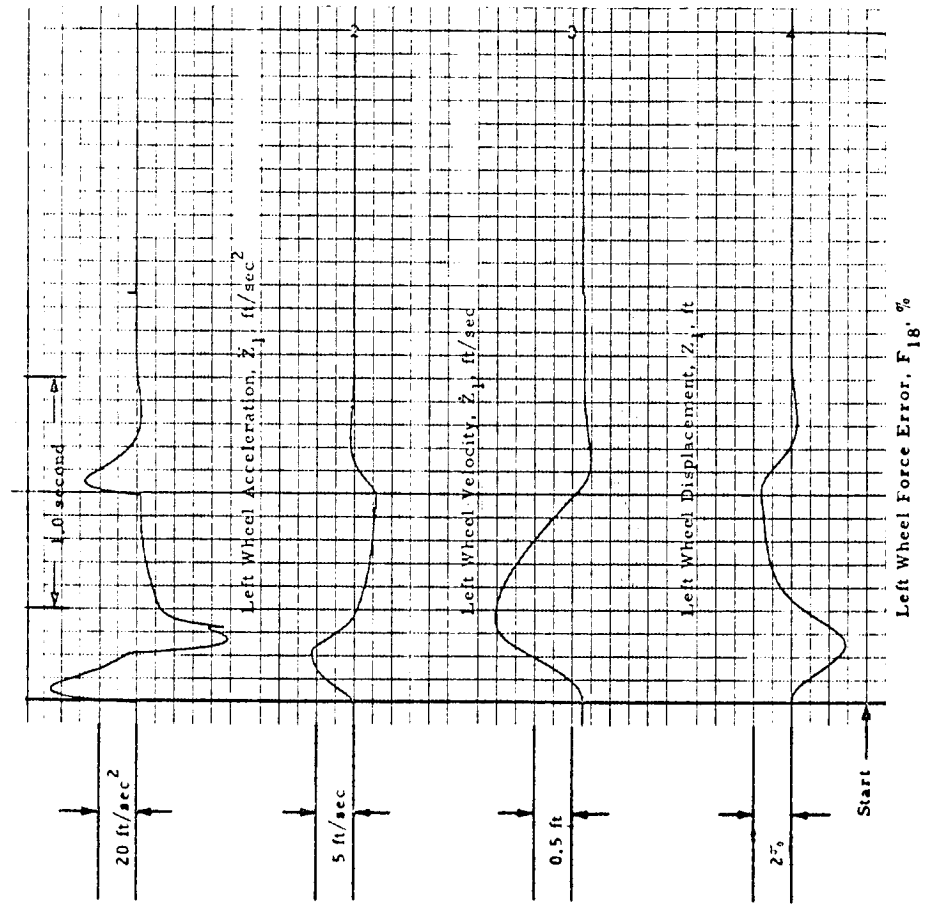
The maximum cable length recommended is that required to satisfy the static error conditions discussed in Section 3 (30 ft minimum) plus the length required for maximum change in lunar terrain elevation change (23 ft). Thus, a maximum cable length of 53 ft is recommended.

◦ Limit Design Condition

A review of the analog results presented indicates severe dynamic conditions for obstacle heights above one foot. Even the conditions for a one foot obstacle appear considerably more severe than the normal driver riding comfort limits. The peak values are compared below:

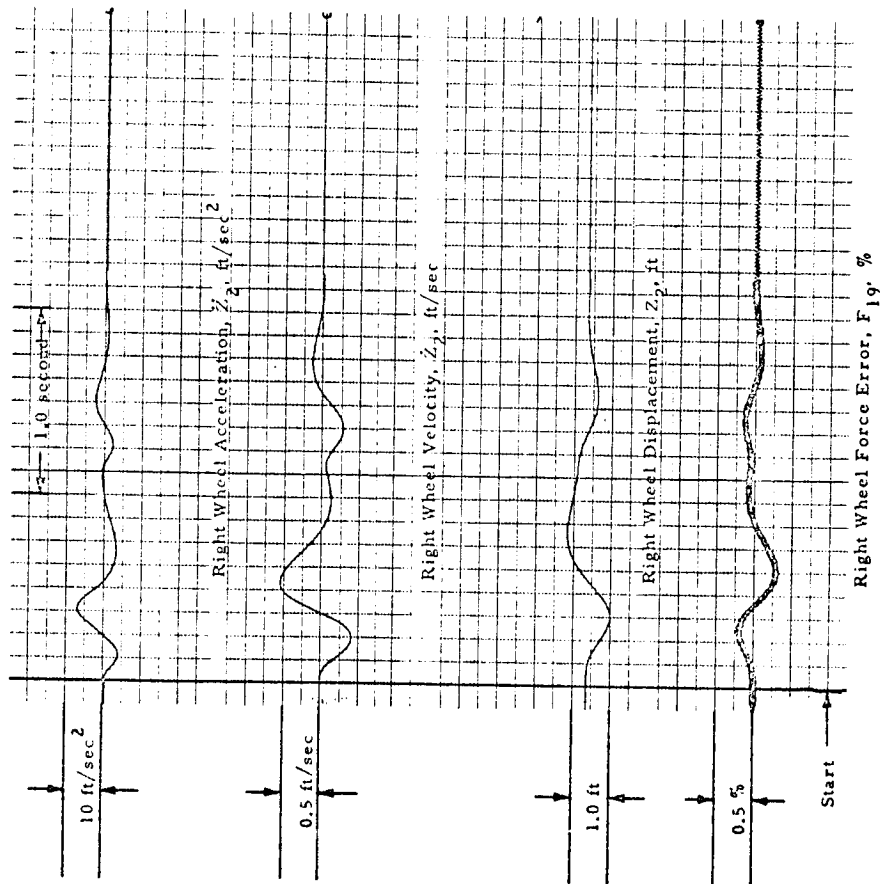
	<u>Riding Comfort Limits</u>	<u>Analog Results (1.0 ft obstacle)</u>	
		<u>LSSM</u>	<u>MOLAB</u>
Vertical Accel. at Vehicle cg (g's)	± 0.37	+0.34 -0.25	+0.75 -0.30
Pitch Accel. (rad/sec ²)	± 2.26	± 5.5	± 6.0
Roll Accel. (rad/sec ²)	± 3.25	± 5.0	± 2.2

From this comparison it is recommended that the dynamic data for a one foot obstacle be representative values for LGS design purposes.



ANALOG SIMULATION
LUNAR GRAVITY SIMULATOR SYSTEM (2D)
Vehicle: LSSM
Configuration: Roll
Obstacle Height: 1.0 ft
Vehicle Velocity: 8.2 ft/sec
Cable Length: 50 ft

Figure 4. 5 - Force Control System Performance with LSSM Left Wheels Engaging Obstacle (Roll Configuration)



ANALOG SIMULATION
LUNAR GRAVITY SIMULATOR SYSTEM (2D)
Vehicle: LSSM
Configuration: Roll
Obstacle Height: 1.0 ft
Vehicle Velocity: 8.2 ft/sec
Cable Length: 50 ft

Figure 4.6 - Force Control System Performance with LSSM Left Wheels Engaging Obstacle (Roll Configuration)

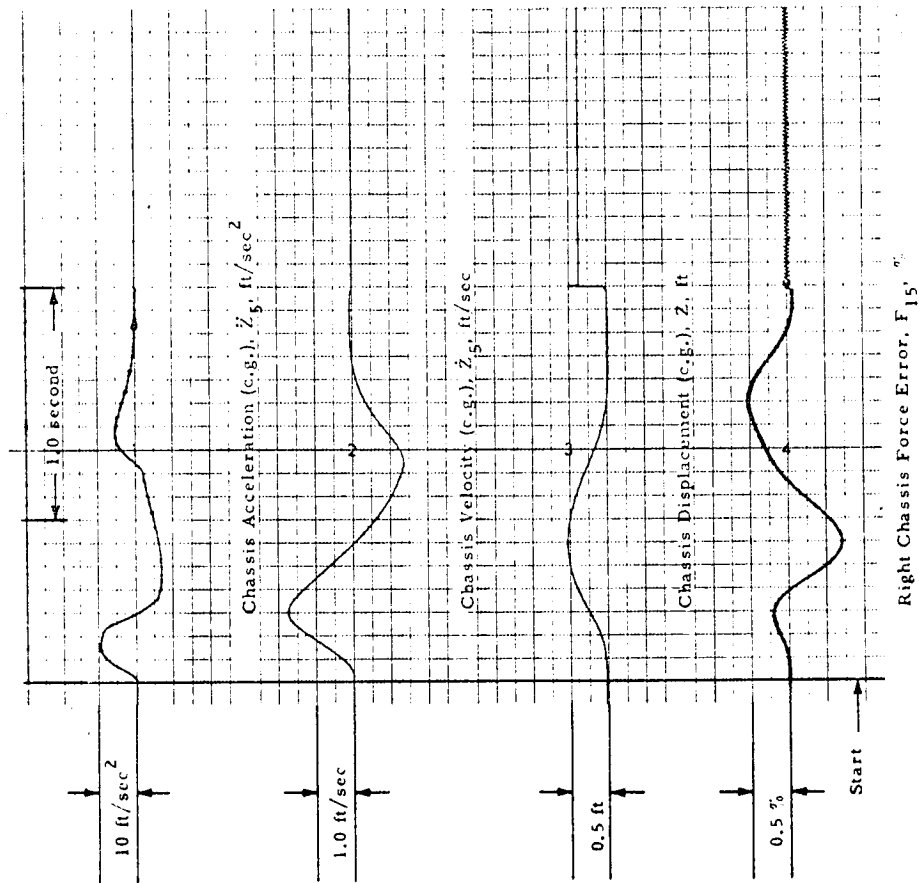
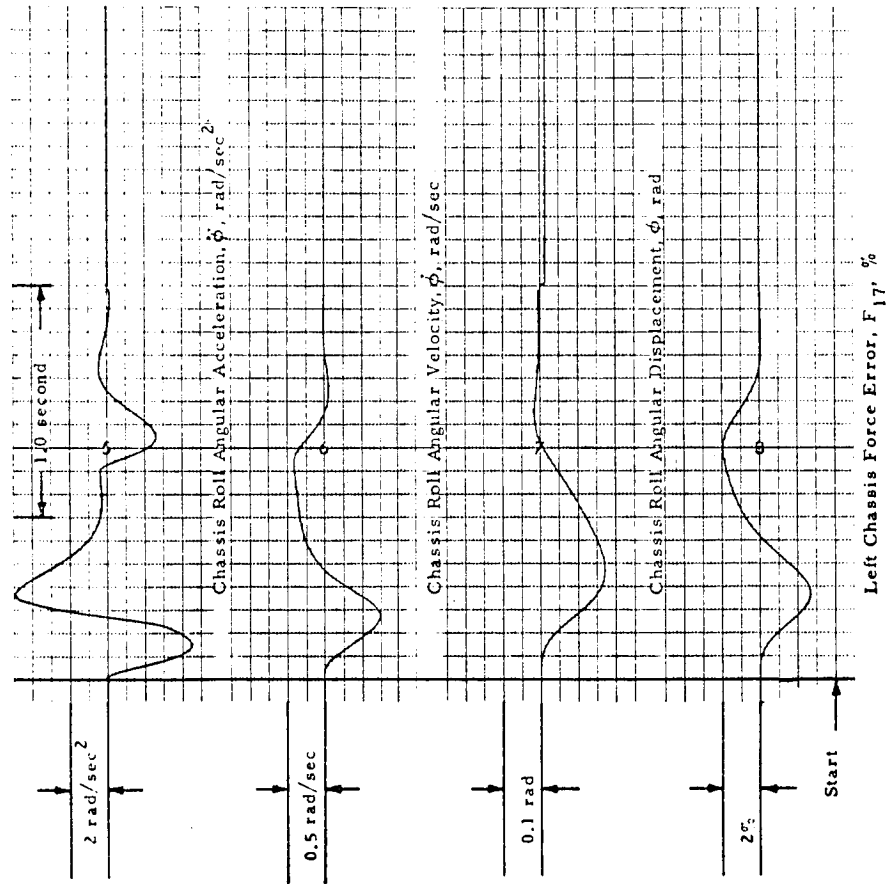
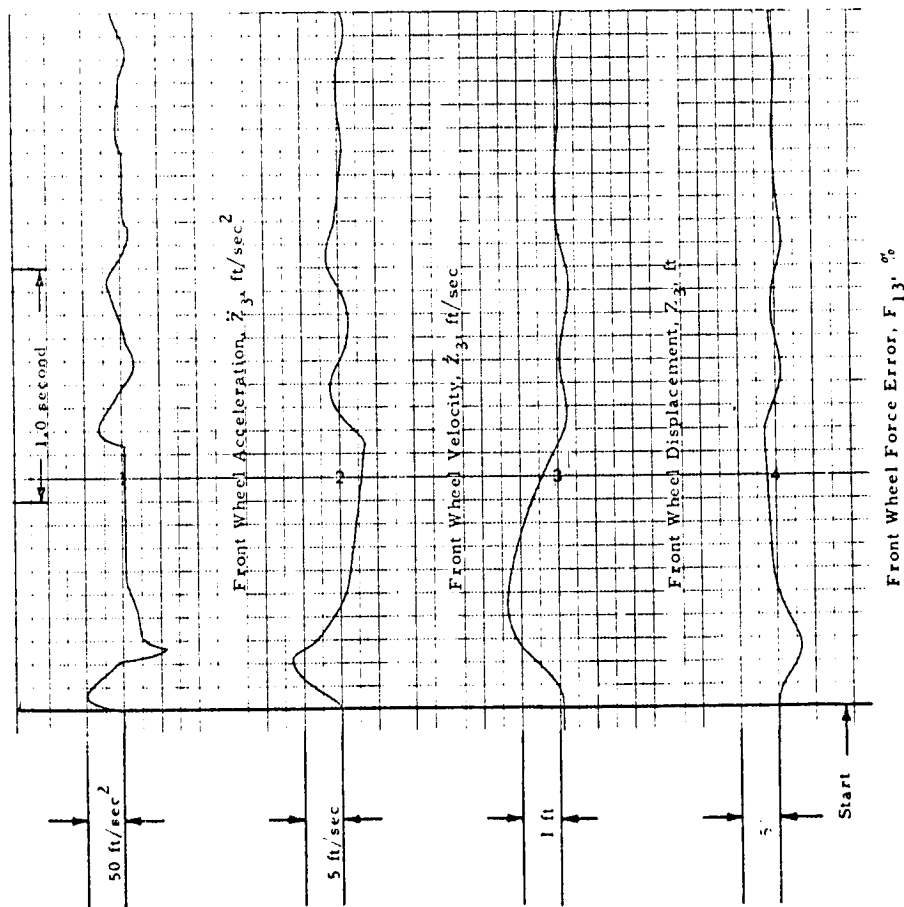


Figure 4.7 - Force Control System Performance with LSSM Left Wheels Engaging Obstacle (Roll Configuration)



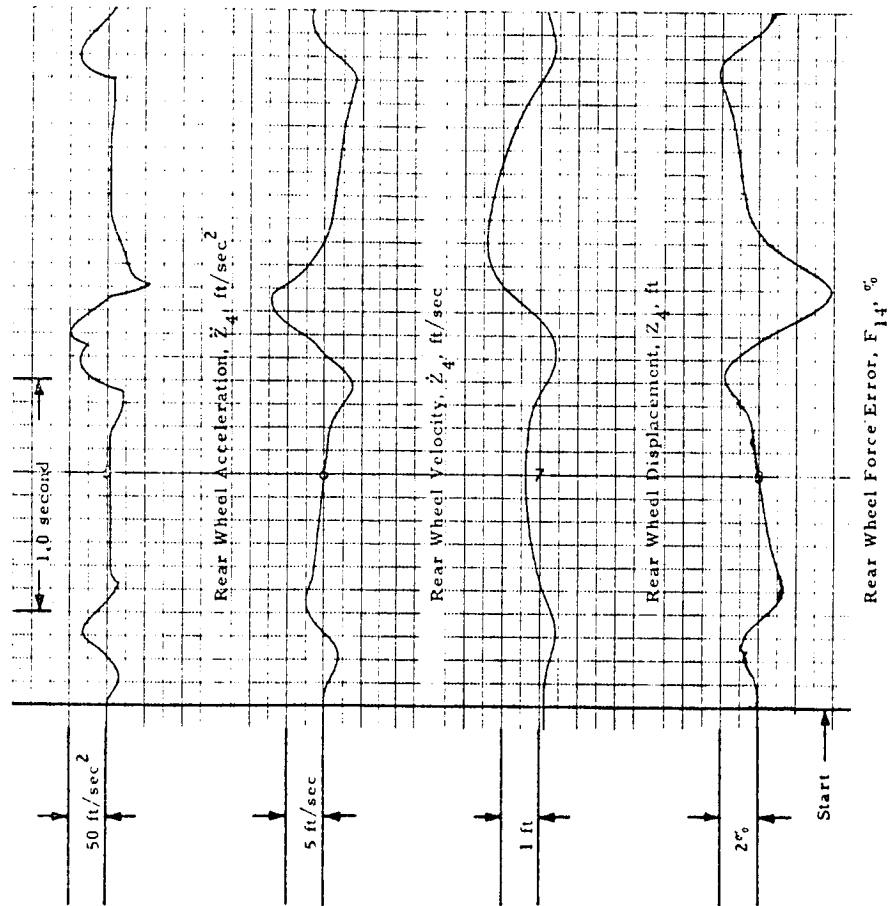
ANALOG SIMULATION
LUNAR GRAVITY SIMULATOR SYSTEM (2D)
Vehicle: LSSM
Configuration: Roll:
Obstacle Height: 1.0 ft
Vehicle Velocity: 8.2 ft/sec
Cable Length: 50 ft

Figure 4.8 - Force Control System Performance with LSSM Left Wheels
Engaging Obstacle (Roll Configuration)



ANALOG SIMULATION
LUNAR GRAVITY SIMULATOR SYSTEM (2D)
Vehicle: LSSM
Configuration: Pitch
Obstacle Height: 1.0 ft
Vehicle Velocity: 8.2 ft/sec
Cable Length: 50 ft

Figure 4.9 - Force Control System Performance with LSSM Front and Rear Wheels Engaging Obstacle (Pitch Configuration)



ANALOG SIMULATION
LUNAR GRAVITY SIMULATOR SYSTEM (2D)

Vehicle: LSSM

Configuration: Pitch

Obstacle Height: 1.0 ft

Vehicle Velocity: 8.2 ft/sec

Cable Length: 50 ft

Figure 4.10 - Force Control System Performance with LSSM Front and Rear Wheels Engaging Obstacle (Pitch Configuration)

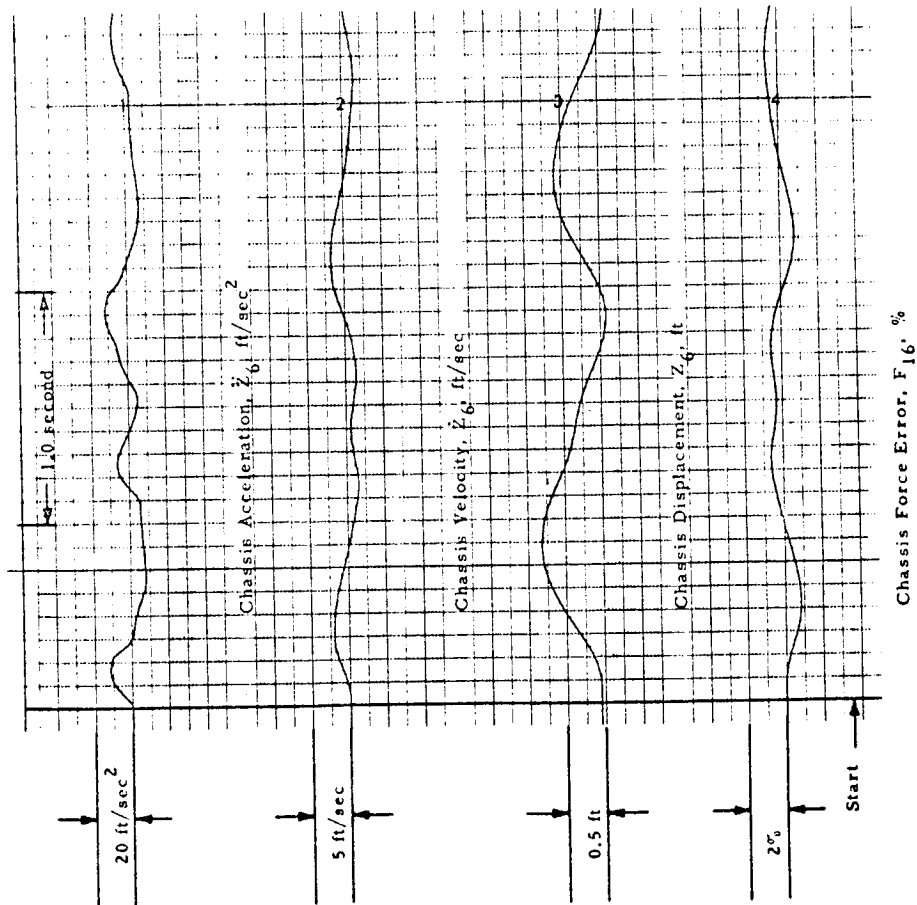


Figure 4.11 - Force Control System Performance with LSSM Front and Rear
Wheels Engaging Obstacle (Pitch Configuration)

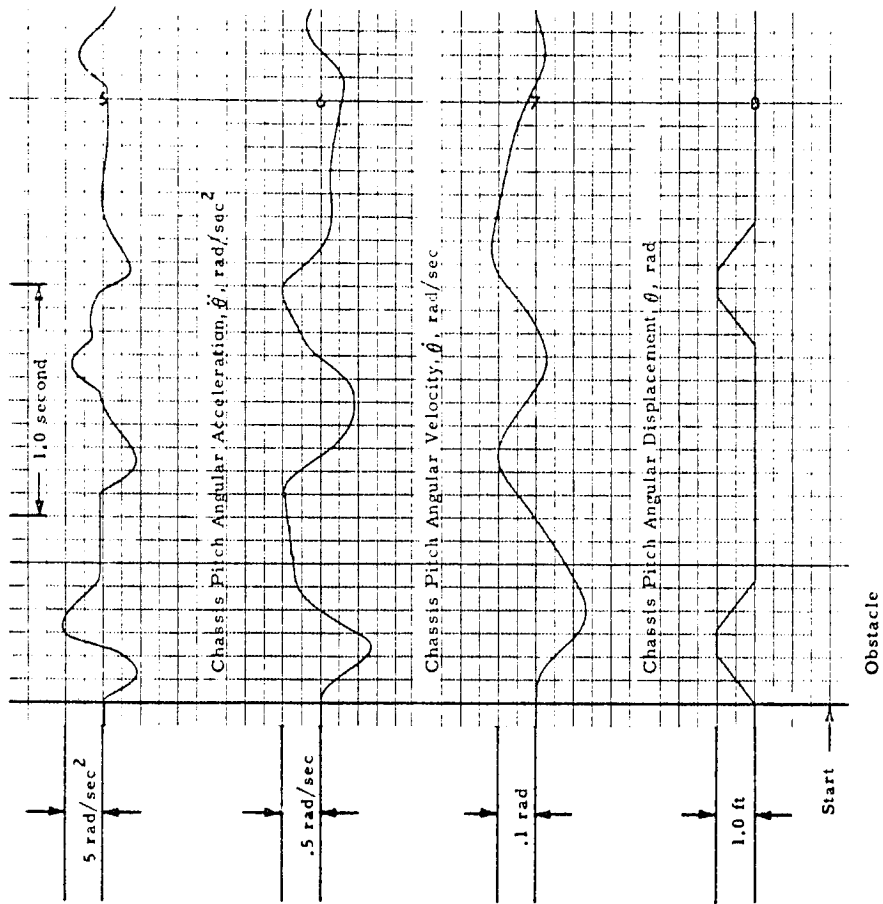
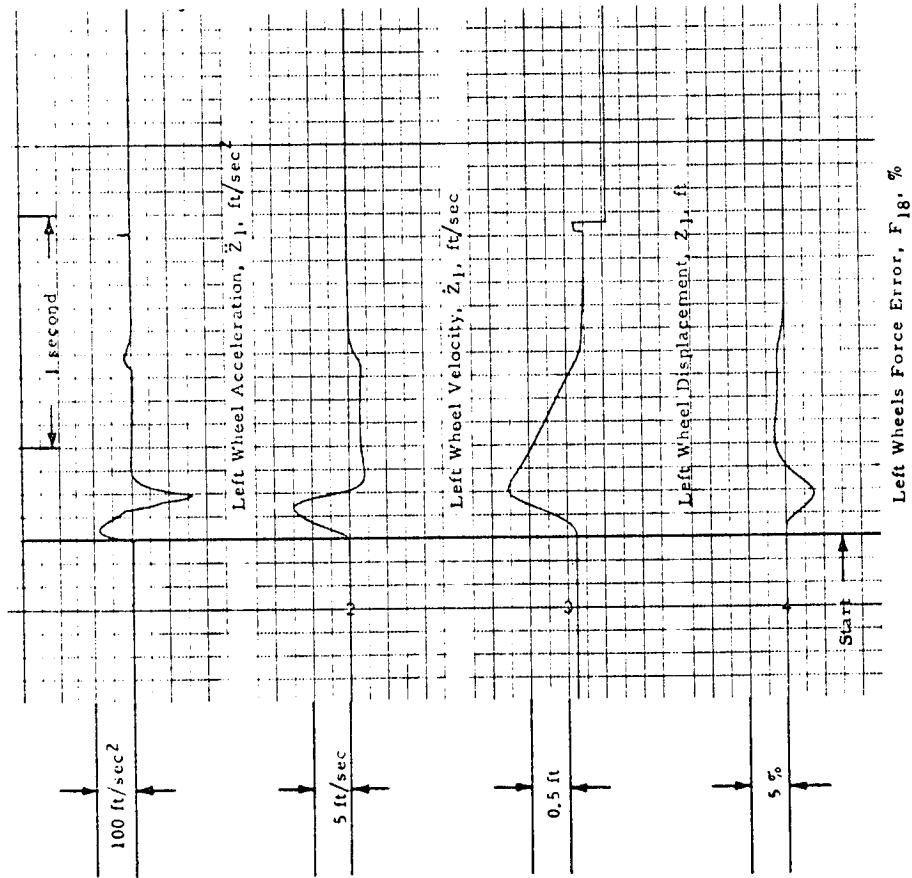


Figure 4.12 - Force Control System
ANALOG SIMULATION
LUNAR GRAVITY SIMULATOR SYSTEM (2D)
Vehicle: LSSM
Configuration: Pitch
Obstacle Height: 1.0 ft
Vehicle Velocity: 8.2 ft/sec
Cable Length: 50 ft

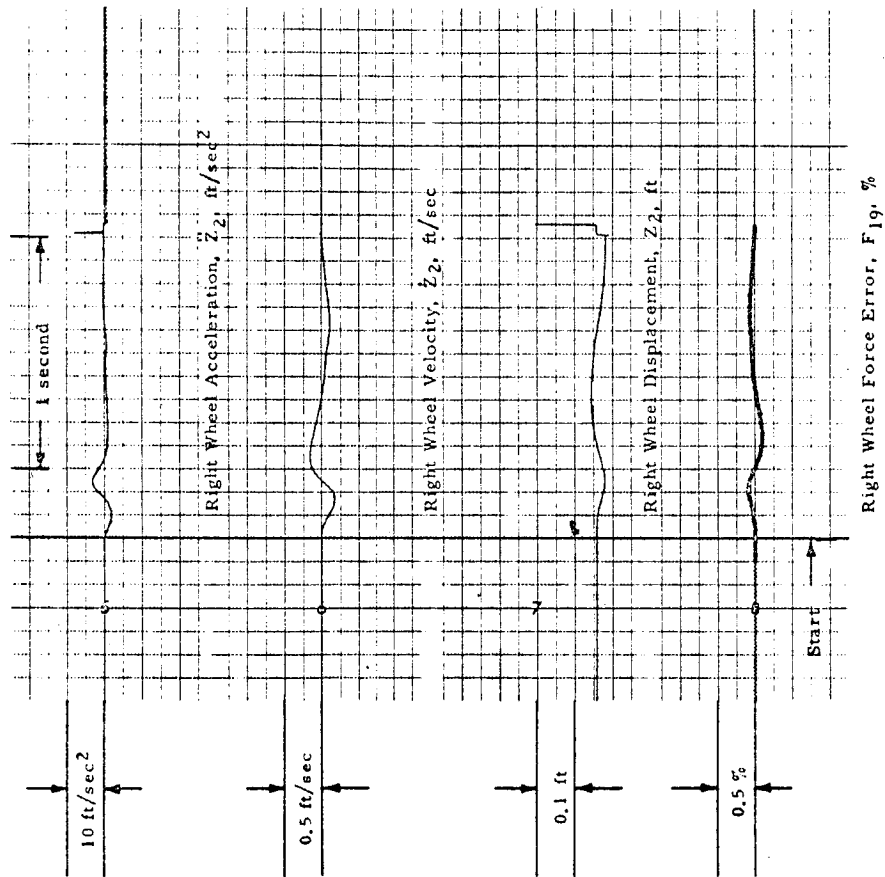
Figure 4.12 - Force Control System Performance with LSSM Front and Rear
Wheels Engaging Obstacle (Pitch Configuration)



ANALOG SIMULATION
LUNAR GRAVITY SIMULATOR SYSTEM (2D)

Vehicle:	MOLAB
Configuration:	Roll
Obstacle Height:	1.0 ft
Vehicle Velocity:	18.25 ft/sec
Cable Length:	50.0 ft

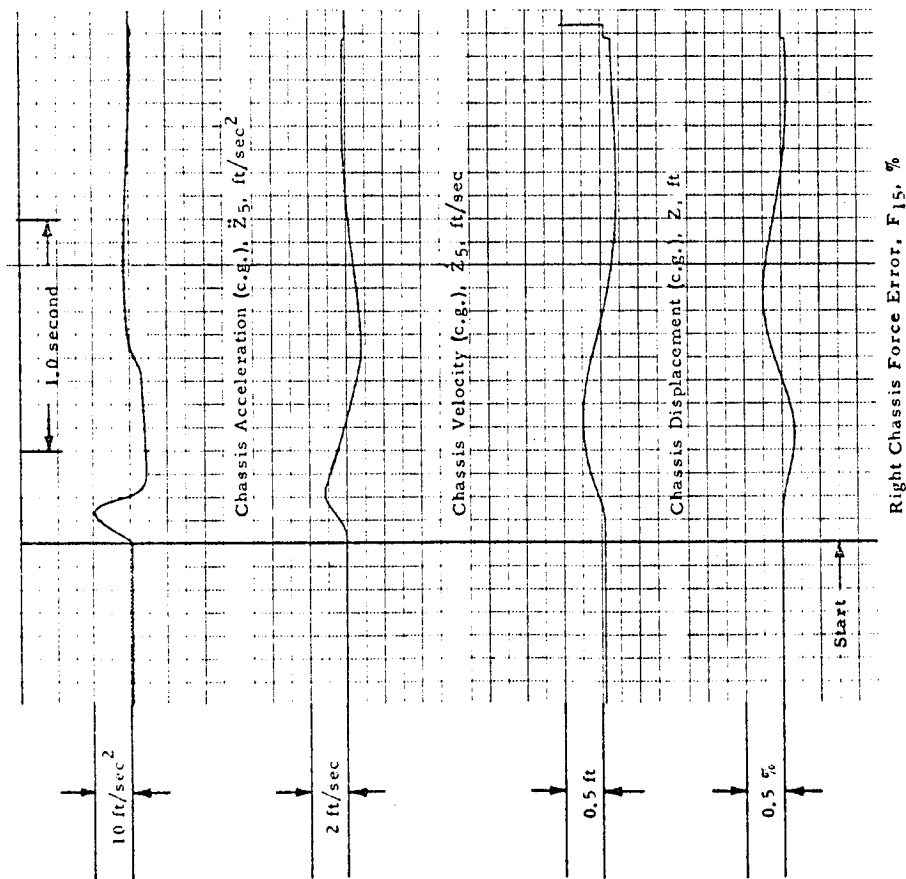
Figure 4.13 - Force Control System Performance with MOLAB Left Wheels Engaging Obstacle (Roll Configuration)



ANALOG SIMULATION
LUNAR GRAVITY SIMULATOR SYSTEM (2D)

Velocity: MOLAB
Configuration: Roll
Obstacle Height: 1.0 ft
Vehicle Velocity: 18.25 ft/sec
Cable Length: 50 ft

Figure 4.14 - Force Control System Performance with MOLAB Left Wheels Engaging Obstacle (Roll Configuration)



ANALOG SIMULATION LUNAR GRAVITY SIMULATOR SYSTEM (2D)

Vehicle: MOLAB
Configuration: Roll
Obstacle Height: 1.0 ft
Vehicle Velocity: 18.25 ft/sec
Cable Length: 50 ft

Figure 4.15 - Force Control System Performance with MOLAB Left Wheels Engaging Obstacle (Roll Configuration)

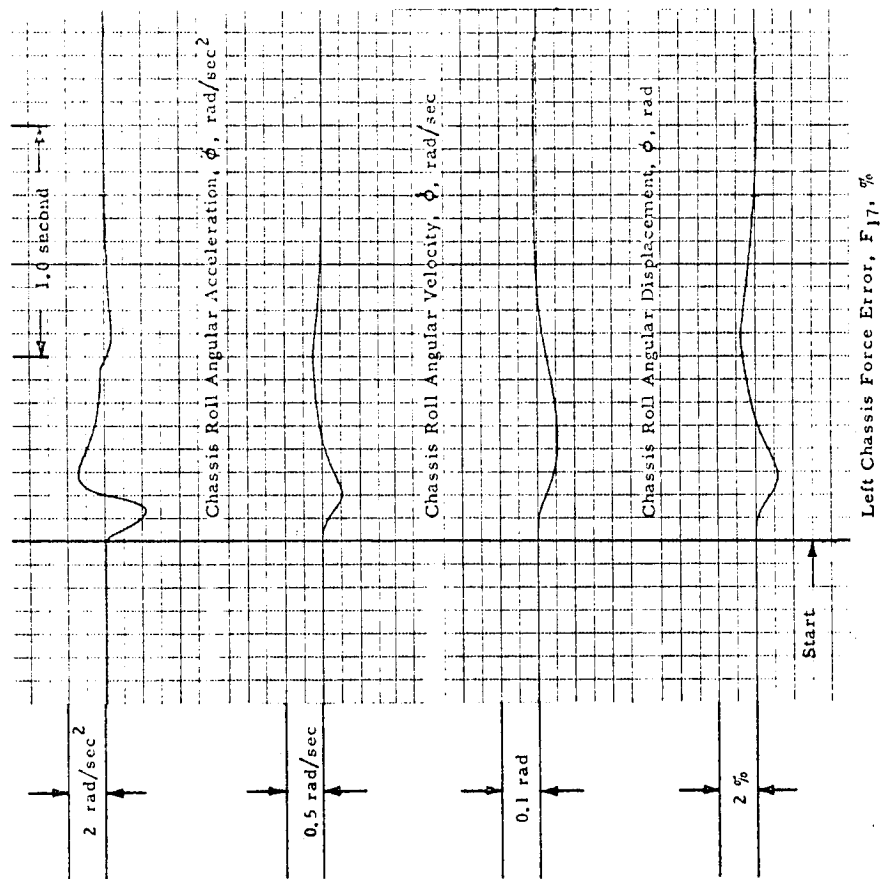
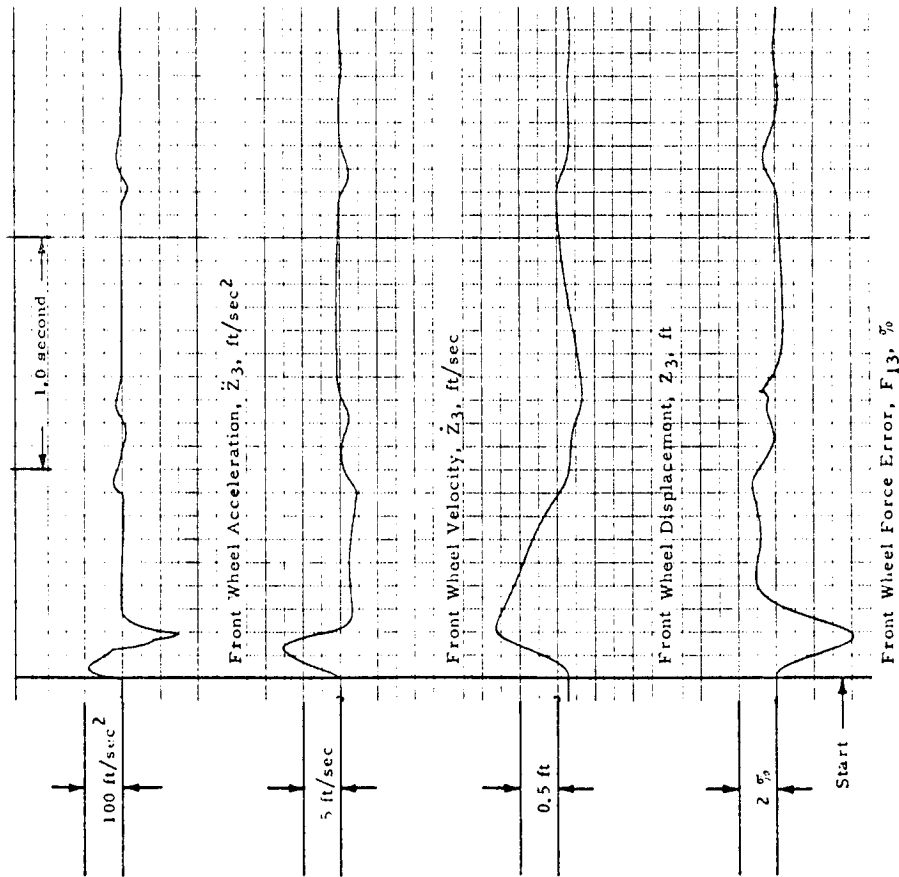


Figure 4.16 - Force Control System Performance with MOLAB Left Wheels Engaging Obstacle (Roll Configuration)



ANALOG SIMULATION
LUNAR GRAVITY SIMULATOR SYSTEM (2D)

Vehicle: MOLAB
Configuration: Pitch
Obstacle Height: 1.0 ft
Vehicle Velocity: 18.25 ft/sec
Cable Length: 50 ft

Figure 4.17 - Force Control System Performance with MOLAB Front and Rear Wheels Engaging Obstacle (Pitch Configuration)

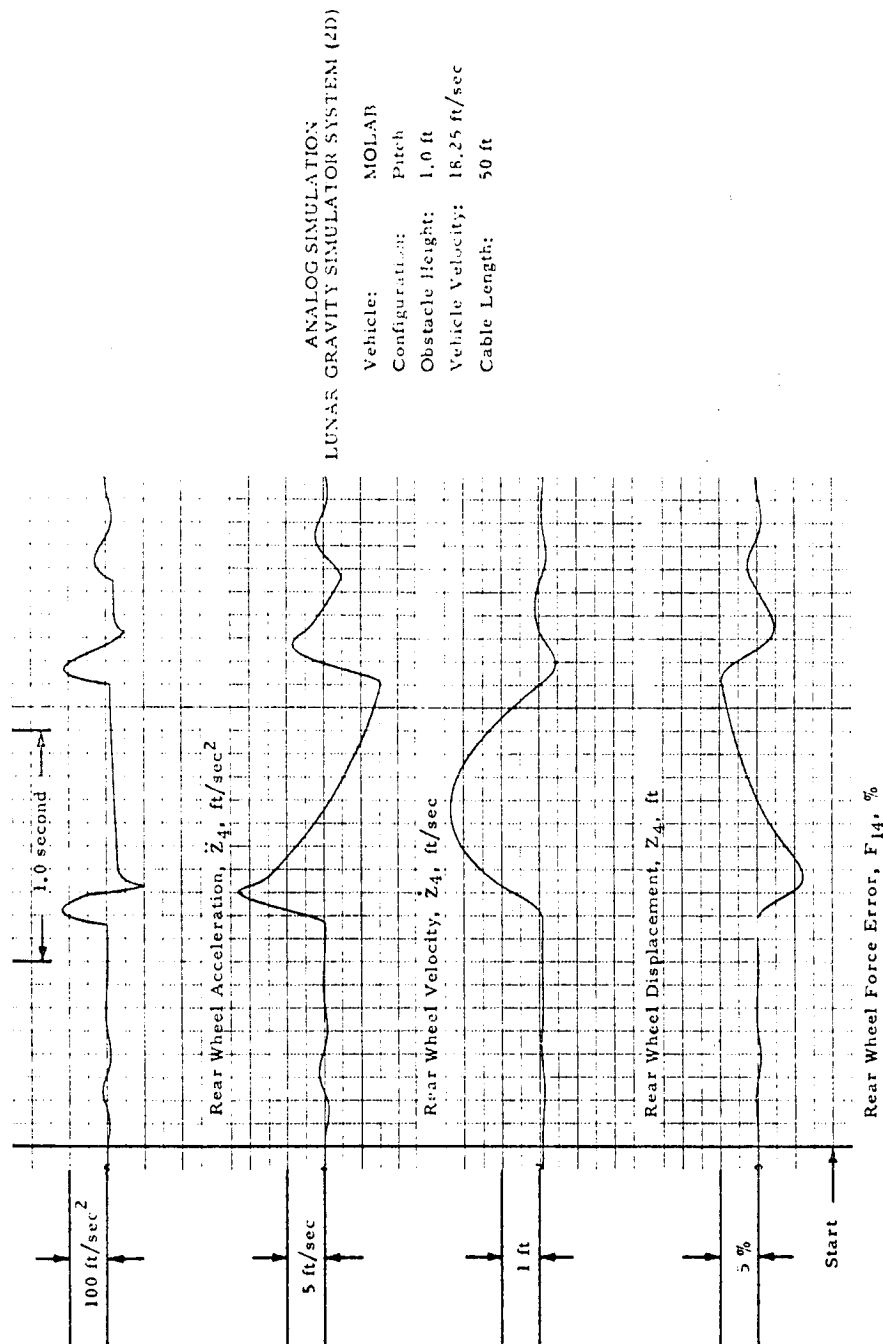


Figure 4.18 - Force Control System Performance with MOLAB Front and Rear Wheels Engaging Obstacle (Pitch Configuration)

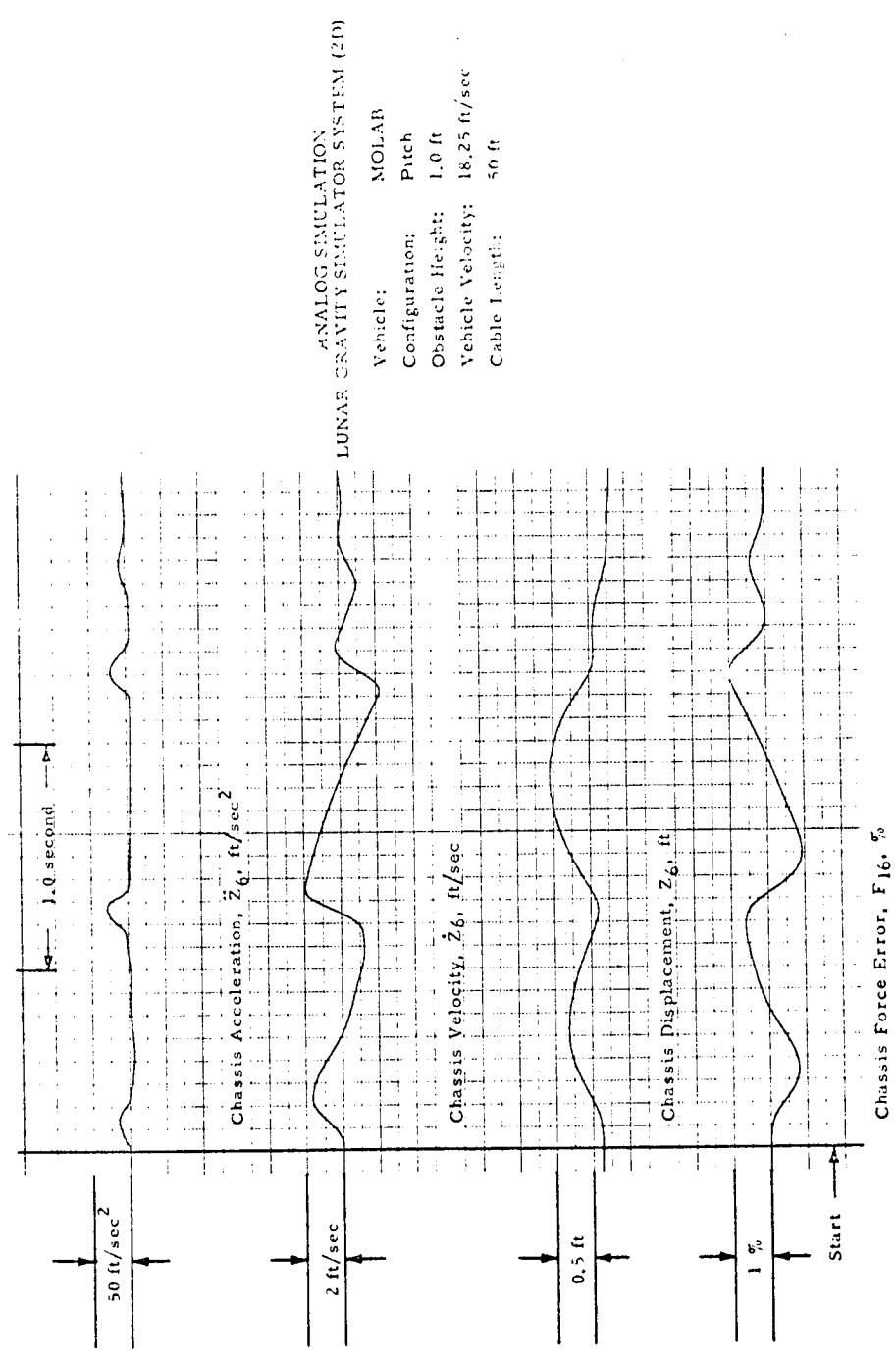


Figure 4.19 - Force Control System Performance with MOLAB Front and Rear Wheels Engaging Obstacle (Pitch Configuration)

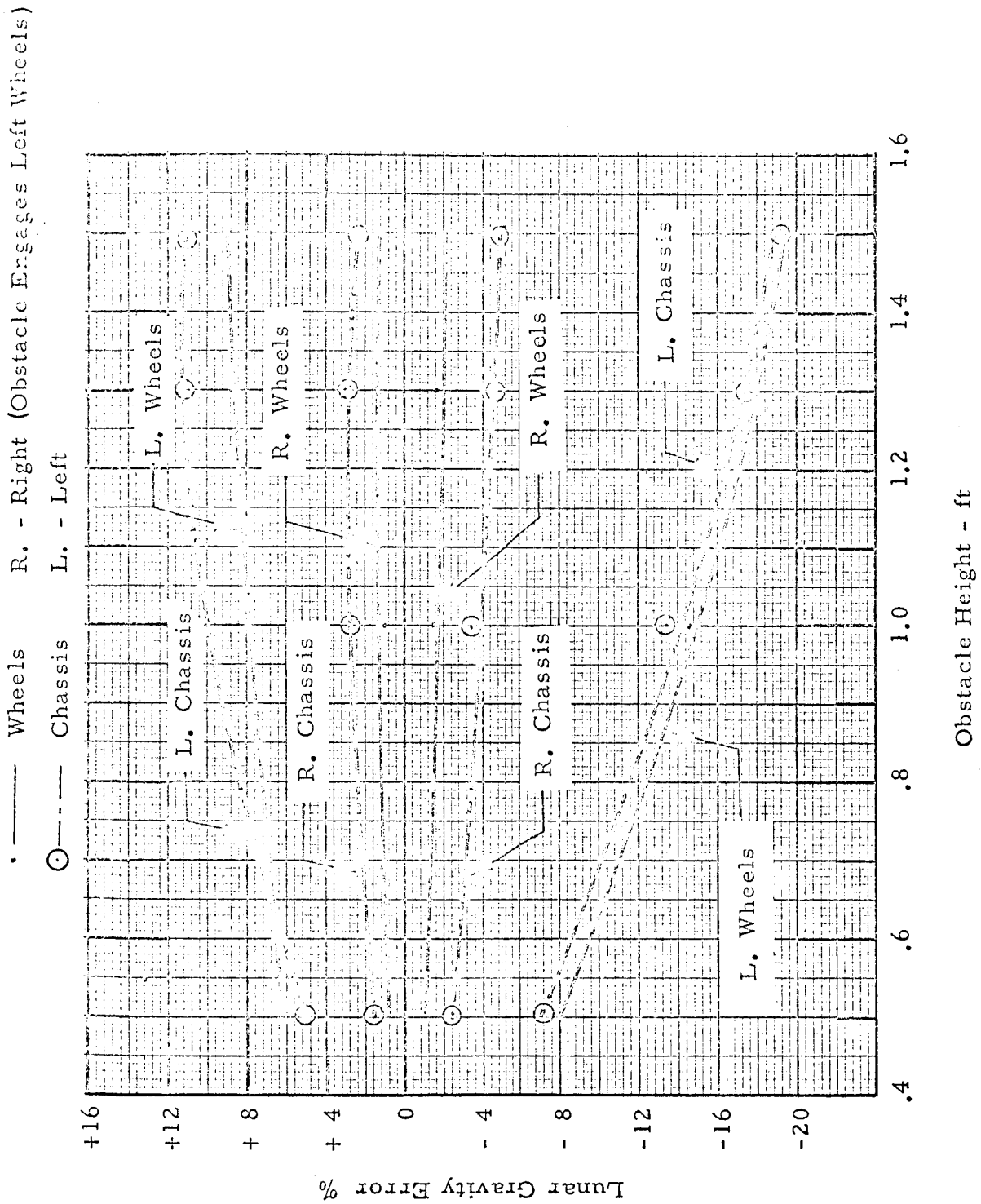


Figure 4.21 - Lunar Gravity Error vs Obstacle Height -
LSSM Vehicle in Roll Configuration

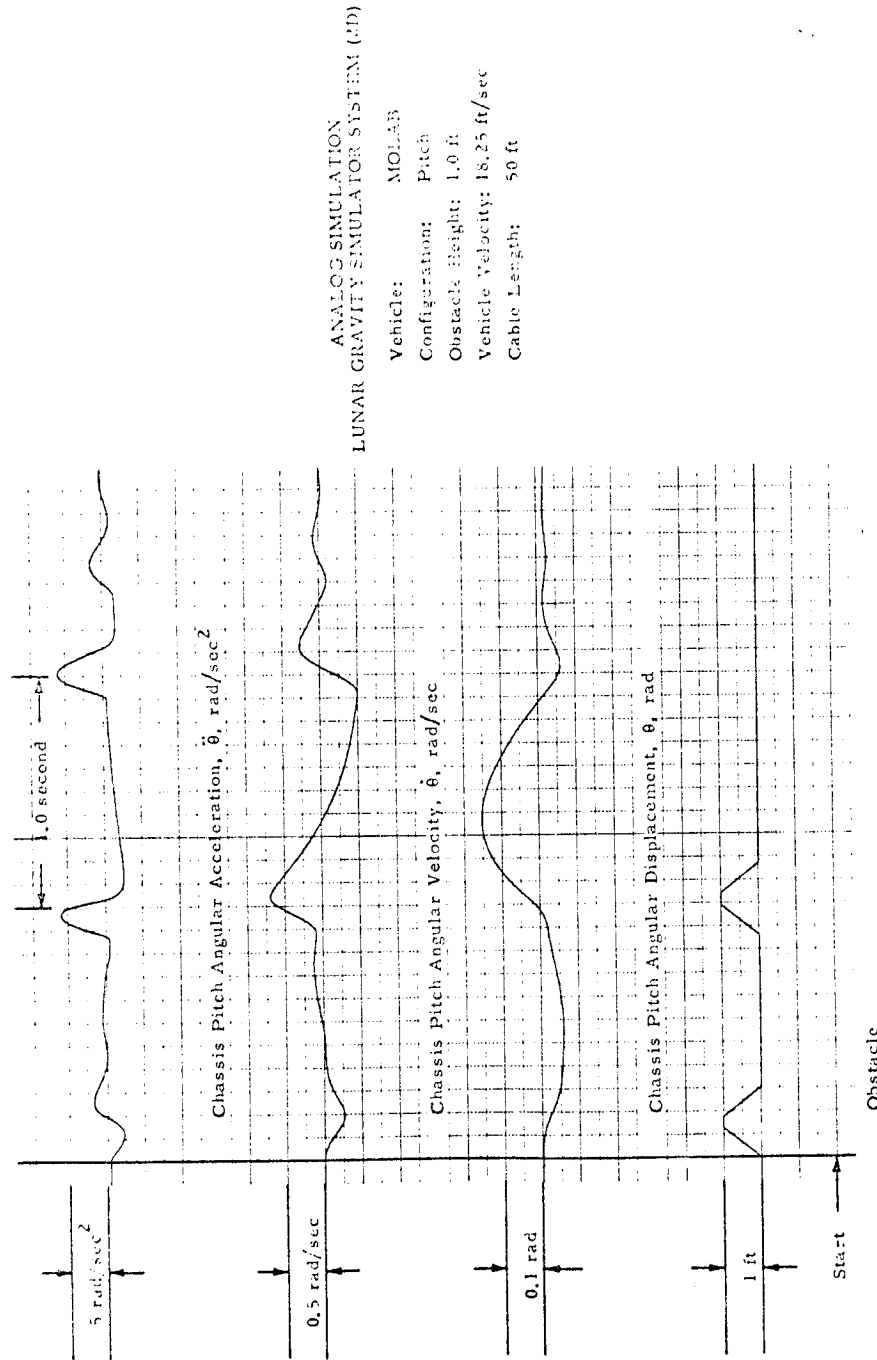


Figure 4.20 - Force Control System Performance with MOLAB Front and Rear Wheels Engaging Obstacle (Pitch Configuration)

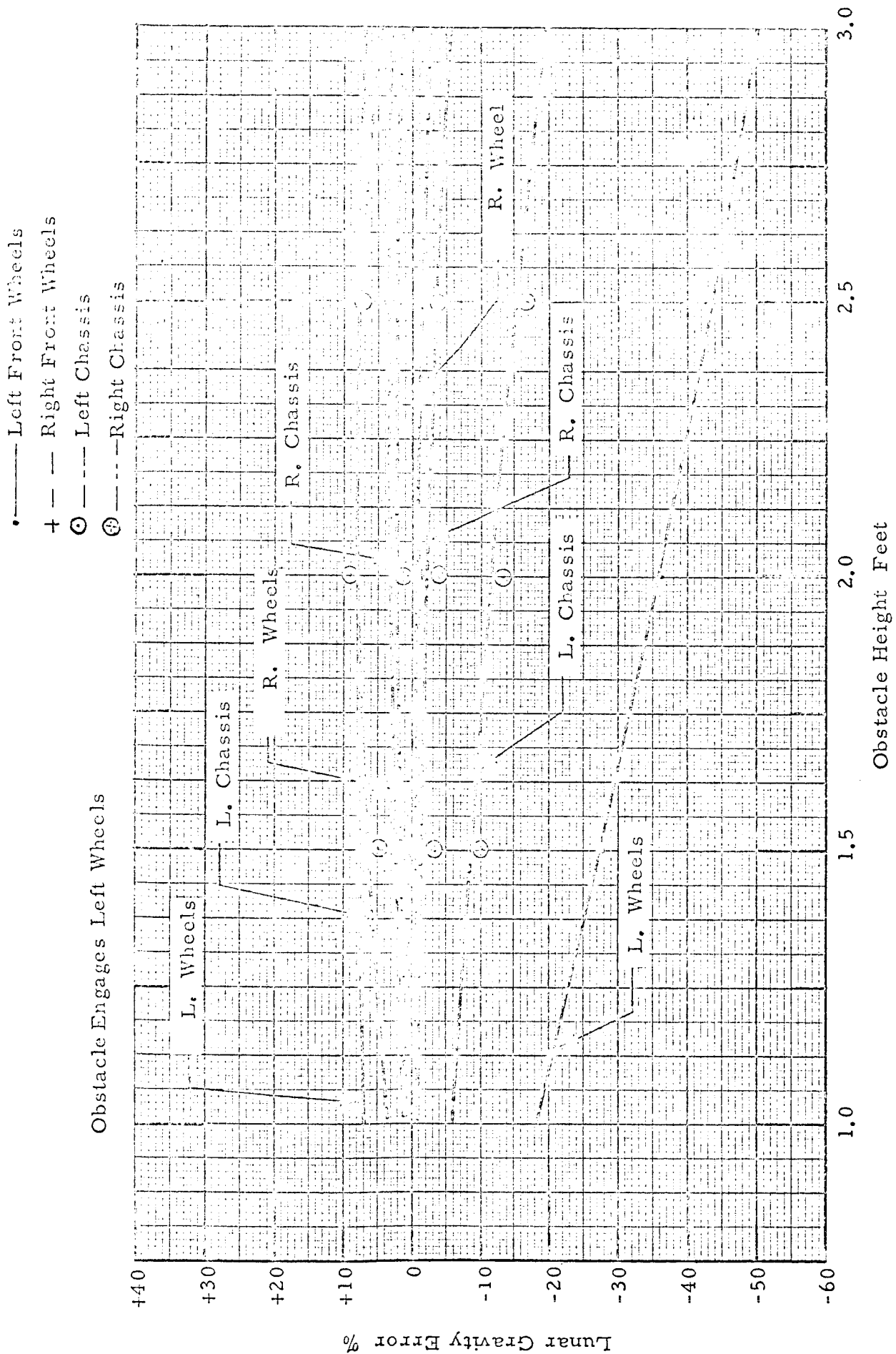


Figure 4.22 Lunar Gravity Error vs Obstacle Height-MOLAB Vehicle in Roll Configuration

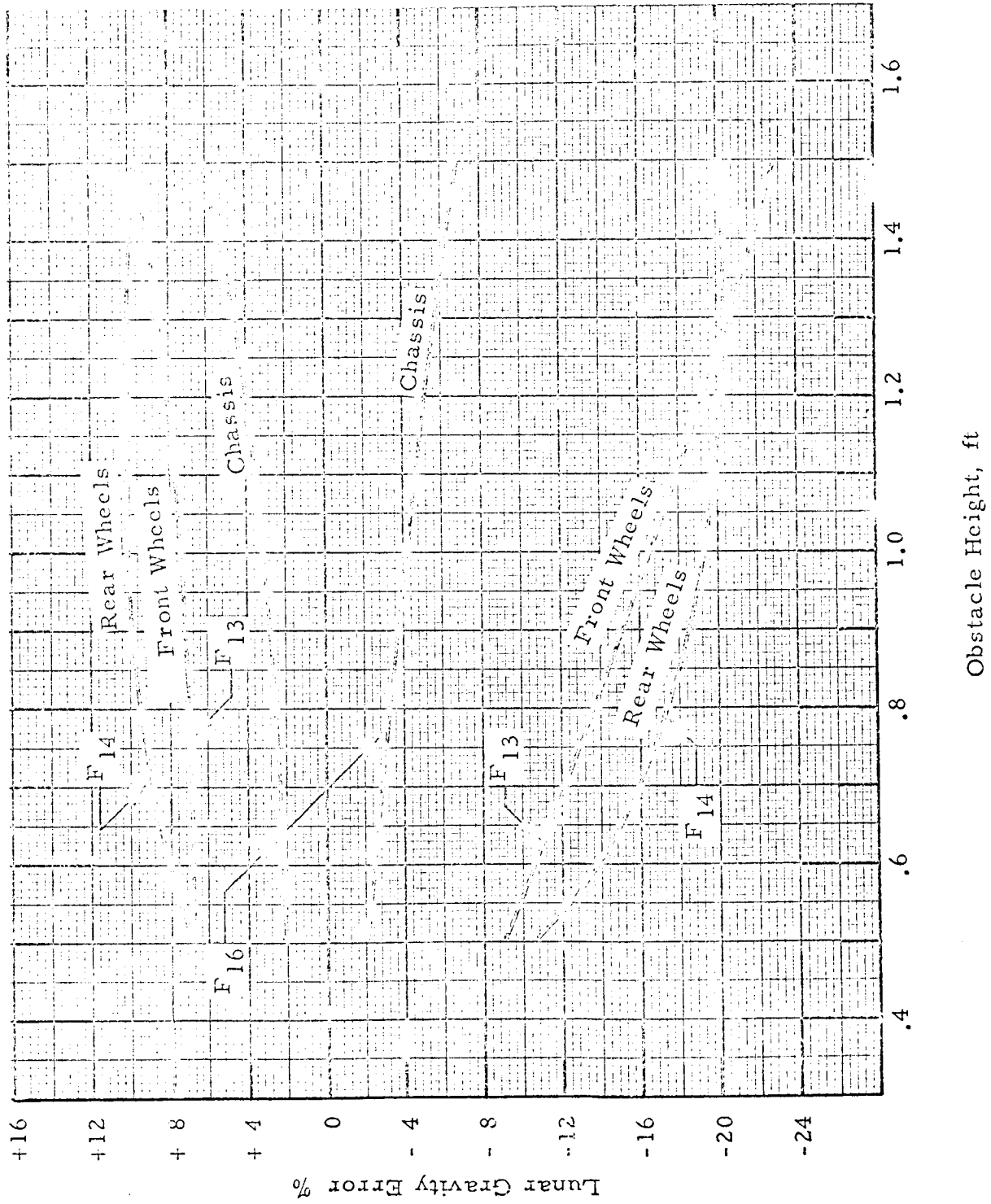


Figure 4.23 - Lunar Gravity Error vs Obstacle Height-LSSM Vehicle in Pitch Configuration

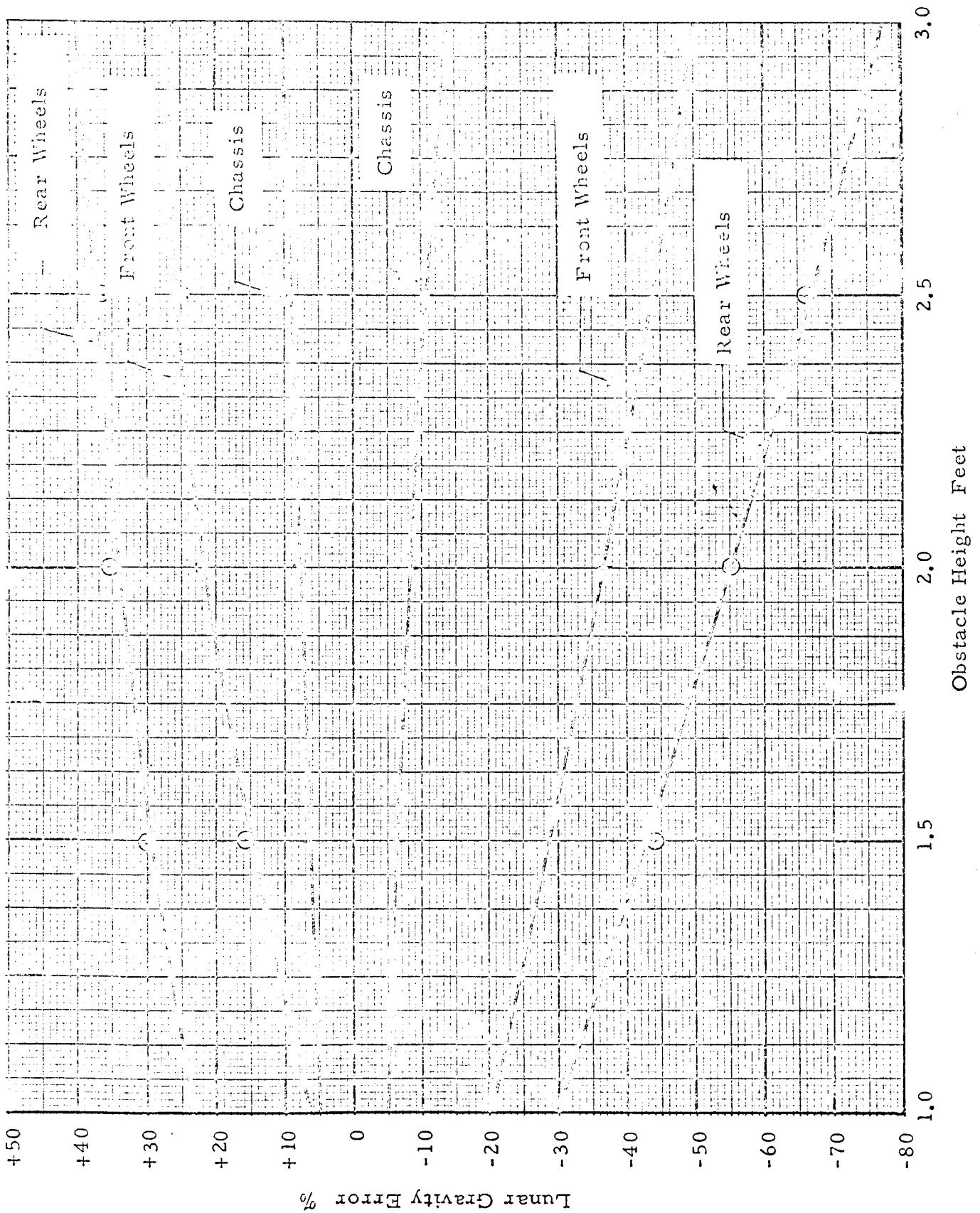


Figure 4.24 - Lunar Gravity Error vs Obstacle Height-MOLAB Vehicle in Pitch Configuration

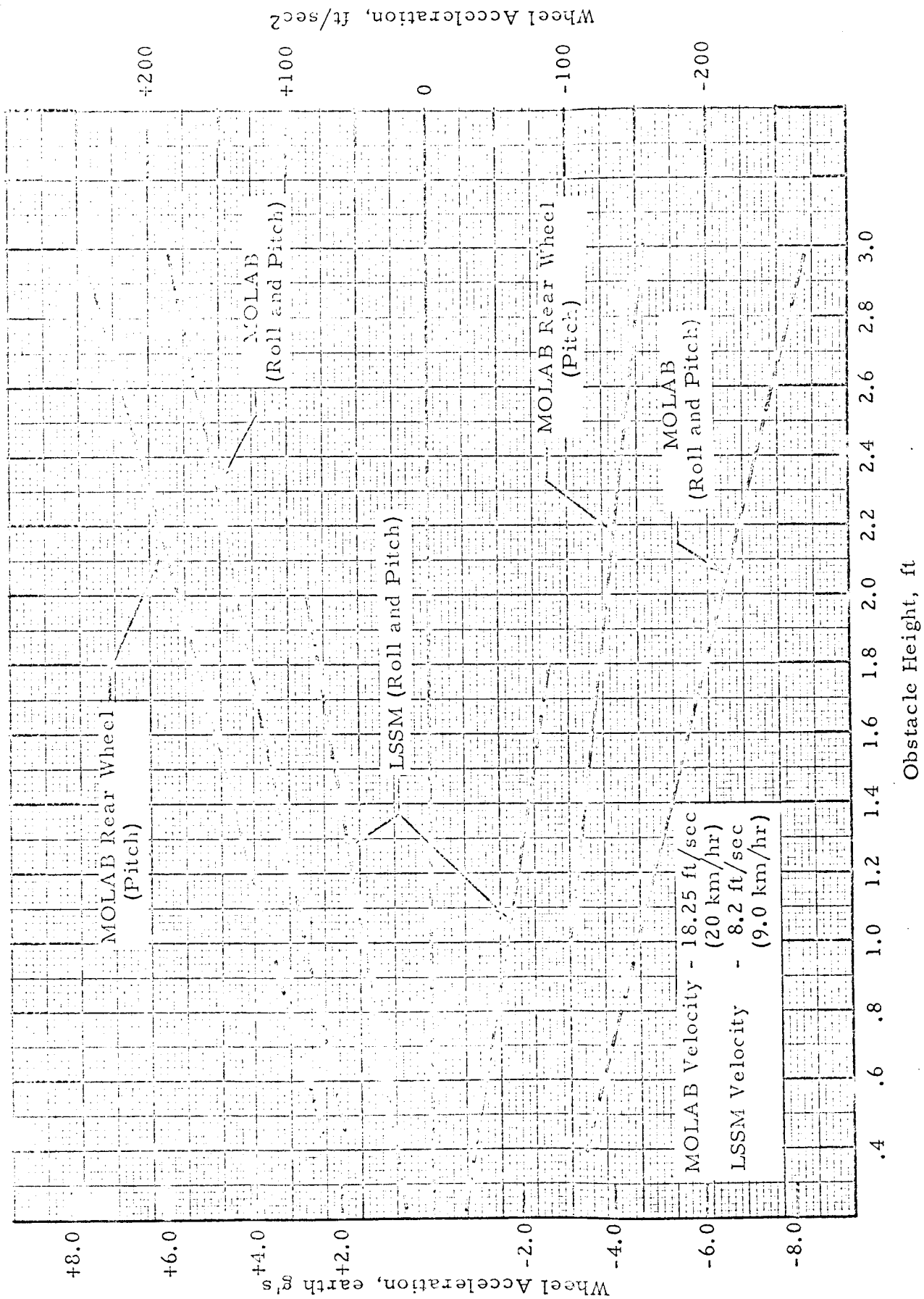


Figure 4.25 - Peak Wheel Accelerations vs Obstacle Height, LSSM and MOLAB

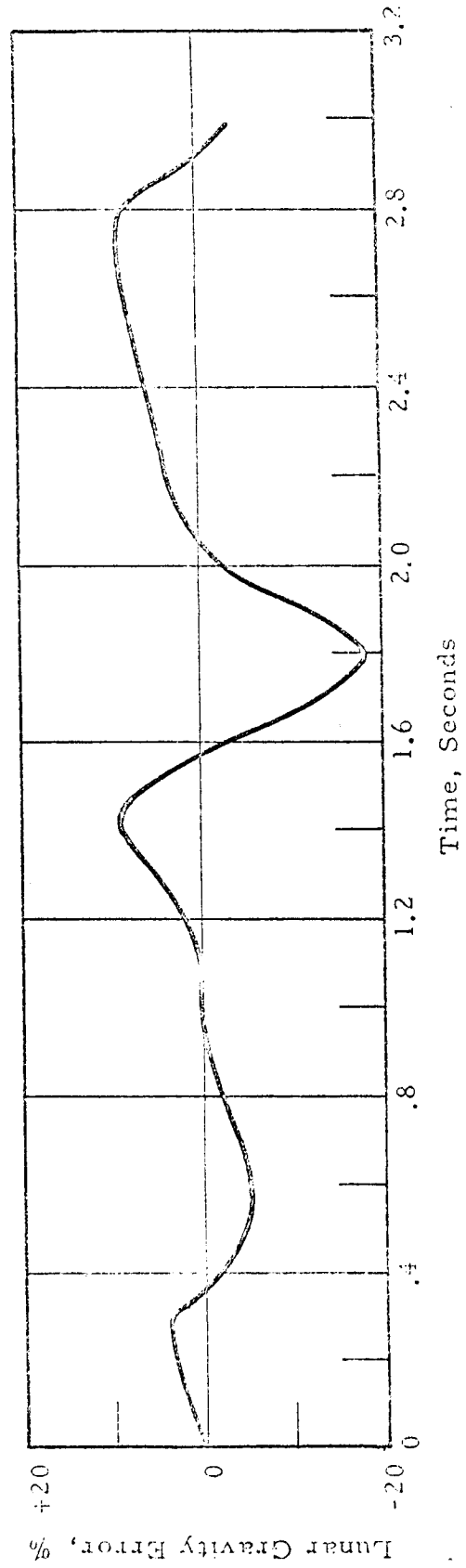
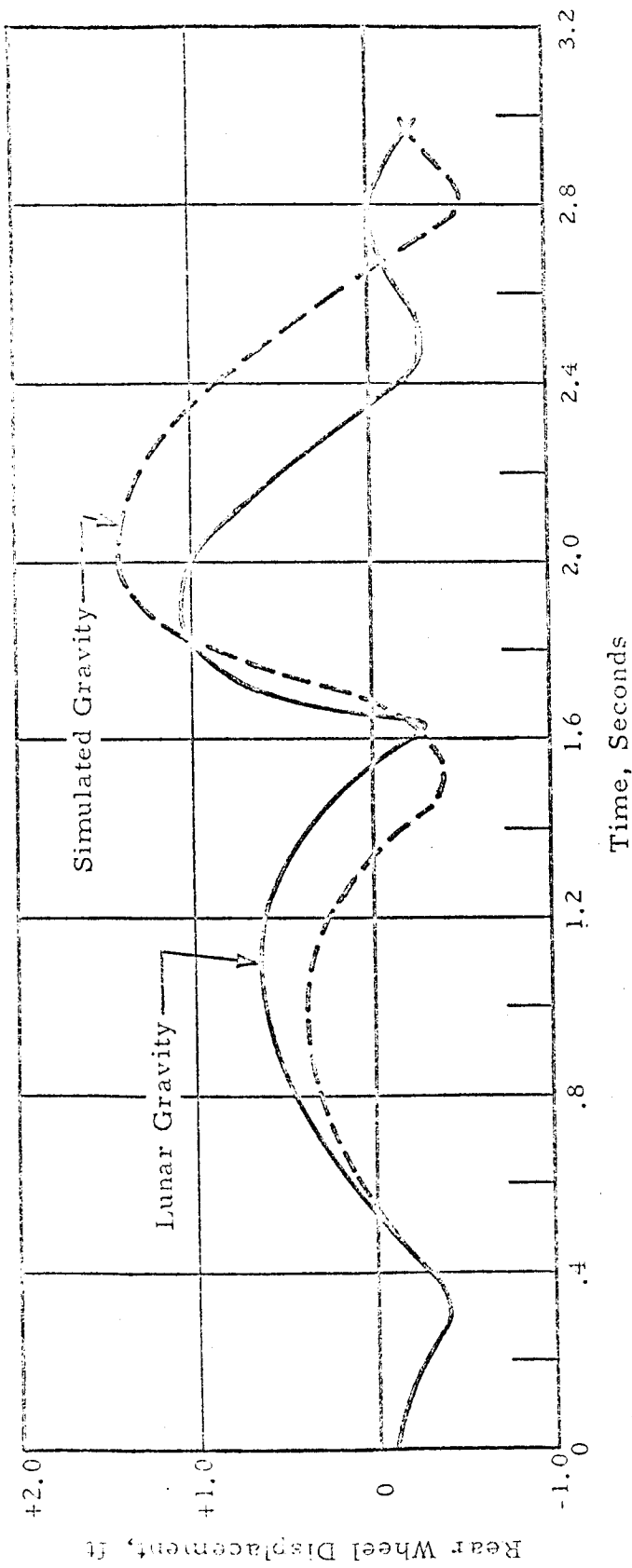


Figure 4.26 - LSSM Rear Wheel Displacement and Lunar Gravity Error

$\dot{x} = 8.2 \text{ ft/sec (9.0 km/hr)}$ Obstacle Height = 1.0 ft

Cable Length = 50 ft Pitch Configuration

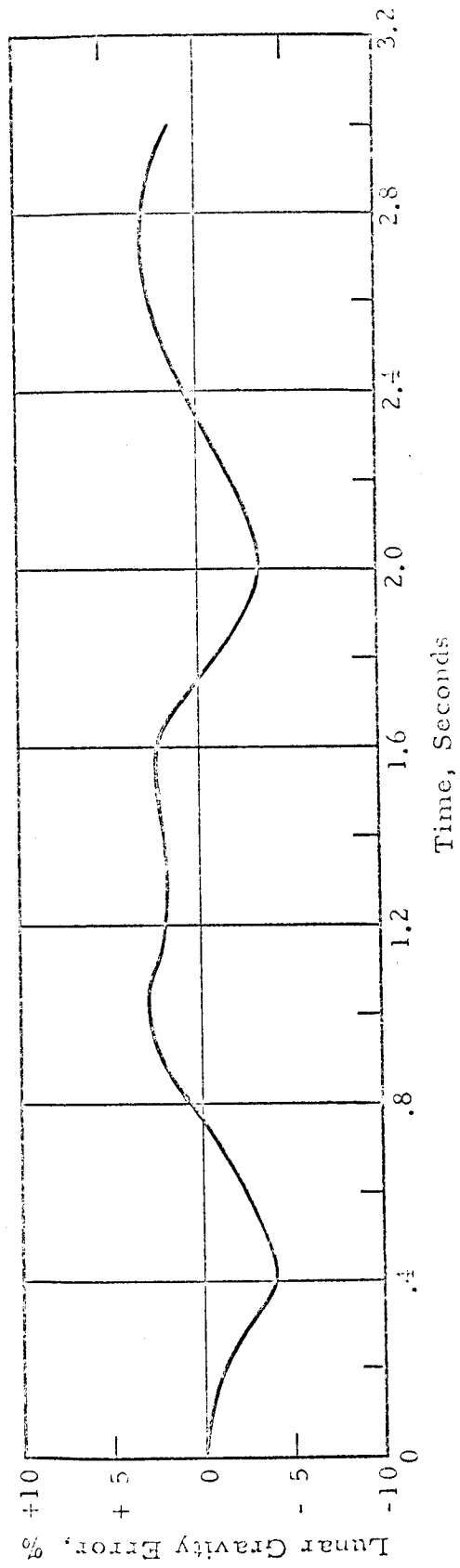
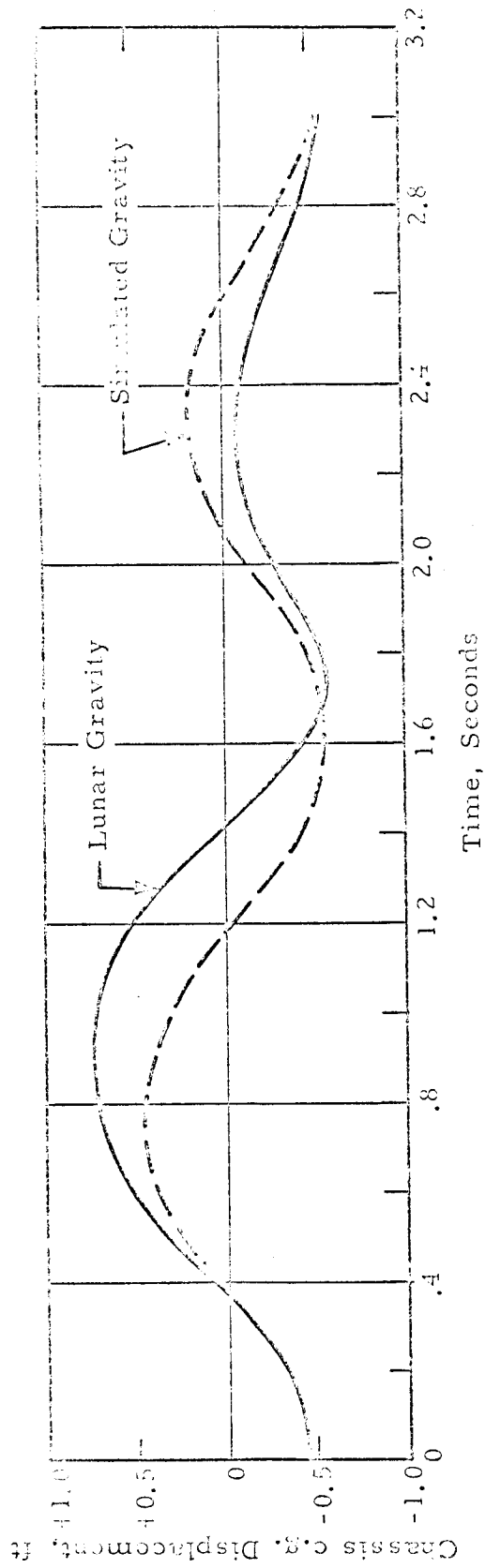


Figure 4.27 - LSSM Chassis c.g. Displacement and Lunar Gravity Error

$\dot{X} = 8.2 \text{ ft/sec (9.0 km/hr)}$ Obstacle Height = 1.0 ft

Cable Length = 50 ft Pitch Configuration

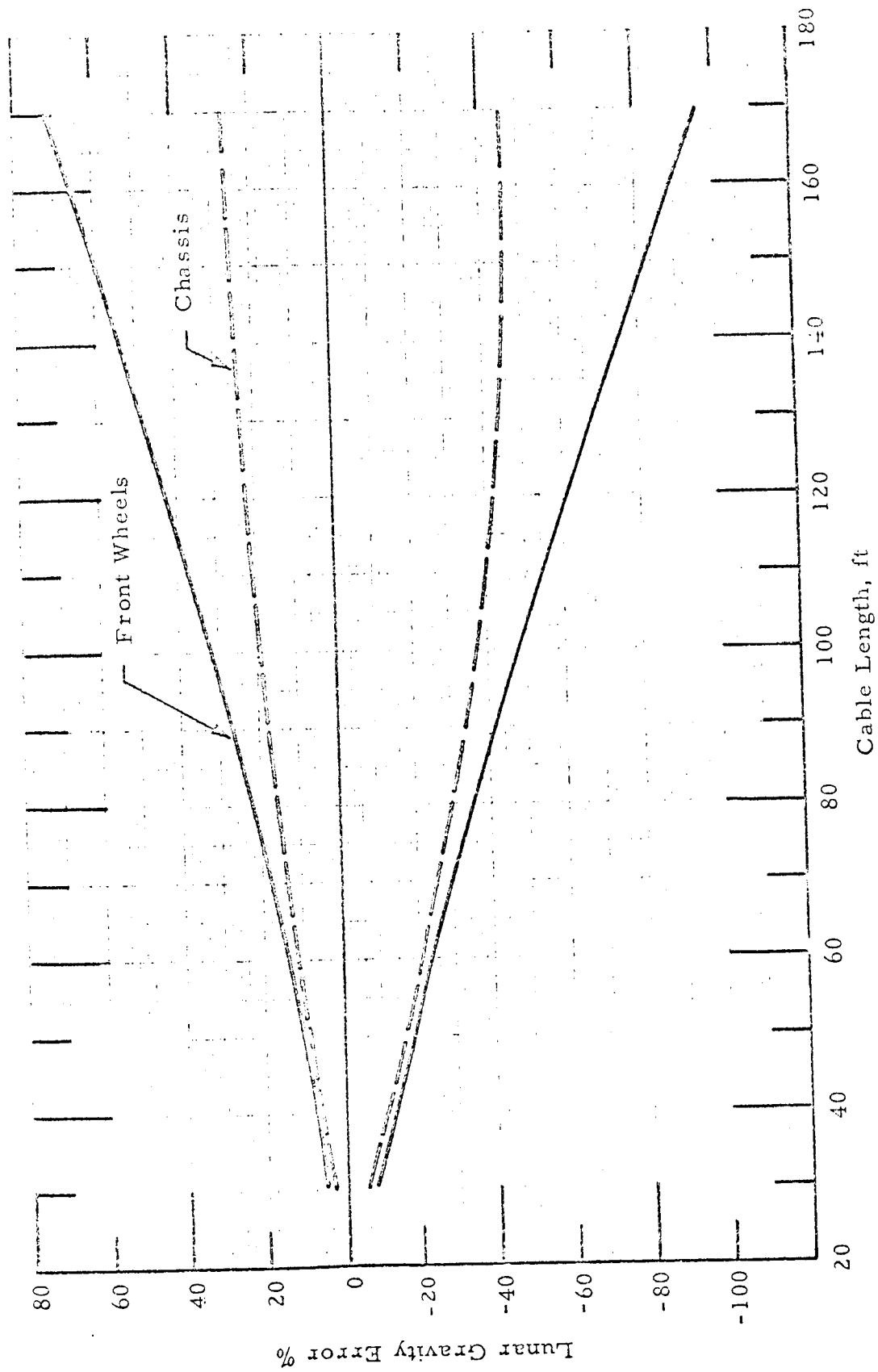


Figure 4.28 - Lunar Gravity Error vs Cable Length for LSSM in Pitch Configuration

4.3 TROLLEY DRIVE SYSTEM

4.3.1 Analog Simulation

The trolley drive system, described in Section 2.2, was simulated on the analog computer for an evaluation of the dynamic response due to severe test cases. The points of interest were:

- o Can satisfactory response be obtained with the control system of Section 2.2 without further compensation.
- o How does the cable length affect the dynamic errors caused by the trolley drive system for both LSSM and MOLAB types of test articles.

The dynamic equations used for the simulation and for the Flow Chart of Section 2 are given below:

$$M \ddot{\xi} + B \dot{\xi} - F_o \alpha = 0 \quad (\text{trolley})$$

$$\frac{I}{R} \ddot{\xi} + \frac{B_M}{R} \dot{\xi} + R F_D - \frac{T_o}{P_o} P = 0 \quad (\text{motor})$$

$$q \dot{\xi} + \frac{2q\zeta_v}{\omega_v} \ddot{\xi} + \frac{q}{2} \ddot{\xi} = k_1^* i - k_2^* P \quad (\text{valve})$$

$$i = k^*(X - \xi) + k_o^*(\dot{X} - \dot{\xi}) \quad (\text{optical sensor})$$

$$\alpha(S) = \frac{1}{L} \frac{X(S) - \dot{\xi}(S)}{(T_\alpha S + 1) \left(\frac{S^2}{\omega_T^2} + \frac{2\zeta_T}{\omega_T} S + 1 \right)} \quad (\text{Transverse Cable Dynamics})$$

Table 4.1

TROLLEY DRIVE SYSTEM PARAMETERS AS USED FOR THE SIMULATION

Coefficients for:	MOLAB	LSSM
M	68.4 slugs	68.4 slugs
B	0	0
F_o	5,660 lbs	1830 lbs
I/R	0.5 slug ft ²	0.5 slug ft ²
B_M	0	0
R	0.26 ft	0.26 ft
T_o/P_o	0.003 ft ³	0.003 ft ³
$q = d/2\pi\eta R$	0.0061 ft ²	0.0061 ft ²
ω_v	628 sec ⁻¹	628 sec ⁻¹
$k^* k_1^*$	1.35	1.35
$k_o^* k_1^*$ (optical sensor)	0.0046	0.0046
k_2^*	$0.207 \times 10^{-7} \text{ ft}^5/\text{lb sec}$	$0.207 \times 10^{-7} \text{ ft}^5/\text{lb sec}$
T_α : L=30'	0.031 sec	0.028 sec
50'	0.052 sec	0.047 sec
90'	0.094 sec	0.085 sec
130'	0.135 sec	0.122 sec
170'	0.177 sec	0.160 sec
ω_T	67.0 sec ⁻¹	73.0 sec ⁻¹
ζ_T (estimated)	0.1	0.1

where

$$\begin{aligned} M &= \text{trolley mass} \\ F_O &= \text{nominal total cable tension} \\ I &= \text{motor and winch moment of inertia} \\ F_D &= \text{trolley driving force} \\ q &= \frac{d}{2\pi\eta R} = \text{relative motor displacement} \end{aligned}$$

The other parameters are defined in Section 2.

The numerical values for all system parameters are listed in Table 4.1.

Disturbance Inputs

In order to simulate worst cases as outlined in the contract specifications, the following types of disturbances were selected for all runs. (See Table 4.2.)

Table 4.2
ACCELERATION DISTURBANCES AS USED DURING DYNAMIC
TROLLEY DRIVE SYSTEM SIMULATIONS

Type of LSV	Initial State	Disturbance	Final State
LSSM	$\dot{X} = \dot{\xi} = V_{\max} = 8.2 \frac{\text{ft}}{\text{sec}}$ $\ddot{X} = \ddot{\xi} = 0$	$\ddot{X} = -2 \text{ g}$ -1.4g -0.8g -0.1g	$\dot{X} = \dot{\xi} = V_{\max} - 4 \frac{\text{ft}}{\text{sec}}$ $= 4.2 \frac{\text{ft}}{\text{sec}}$
MOLAB	$\dot{X} = \dot{\xi} = V_{\max} = 18.25 \frac{\text{ft}}{\text{sec}}$ $\ddot{X} = \ddot{\xi} = 0$	$\ddot{X} = -2 \text{ g}$ -1.4g -0.8g -0.1g	$\dot{X} = \dot{\xi} = V_{\max} - 4 \frac{\text{ft}}{\text{sec}}$ $= 14 \frac{\text{ft}}{\text{sec}}$

Maximum velocity as initial state was considered the most severe case because this implied that the trolley had to be decelerated from the state of maximum kinetic energy.

The duration of the decelerating disturbance was varied such that a constant velocity reduction of 4 ft/sec was obtained. This was considered a realistic procedure because it resulted in very short pulses for the high-g cases and longer pulses for low decelerations as may be expected from typical obstacle and terrain geometry.

During the simulations, the cable length was varied from 30 ft to 170 ft for each type of vehicle and disturbance.

Two typical simulations at maximum deceleration are recorded in Figure 4.29 for the LSSM and in Figure 4.30 for the MOLAB.

Errors at Constant Velocity - There is a steady-state horizontal displacement $(X - \xi)_{ss}$ and cable misalignment α_{ss} due to the constant velocity $\dot{X} = \dot{\xi} = V_{\max}$ prior to the disturbance in each case. For the 50 ft cable length, the maximum steady-state displacements and misalignments were found to be

$$\text{LSSM: } \text{Max } (X - \xi)_{ss} = 0.04 \text{ ft} = 0.48 \text{ in.}$$

$$\text{Max } \alpha_{ss} = 0.0008 \text{ rad} = 0.046 \text{ deg}$$

$$\text{MOLAB: } \text{Max } (X - \xi)_{ss} = 0.085 \text{ ft} = 1.02 \text{ in.}$$

$$\text{Max } \alpha_{ss} = 0.0017 \text{ rad} = 0.1 \text{ deg}$$

More meaningful data are obtained by expressing these errors in terms of erroneous horizontal forces acting on the LSV.

As can be read from Figure 4.31 the horizontal force and corresponding acceleration error is

$$\begin{aligned} \Delta F_H &\approx -F_o \alpha \\ \Delta \ddot{X} &= \frac{\Delta F_H}{m} = \frac{-5/6 m g \alpha}{m} = \frac{5}{6} \alpha g \end{aligned} \tag{4.1}$$

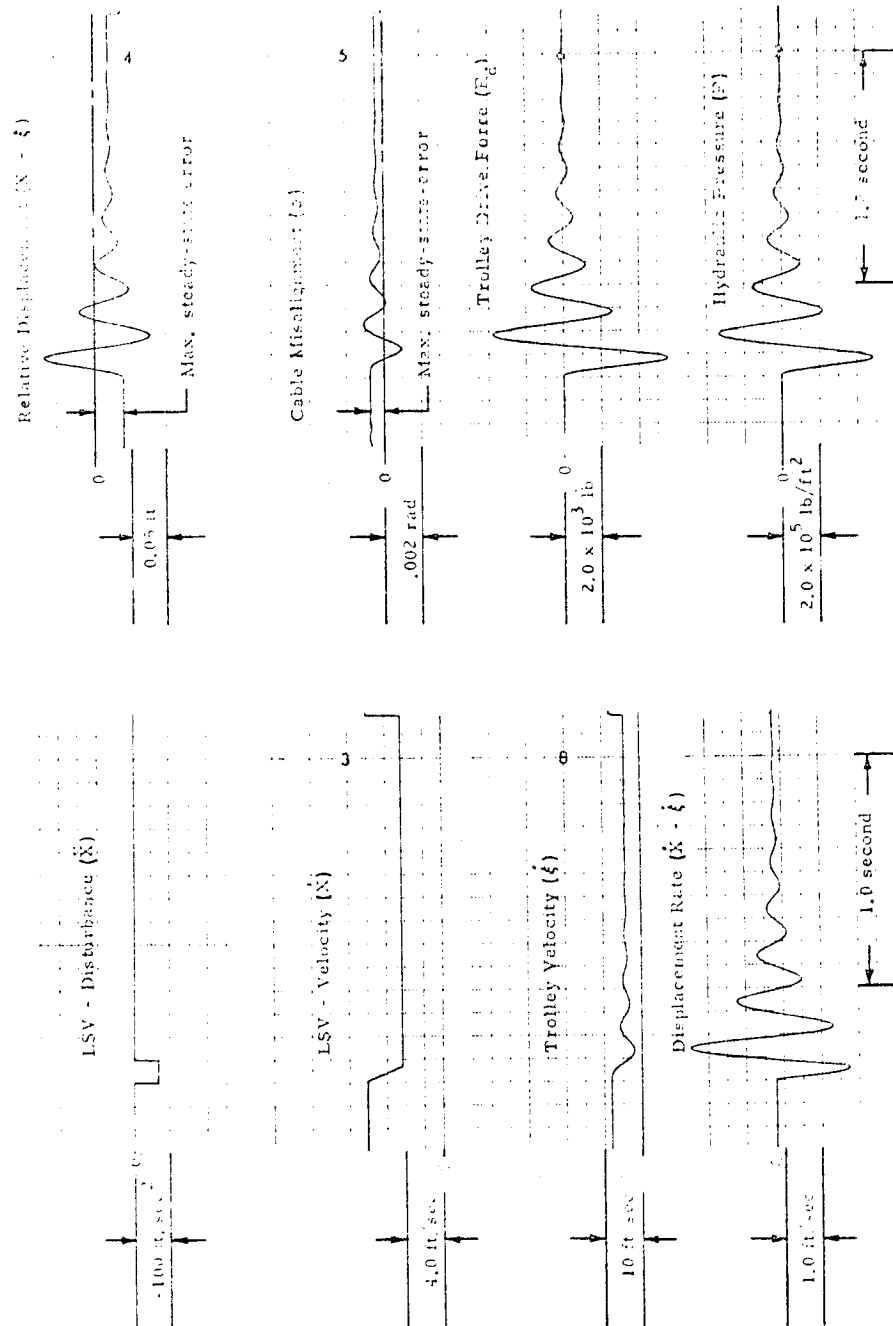
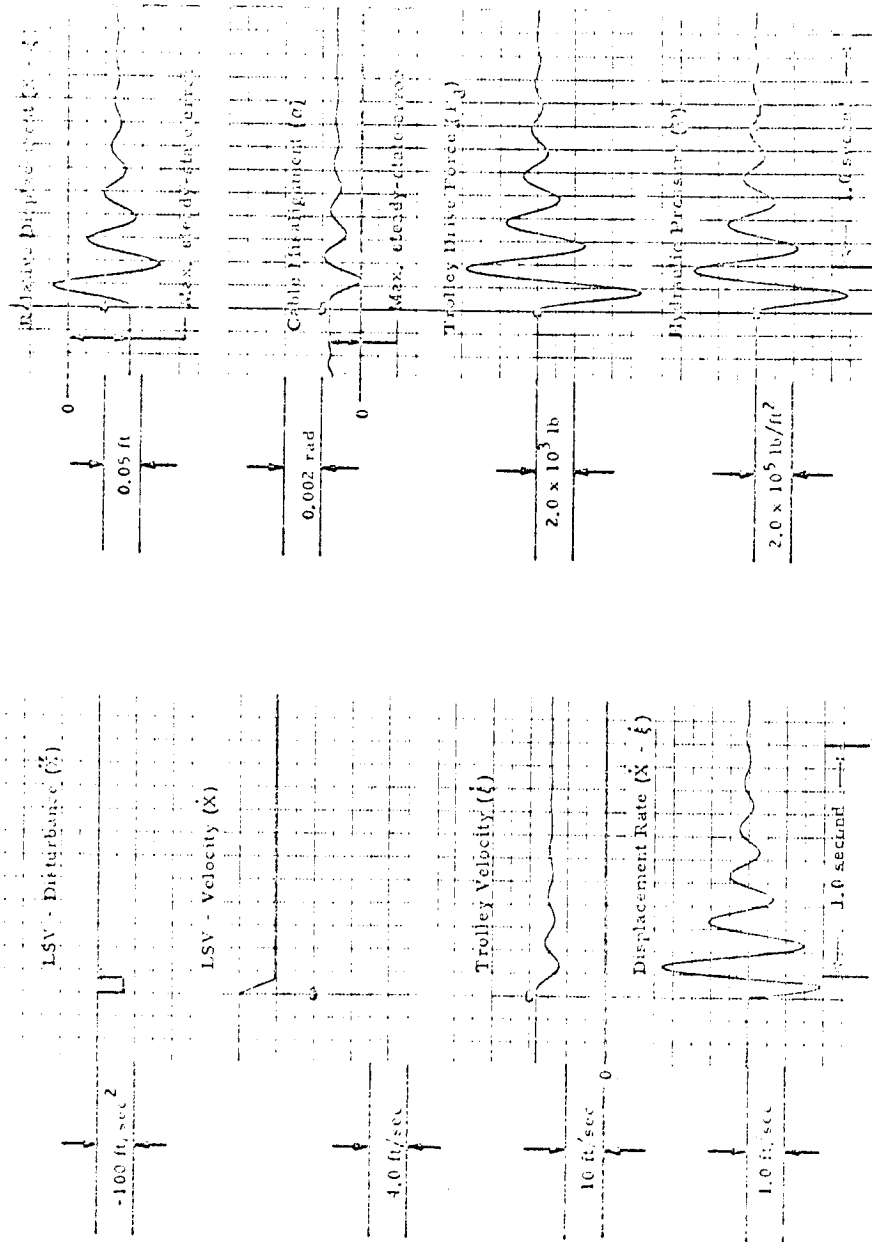


Figure 4.29 - Trolley Drive System Response Characteristics (LSSM Vehicle)



$\ddot{X} = -2g$
 $\dot{X} = \dot{X}_0 = 18.25 \text{ ft/sec (initial)}$
 Cable Length = 50 ft

Figure 4.30 - Trolley Drive System Response Characteristics (MOLAB Vehicle)

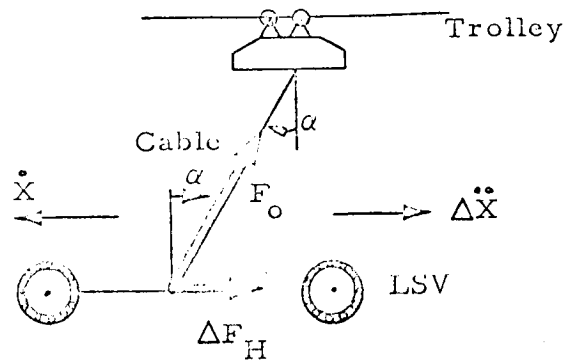


Figure 4.31 - Trolley/LSV Force Diagram

Using Equation (4.1), the maximum steady-state acceleration errors for the two cases of Figures 4.29 and 4.30 are

$$\text{LSSM: } \text{Max } \Delta \ddot{X}_{ss} = -0.0007g$$

$$\text{MOLAB: } \text{Max } \Delta \ddot{X}_{ss} = -0.0017g$$

The corresponding values for the full range of cable lengths investigated are plotted in Figures 4.32 and 4.33 as maximum steady-state errors. These values seem well within the admissible range.

A 5 Hz oscillation is observed due to the disturbing deceleration. The assumed hydraulic system pressure of 3000 psi is slightly exceeded during the first peak. It is possible to increase system pressure up to 4500 psi using the same hardware as described in Section 2. A slight increase to 3500 psi would be sufficient, however, to prevent pressure saturation in this worst case. Less overshoot and better damping can be obtained in the final design by adding a compensating filter.

Peak Errors after Disturbance \ddot{X}

Larger errors are encountered during transients caused by decelerations \ddot{X} . The peaks for these errors under various cable lengths are plotted in Figure 4.32 for the LSSM and in Figure 4.33 for the MOLAB. As the acceleration error is proportional to the cable misalignment α , more favorable results are obtained with increasing cable length. This trend is due to the displacement sensing concept applied where there are virtually no adverse effects of large cable lengths on the sensor performance. It is felt that with the angle sensing concept, it would be difficult, if not impossible, to obtain as tight a control as is predicted for the displacement sensing or optical sensing method.

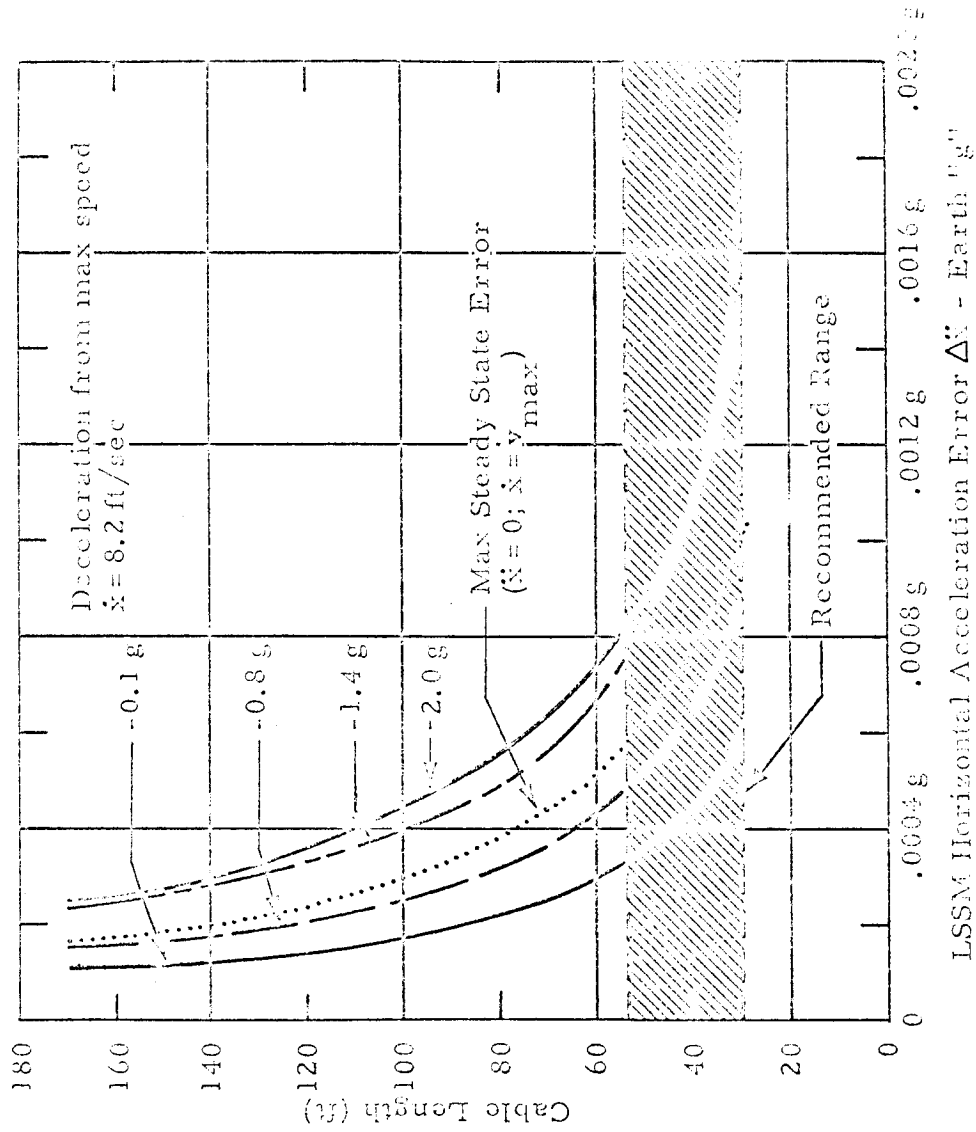


Figure 4.32 - Effect of Cable Length on the Horizontal Acceleration Error for Various Decelerations. \dot{x} from max LSSM - Velocity $\dot{x} = 8.2$ ft/sec. Trolley Drive System Senses Displacement ($x - \hat{x}$) and Displacement rate ($\dot{x} - \dot{\hat{x}}$) as Described in Section 2.2.

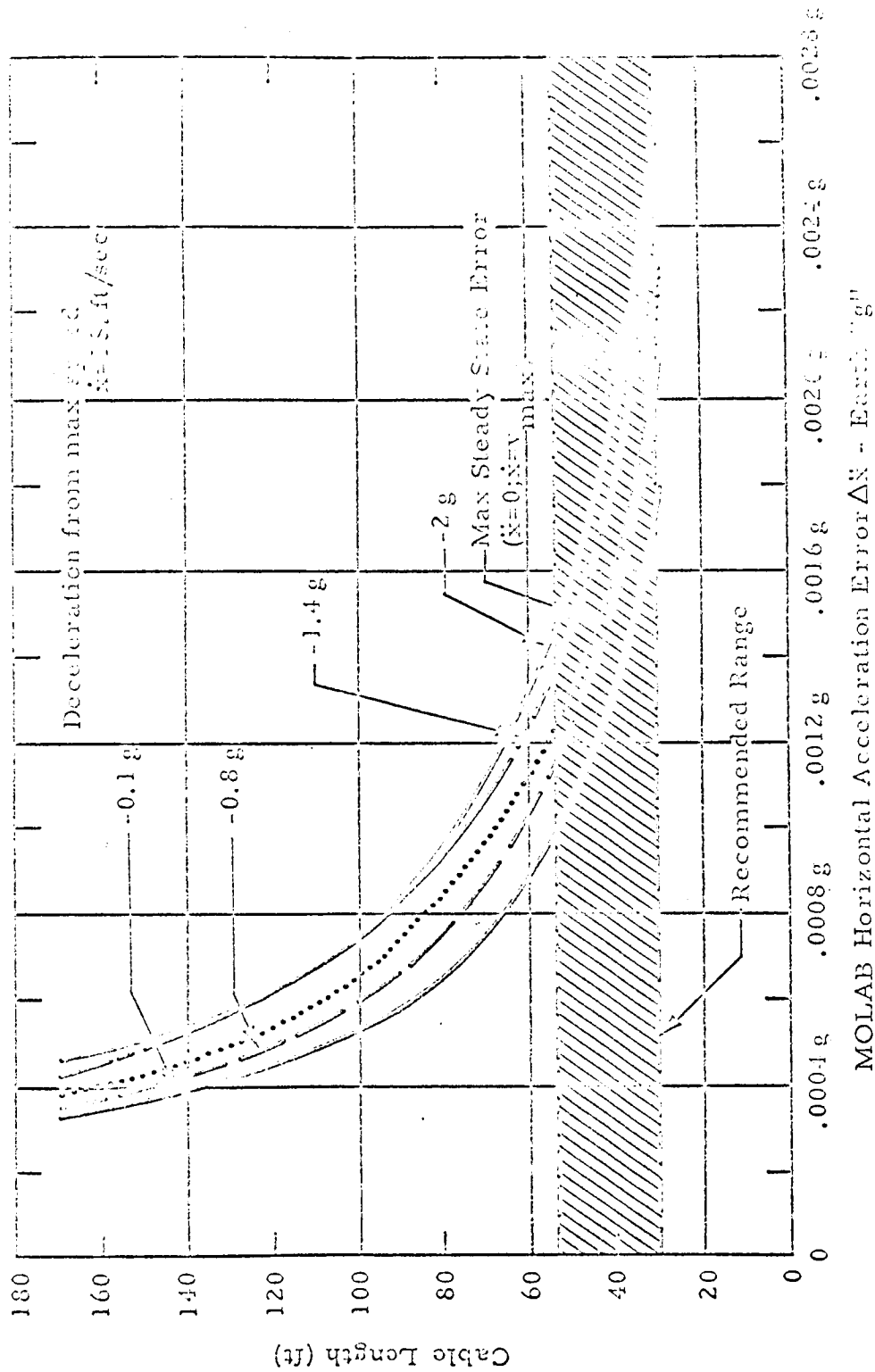


Figure 4.33 - Effect of Cable Length on the Horizontal Acceleration Error for Various Decelerations, \ddot{x} from max MOLAB - Velocity $\dot{x} = 18.25 \text{ ft/sec}$. Trolley Drive System Senses Displacement ($x - \xi$) and Displacement rate $\dot{x} - \dot{\xi}$ as Described in Section 2.2.

Section 5

2-D LCS DESIGN AND COMPONENT SPECIFICATIONS

5.1 LCS SYSTEM DESCRIPTION - 2-D CONFIGURATION

Figure 5.1 illustrates the basic design concept for the two-dimensional LCS system configuration. This system would consist of the following sub-assemblies: the lunar surface vehicle chassis and wheel interfaces, suspension cables and winches, vehicle suspension platform (main vehicle and trailer), the suspension platform support trolley and drive mechanism, the overhead rail support structure, and the suspension system control and checkout console.

5.1.1 Vehicle Chassis and Wheel Interface

The vehicle chassis support frame would be constructed of a simple lightweight tubular truss frame, with the lower end attached to hard points on the chassis primary structure. The upper end would terminate with an omni-ball joint, located on the vehicle pitch axis and permitting complete suspension cable freedom through a 35° cone (static condition). The same type of structure would be located at the CG of the vehicle trailer (Boeing configuration only). The force sensing of the vehicle would be accomplished by placing a load cell between the omni-ball joint and the suspension cable. The vehicle wheel interface would consist of a support frame assembly that would attach to the outer face of the vehicle wheel hub. The assembly is composed of a mounting flange that would act as the interface for a bearing located in a housing, connected to a tubular frame yoke. The yoke ends would support ball end joints that would be located at the wheel suspension system roll axis (through CG). Two cables would attach to the joints and be connected together above the CG. This arrangement would also allow for a 35° cone of cable freedom. The force sensing would be provided by instrumenting the yoke with strain gages, thereby measuring frame deflection.

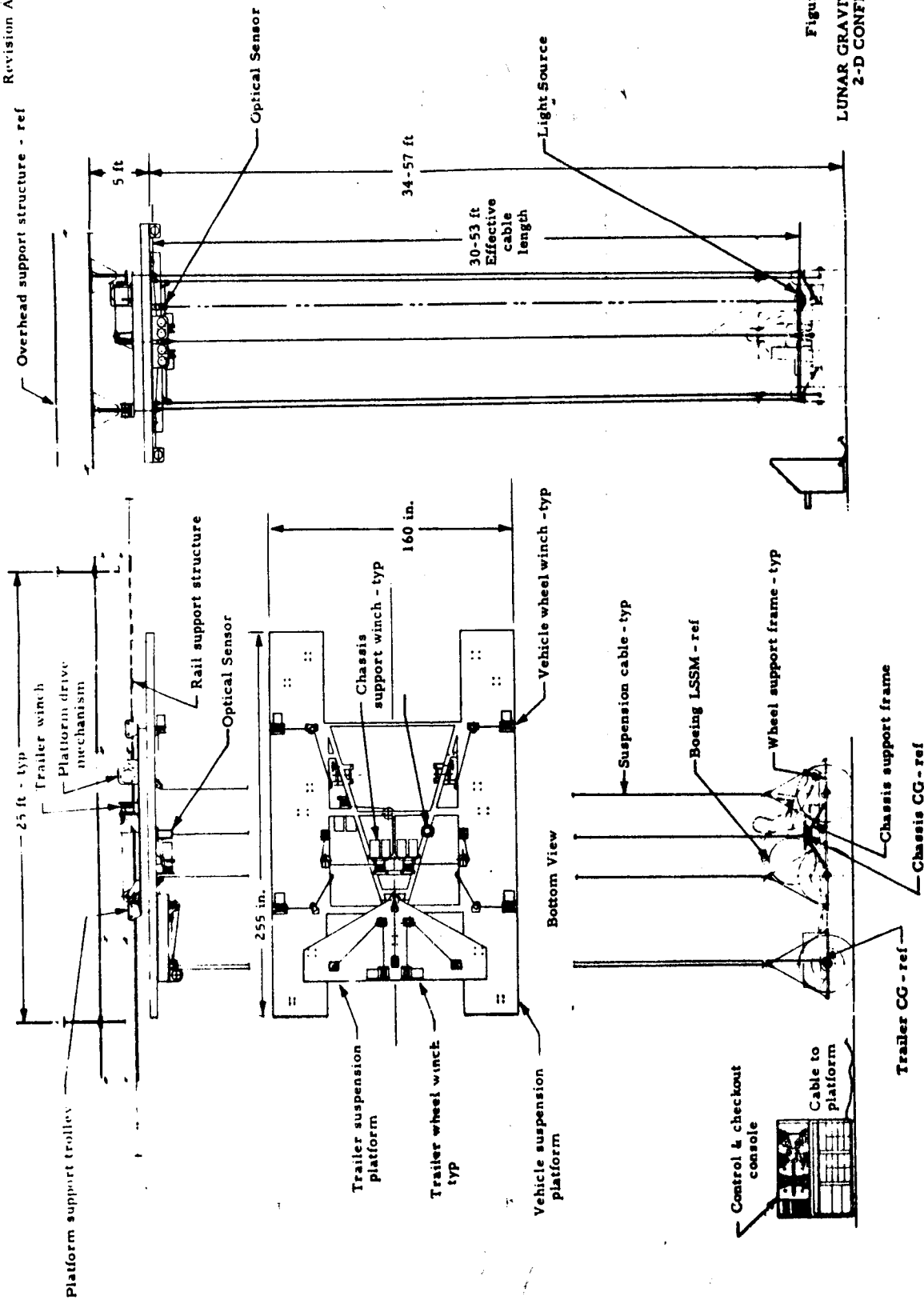


Figure 5.1

LUNAR GRAVITY SIMULATOR
2-D CONFIGURATION

5.1.2 Suspension Cable and Winch Subassembly

The $1/6$ g condition of the LSV will be maintained by supporting $5/6$ of the weight of the vehicle chassis and wheels by the use of constant force suspension cables, attached to the interface and that are reeved by hydraulic powered, servo actuated drum winches, mounted on the suspension platform. The length of the cables will be about 60 feet. The cables will have an electrical conductor core for signal transmission.

5.1.3 Vehicle Suspension Platform

The vehicle suspension platform consists of a main vehicle support structure and a trailer support structure that are mounted on the bottom of the main structure. The trailer structure is mounted to a bearing on the main structure. The bearing will be locked out for the 2-D mode, but used to pivot the trailer in the 3-D configuration. The support structures are composed of lightweight welded aluminum channels and I-beams. The outer sections of the main platform and the trailer support will have an aluminum Honeycomb panel covering on the bottom, with winch and cable pulley mounting holes on a grid pattern, with three-inch centers. This will facilitate almost any mounting location. A suspension platform weight summary is shown in Table 5.1.

5.1.4 Support Trolley and Drive Mechanism

The suspension platform will be attached to a rail support structure by four trolley assemblies, one at each corner of the main load carrying structure. The platform will be driven fore and aft by two servo actuated, hydraulic motor driven capstans. A cable will run the full length of each of the rail support structures, and will be looped around each capstan. Each end of the cables will be anchored with an adjustable tensioning element.

Table 5.1
VEHICLE SUSPENSION PLATFORM
WEIGHT SUMMARY

<u>Component</u>	<u>Weight, lb</u>
<u>Vehicle Platform</u>	
Structure	921
Honeycomb panels	222
Wheel winches and pulleys (4 sets)	128
Chassis winches and pulleys (3 sets)	285
Trolley assembly (4 sets)	220
Captan and motor (2 sets)	120
Hydraulic power supply and electric drive motor	520
	<hr/>
Sub-Total	2416
 <u>Trailer Platform</u>	
Structure	128
Wheel winches and pulleys (2 sets)	64
Honeycomb panels	54
	<hr/>
Total	2642

5.1.5 Rail Support Structure

The rail support structure will consist of two steel I-beams, approximately 250 feet in length. The rail may house linear commutators that will contact electrical wipers on the suspension platform, to transmit force control sensing, servo amplifier, and other types of signals between the force sensors at the vehicle and the control/checkout console and servo valves on the cable winches. This system appears sound, but further study should be undertaken to assure good signal transmission. The rail support structure will need overhead support at about 25 feet intervals and be capable of supporting a 12,000 lb rolling load and the load from the crane rail (two rails at 80 lb/ft).

5.1.6 Suspension System Control and Checkout Console

The suspension system control and checkout console will consist of a modified component rack cabinet with the representative vehicle schematic on an inclined panel. Each wheel and chassis attachment point will be shown with a digital voltmeter and adjusting potentiometer located adjacent. A checkout panel would also be included with a functional array of illuminated push button switches, that would check a system and readout to a common digital voltmeter. The console may be used to calibrate the system by the following procedure:

- Adjust wheel suspension control potentiometers until the proper weight is reached (the wheel suspension weight would have already been established).
- Adjust vehicle chassis control potentiometer until the vehicle is lifted off the ground. (Align CG if vehicle does not rise in a level fashion.)
- Calculate 5/6 of vehicle chassis and wheel suspension system weight and adjust potentiometers to read this weight.

The console would contain up to 40 servo amplifiers for the force control system and trolley drive system. Additionally, appropriate power supplies will be required for the servo amplifiers and other electrical elements. In all probability, temperature conditioning of the console will be required for the critical electronic elements.

5.2 STRUCTURAL ANALYSIS OF THE LGS SUSPENSION PLATFORM

A structural analysis of the main platform was performed by the Structural Analysis group using the Lockheed FRAME computer program. The platform structure was designed using aluminum beam and channel sections. All members are welded at the joints, resulting in an indeterminate structure. Beam sizes were selected by a preliminary analysis.

The math model used for analysis was composed of 45 members and 31 joints as shown in Figure 5.2. The pivot point (Joint 31) was selected as the origin of the coordinate system and the 2-3 axes form a plane of symmetry.

The applied load conditions were the 10,000 pound scaled-up versions of the Boeing MOLAB and the Bendix MOLAB vehicles plus the platform structural and component weights and forces.

The computer output gives the deformation at each joint and the resultant forces and moments for each loading configuration in three orthogonal planes. In addition, stiffness and flexibility matrices of the structure is included in the results.

The input structural member sizes and weights are tabulated in Table 5.2. The recommended changes in structural member sizes listed in the comments are based on the vertical joint deflections listed in Table 5.3. Stresses and deflections in the other planes were negligible. Additional computer runs should be made to assure that the complete structure is adequate and attempt substitution of lighter members to minimize the structural weight. Also, a frequency analysis is needed to determine the platform's natural frequency at key support points. These tasks should be the initial steps for the detail design of the suspension platform structure.

Table 5.2
MAIN SUPPORT PLATFORM STRUCTURE

Member No.	Connects Joints	Member Size, Type, wt/ft	Length (in)	Comments
1	1 3	4 in channel 1.85	35.00	<div> <div>↓</div> <div>Increase to 6 in channel 2.83</div> <div>↓</div> <div>Decrease to 12 in channel 7.41</div> <div>↓</div> <div>Increase to 12 in channel 2.83</div> </div>
2	4 2	↓	35.00	
3	7 1		70.00	
4	2 8		70.00	
5	3 9		70.00	
6	4 10		70.00	
7	5 6	12 in I-Beam 10.99	14.00	
8	5 7	↓	38.00	
9	6 8		38.00	
10	7 9	6 in channel 2.83	35.00	
11	10 8	↓	35.00	↓
12	5 11	12 in channel 7.41	10.98	
13	6 12	↓	10.98	
14	11 29		19.87	
15	12 30		19.87	
16	11 12		20.40	
17	29 30	6 in channel 2.83	32.00	
18	29 13	12 in channel 7.41	37.12	
19	30 14	↓	37.12	
20	7 15	12 in I-Beam 10.99	65.00	
21	8 16	↓	65.00	
22	9 19	6 in channel 2.83	65.00	
23	10 20	↓	65.00	
24	13 14		53.70	
25	13 15	12 in I-Beam 10.99	18.15	
26	14 16	↓	18.15	
27	15 17		15.00	
28	16 18		15.00	
29	17 19		20.00	
30	18 20		20.00	

Table 5.2(Continued)
MAIN SUPPORT PLATFORM STRUCTURE

Member No.	Connects Joints		Member Size, Type, wt/ft	Length (in)	Comments
31	13	21	12 in channel 7.41	61.73	<div style="display: flex; align-items: center; justify-content: center;"> <div style="margin-right: 10px;">↓</div> <div style="margin-right: 10px;">↓</div> <div style="margin-right: 10px;">↓</div> <div style="margin-right: 10px;">↓</div> <div style="margin-right: 10px;">↓</div> <div style="margin-right: 10px;">↓</div> <div style="margin-right: 10px;">↓</div> <div style="margin-right: 10px;">↓</div> <div style="margin-right: 10px;">↓</div> <div style="margin-right: 10px;">↓</div> </div>
32	22	14		61.73	
33	15	21	12 in I-Beam 10.99	59.00	
34	16	22		59.00	
35	19	23	6 in channel 2.83	59.00	
35	24	20		59.00	
37	21	22		90.00	
38	23	21		35.00	
39	22	24		35.00	
40	25	21	4 in channel 1.85	61.00	
41	22	26		61.00	<div style="display: flex; align-items: center; justify-content: center;"> <div style="margin-right: 10px;">↓</div> <div style="margin-right: 10px;">↓</div> <div style="margin-right: 10px;">↓</div> <div style="margin-right: 10px;">↓</div> <div style="margin-right: 10px;">↓</div> </div>
42	23	27		61.00	
43	28	24		61.00	
44	27	25		35.00	
45	26	28		35.00	

Table 5.3
VERTICAL DISPLACEMENT OF JOINTS

Joint No.	Vertical Displacement		Recommendations and Comments
	Bocing MOLAB	Bendix MOLAB	
1	.100 (.029)	.917 (.268)	Increase Member 3 to 6 in channel
2	.102 (.029)	.920 (.269)	Increase Member 4 to 6 in channel
3	.146 (.043)	1.361 (.398)	Increase Member 5 to 6 in channel
4	.148 (.043)	1.363 (.398)	Increase Member 6 to 6 in channel
5	.037 (.061)	-.012 (-.019)	Reduce Members 7, 8 to 12 in channel
6	.037 (.061)	-.012 (-.019)	Reduce Members 7, 9 to 12 in channel
7	0	0	—
8	0	0	—
9	.077 (.008)	.393 (.039)	Increase Member 10 to 12 in channel
10	.078 (.008)	.393 (.039)	Increase Member 11 to 12 in channel
11	-.144	-.089	—
12	-.144	-.089	—
13	-.135	-.275	—
14	-.137	-.275	—
15	-.013	.088	—
16	-.014	.086	—
17	.088	.398 (.250)	Due to the Redistribution of the Loads, the Deflections of these Joints should be Reduced to Acceptable Limits
18	.088	.397 (.250)	
19	.223	.807 (.290)	
20	.224	.807 (.290)	
21	0	0	—
22	0	0	—
23	.391 (.039)	.840 (.084)	Increase Member 38 to 12 in channel
24	.391 (.039)	.841 (.084)	Increase Member 39 to 12 in channel
25	.761 (.222)	.014 (.004)	Increase Member 40 to 6 in channel
26	.721 (.211)	.015 (.004)	Increase Member 41 to 6 in channel
27	1.116 (.326)	.977 (.286)	Increase Member 42 to 6 in channel
28	1.084 (.317)	.981 (.287)	Increase Member 43 to 6 in channel
29	-.277	-.215	—
30	-.277	-.215	—
31	-.076	-.060	—

NOTE: The deflections in parenthesis are the estimated deflections after the recommended changes in structural members.

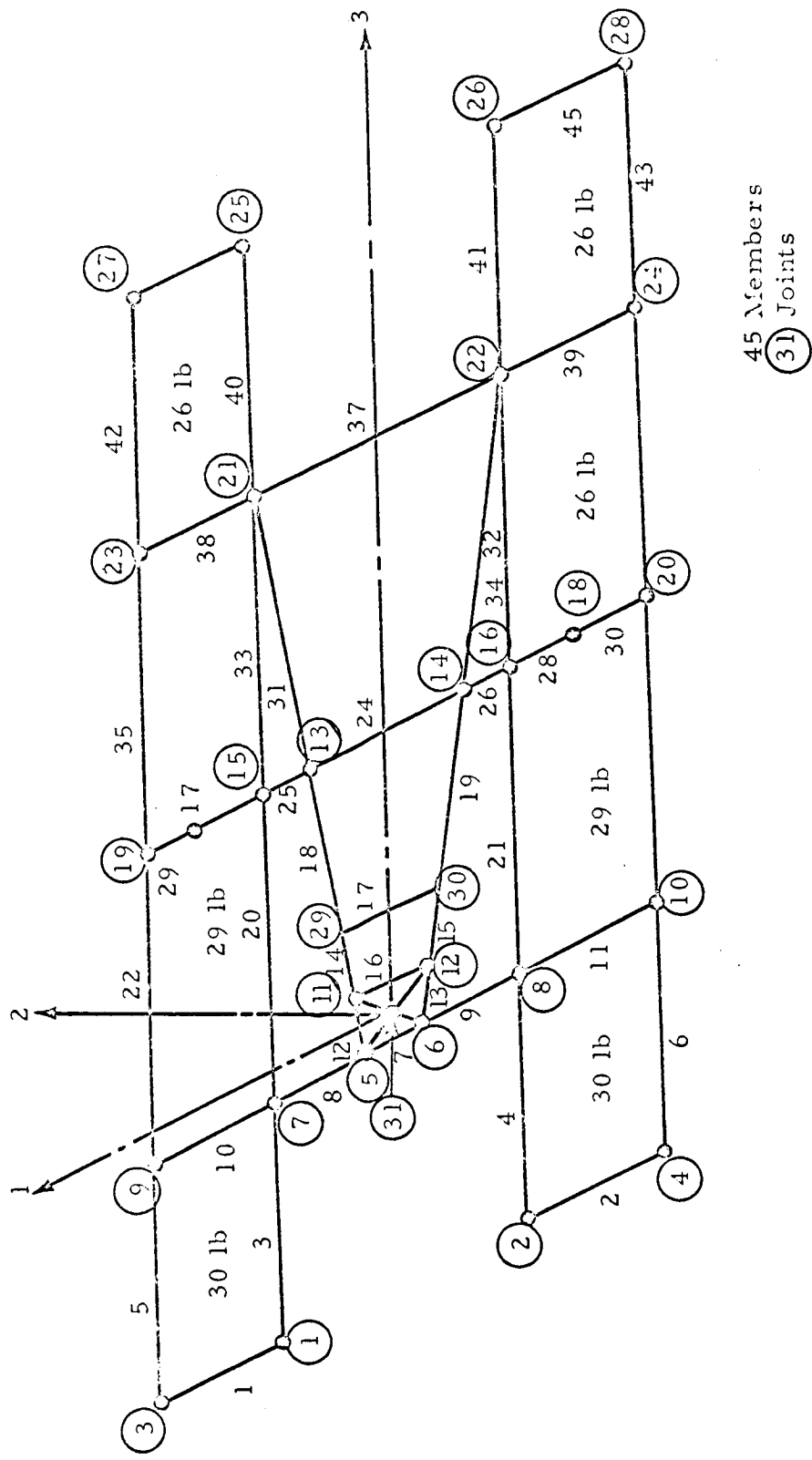


Figure 5.2 - Joint-Member Orientation

5.3 WHEEL SUPPORT SYSTEM

In the First Interim Report, Reference 1, it was recommended that the wheel suspension systems should be given further study. The chart in Figure 5.3 compares three potential wheel support methods. The curved beam support has the prime drawback of interference under design roll and pitch conditions. The axial hub support is adequate on all respects, except it will have a large offset moment. The frame support system was selected for a more detailed study because it minimized the objectionable features of both the other systems.

Figure 5.4 illustrates the proposed wheel frame support configuration. A tubular frame is attached to the bearing housing and the ends are curved such that the line of action passes through the wheel's center of gravity. Strain gauges are mounted as close to the center of the bearing housing as possible. This is to minimize the error caused by the suspension system's inertia during vertical accelerations. This is discussed in detail in Section 5.3.2. Other features include a bearing in the mounting flange and universal joints at the cable attachment points, providing the necessary freedom in wheel pitch and roll motions.

5.3.1 Frame Support Analysis

The frame support concept was analyzed for a natural frequency of 40 cps for 4 configurations: Bendix LSSM, Boeing LSSM, Bendix MOLAB, Boeing MOLAB. The respective wheel weights used were 80, 60, 212, and 160 lbs.

The equation for natural frequency is from Reference 3. The natural frequencies of beams in flexure are:

$$f_n = C_n r/L^2 \times 10^4 \times Km$$

$$f_n = n^{th} \text{ natural frequency, cps}$$

$$C_n = \text{frequency constant - as listed in table according to support method and mode}$$

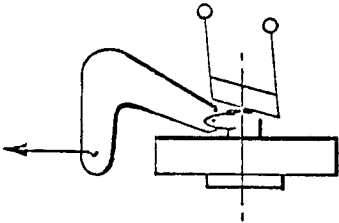
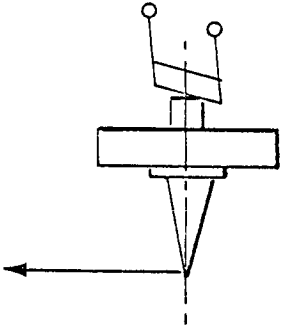
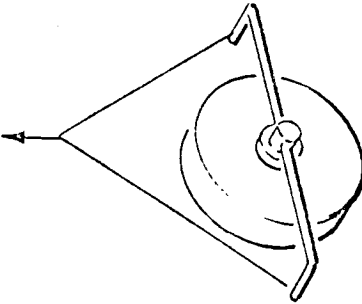
Type	 1 Curved Beam	 2 Axial Hub Support	 3 Frame Support
Weight Factor	Medium	Light	Heavy
Offset Error	Small	Maximum	Minimum
Interference (Roll & Pitch)	Chassis or Wheel Interference on Roll	None	None
Cost	Moderate	Minimum	Moderate
<u>Preferred System</u>			

Figure 5.3 - Comparison of Wheel Suspension Systems

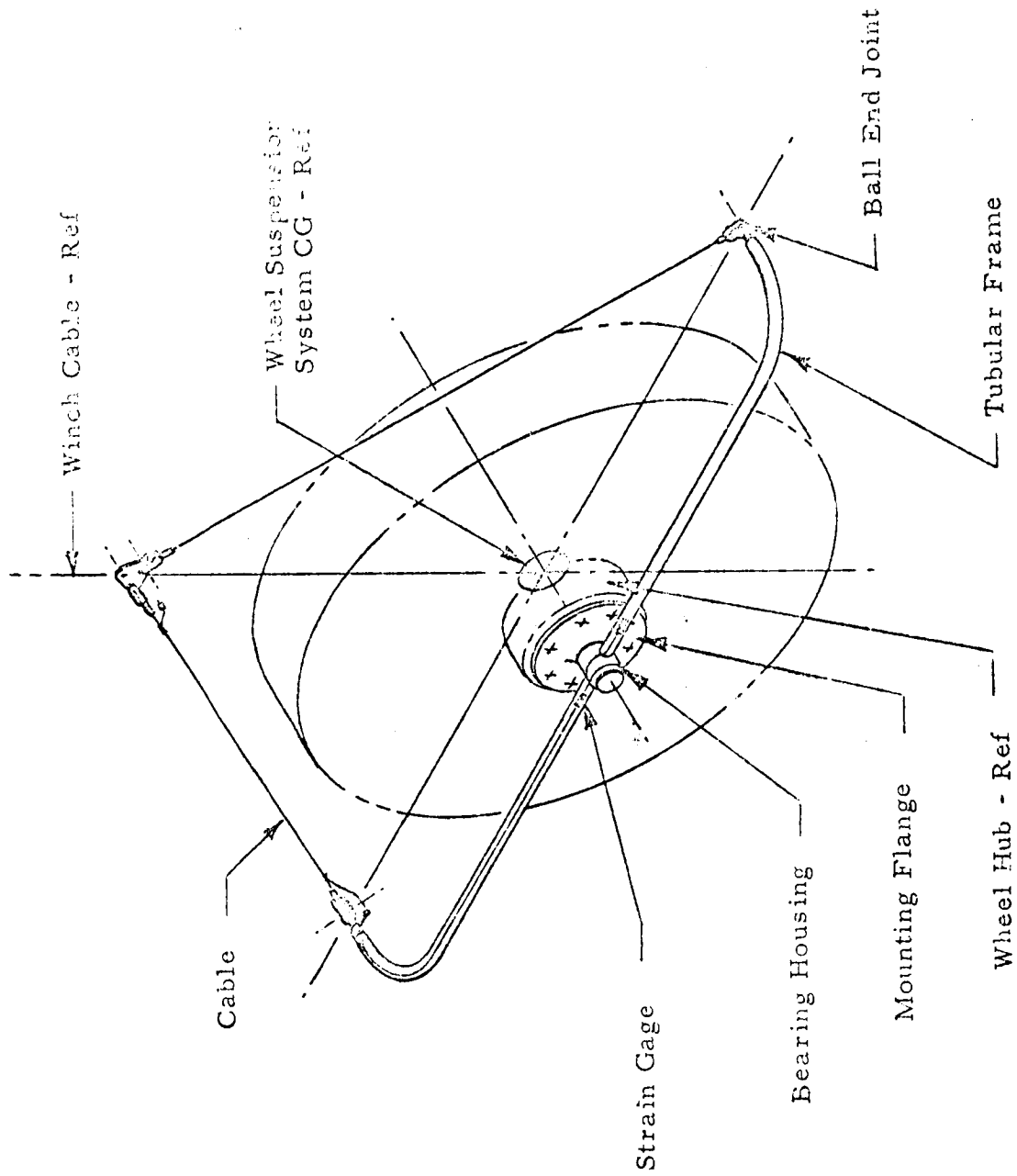


Figure 5.4 - LGS Wheel Support Frame

r = radius of gyration of cross-section = $\sqrt{I/A}$ inches

L = beam length inches

K_m = material constant (Table 6.10) = 1.00 for steel, (.985 for aluminum)

The support frame is free to rotate about the axle pitch axis. The type of fixity used is that of a cantilever beam for each end of the support with $n = 1$, therefore, $C_n = 11.30$.

The frequency equation was transposed so that radius of gyration,

$$r = f_n L^2 / C_n \times 10^4 \times K_m$$

Tubular cross-sections were chosen on the basis of the radius of gyration calculation.

Stresses were checked by the formulae from Reference 4 , which defines

$$S_{n(max)} = 1/2 Z (M + \sqrt{M^2 + M_t^2})$$

where:

$S_{n(max)}$ = maximum normal stress

Z = section modulus (I/c)

M = bending moment

M_t = torsional moment

Also, from Reference 4 ;

$$S_{s(max)} = 1/2 Z \sqrt{M^2 + M_t^2}$$

where

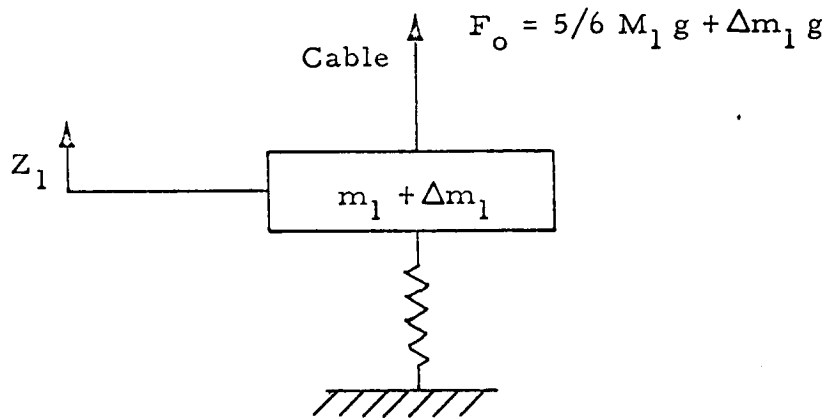
$S_{s(max)}$ = maximum shear stress

The results of these analyses are plotted as Support Frame Weight vs Wheel Diameter for the 4 lunar vehicles (Figure 5.5). The comparison between steel and aluminum is shown. Aluminum fabrication is more desirable for minimizing weight especially for larger wheel sizes, and for minimizing error due to wheel accelerations.

5.3.2 Dynamic Error from Frame Support Mass

The error introduced by vertical wheel acceleration due to the additional inertia of the suspension system must be analyzed:

At nominal state:



During Transients

$$\text{Ideal cable force } F = F_o + \Delta m_1 \ddot{z}$$

Now, applying this to the LSSM vehicle as an example:

$$\begin{aligned} w_1 &= 80 \text{ lbs} \\ 5/6 m_1 g &= 67 \text{ lbs} \quad \therefore F_o = 67 + 8 = 75 \text{ lbs} \\ \Delta m_1 g &= 8 \text{ lbs} \end{aligned}$$

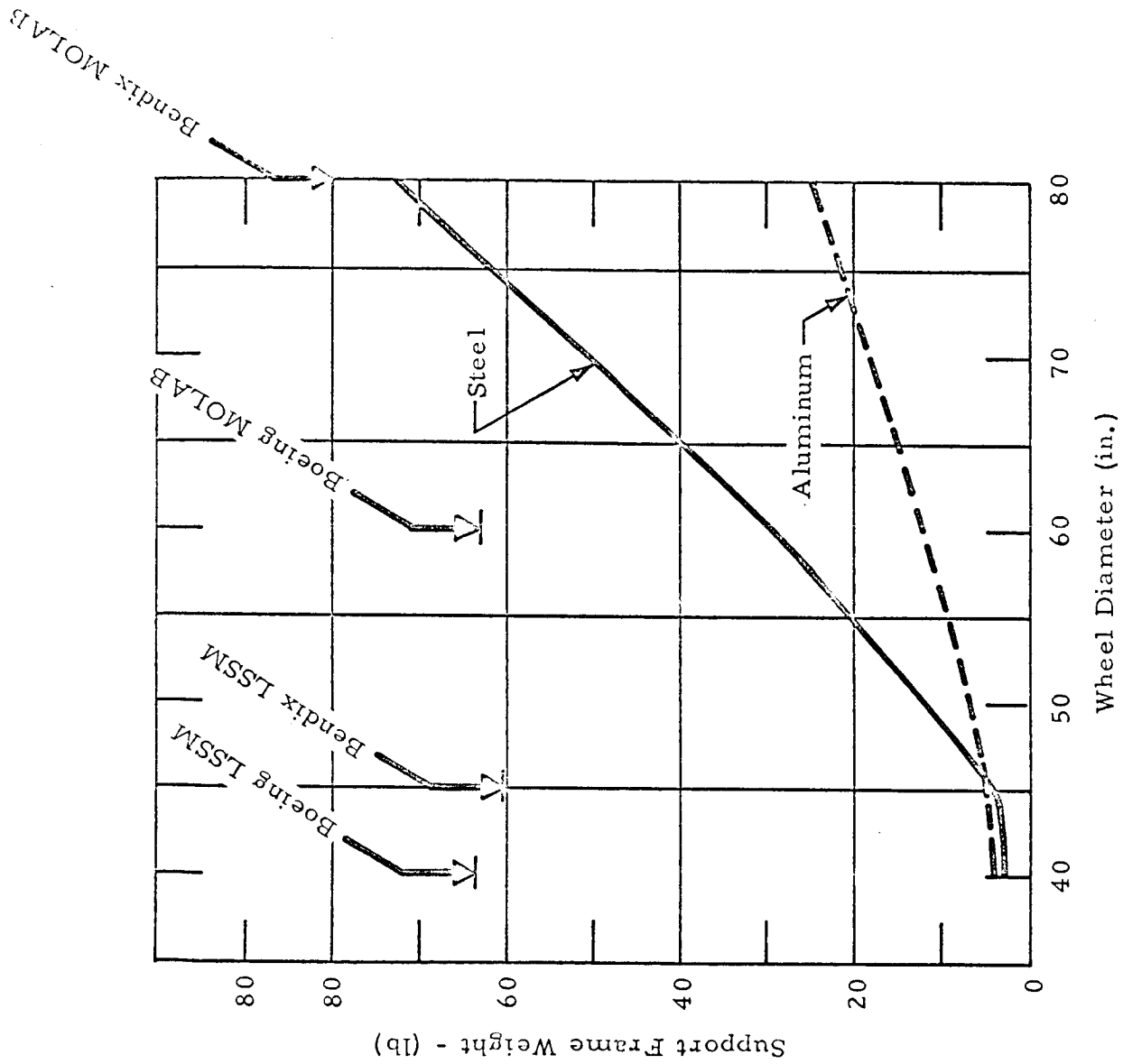


Figure 5.5 - Support Frame Weight vs Vehicle Wheel Diameter

Using the 2 g acceleration (design limit)

$$F_{\text{ideal}} = F_o + 2(8) = 83 \text{ lbs}$$

or

$$F_{\text{ideal}(\text{peak})} = 1.24 F_o$$

This means that during the peak of the wheel hub acceleration, the cable should ideally support 1.24 times its nominal load in order to compensate for the suspension system weight.

Therefore, although the suspension system weights only 10 percent of the wheel weight, it introduces a 24 percent error in cable force (or 120 percent lunar g error). This emphasizes the need to minimize the suspension system weight. Additional studies must be made to utilize higher strength-to-weight materials such as magnesium, fiber glass wound beams and other light construction mediums.

It should be pointed out that for the LSSM vehicle, a 2 g vertical acceleration is equivalent to a 1 foot obstacle, as shown in Figure 4.1, in Section 4.2. By limiting the obstacle height to 1/2 foot, this decreases by half the error in cable force.

The dynamic error from the frame support mass may be minimized by mounting the force sensing strain gauges on the tabular frame as near as possible to the wheel's center. Typical strain gage locations are shown in Figure 5.4.

5.4 WINCH AND MOTOR SYSTEMS

Winch and motor systems were designed to provide the constant force for supporting the LSV chassis and wheel assemblies. A cable winch drive assembly provides the necessary cable storage for a wide range of LSV vertical displacement (7 meters or approximately 21 ft). The winch drum is driven by a hydraulic motor which provides the torque necessary for a constant force in the cable. The following paragraphs describe the winch and motor system design parameters and preliminary system specifications.

In general, the winch and motor systems for the wheel and chassis suspension devices were designed to minimize the control requirements by emphasizing low inertia systems. This criterion was particularly significant because of the transient characteristics of the LSV support points and the desire to minimize force error at these points. The low inertia criteria essentially dictated a low-drive ratio between the motor and the winch drum, because the effective inertia of the motor rotating parts varied as the square of the drive ratio. Thus, a direct drive or 1:1 drive ratio was highly desirable.

Preliminary specifications for the chassis and wheel winch systems are outlined in Table 5.4. The cable nominal force range and the torque range are based on an LSV gross-weight range of 1,000 - 10,000 lb (450-4500 Kg). Wheel and chassis weights were proportioned approximately in accordance with the LSSM and MOLAB vehicles.

5.4.1 Winch Design

The winch designs for the chassis and wheel systems were patterned after conventional light-weight aircraft winch systems. The configurations are shown in Figures 5.6 and 5.7. The winch drums are designed to store a minimum of 25 ft (7.62 m) of cable in order to compensate for the LSV vertical translation. The drum pitch diameter was established at 6.0 in. (15.5 cm) or 20 times the maximum cable diameter of the chassis suspension cables (5/16").

Table 5.4
PRELIMINARY
LGS MOTOR/WINCH SPECIFICATIONS

LGS MOTION/WINCH DATA

Characteristic	Units	Chassis		Wheel	
		Min	Max	Min	Max
<u>Cable Data</u>					
Nominal Force	lb	354	3670	34.0	300
Diameter	in./ft	5/64	5/16	1/32	5/64
Weight/Feet	lb/ft	.0111	.167	.0016	.0111
Met. Area	ft ²	19.7 x 10 ⁻⁶	296 x 10 ⁻⁶	2.8 x 10 ⁻⁶	19.7 x 10 ⁻⁶
Met. Density	lb-sec ² /ft ⁴	17.5	17.5	17.5	17.5
Mod. Elasticity	lb/ft ²	18.2 x 10 ⁸	18.2 x 10 ⁸	18.2 x 10 ⁸	18.2 x 10 ⁸
Construction	—	7 x 7	7 x 7	1 x 7 & 1 x 19	1 x 7 & 1 x 19
<u>Winch Data</u>					
Pitch Diameter	in.	6.0	6.0	6.0	6.0
Nominal Torque	lb-in.	1060	11,000	102	900
Angular Velocity (St.State)	rpm	0	+ 20	0	+ 20
Cable Stor. Length	ft	25	25	25	25
Drive Ratio	— 2	3.14:1	3.14:1	1:1	1:1
Equiv. Mtr. Inertia	lb-in ²	155	310	9.53	9.53
Drive/Drum Inertia	lb-in ²	87	92	18.1	18.1
Total Mtr./Winch Inertia	lb-in.	242	402	27.6	27.6
*Angular Velocity (Peak Dynamic)	rpm	—	75	—	200
<u>Motor Data</u>					
Vickers Designation	—	MF-3921-30	MF-3921-30	MF-3918-25	MF-3918-25
No. Required	—	1	2	1	1
Torque at 3000 psi	in.-lb	—	1752	—	948
Displacement	in. 3/rev	3.671 (ea)	3.671 (ea)	1.986	1.986
Max. rpm at 3000 psi (Intermittent)	rpm	—	4000	—	4600

* Based on 1.0 ft obstacle at maximum vehicle velocity (LSSM and MOLAB)

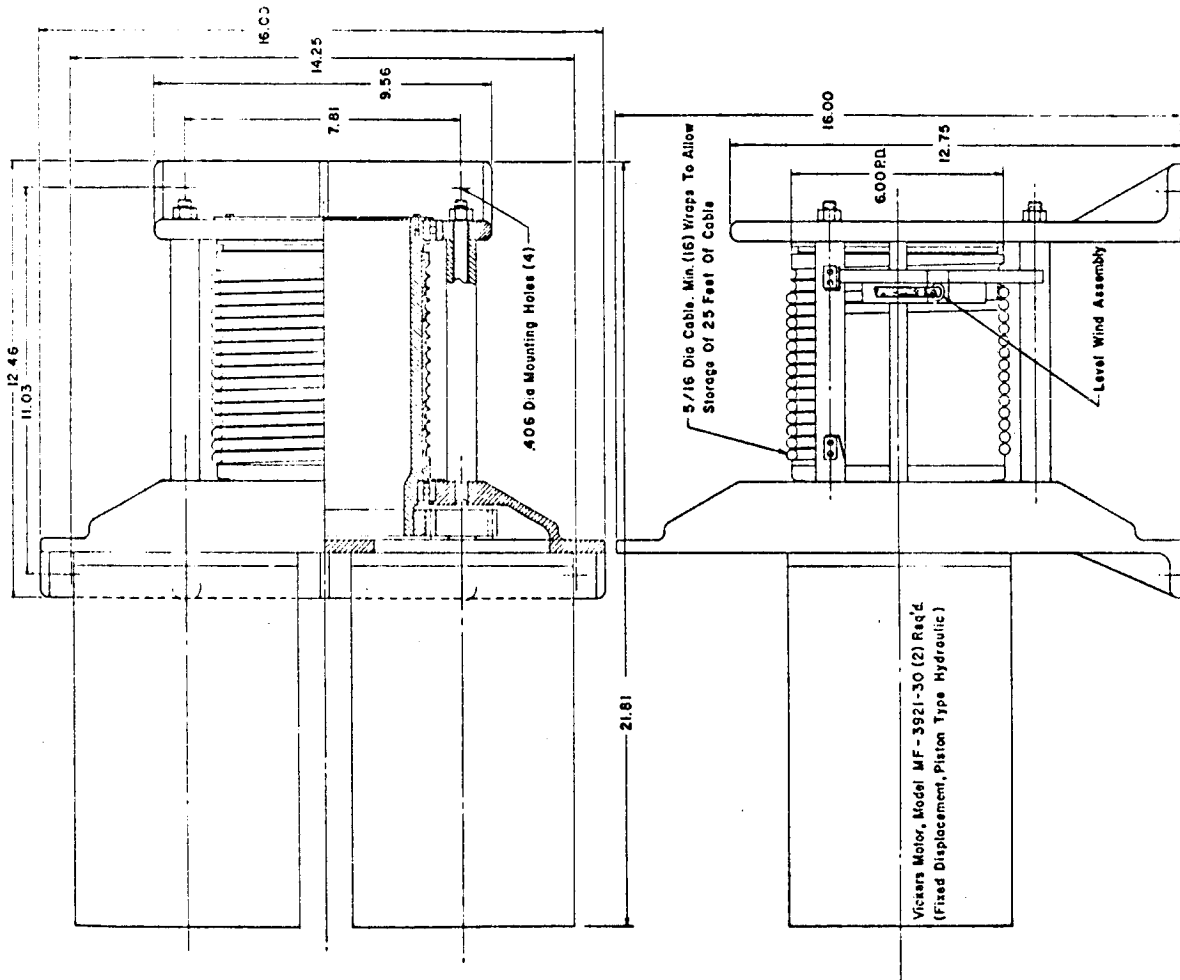


Figure 5.6 - Winch Assembly for Chassis Suspension System

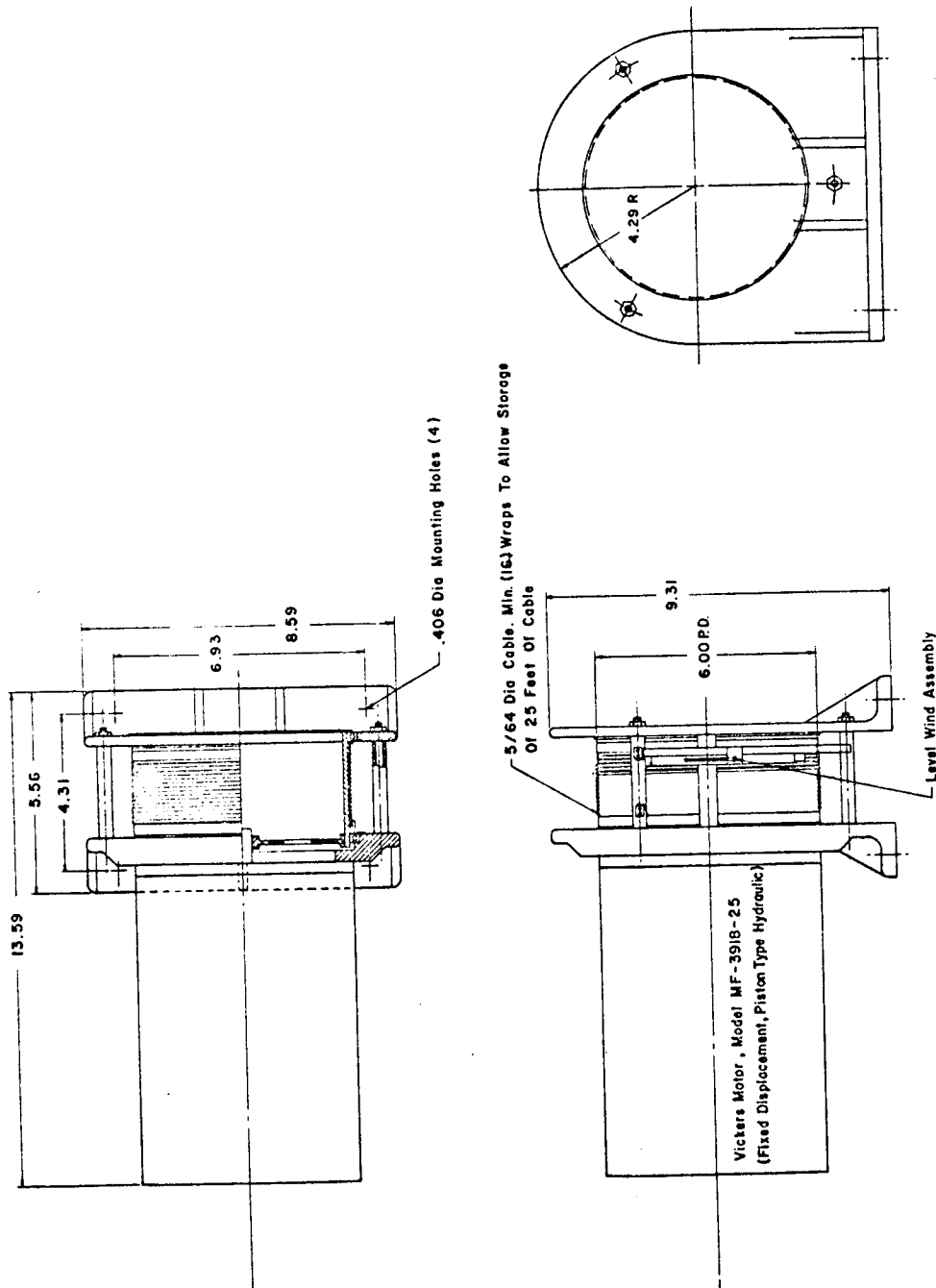


Figure 5.7 - Winch Assembly for Wheel Suspension System

Wheel suspension winch drums were made the same pitch diameter as the chassis drums. The winch drums in both cases are a split shell design (Figures 5.6 and 5.7) to accomodate a wide range of cable diameters required to suspend the 1000 lb (454 Kg) to 10,000 lb (4536 Kg) LSV weight range. Grooves in the drum shell and a cable device maintain the cable at a constant pitch radius for the full length of cable travel (or drum angular displacement).

5.4.2 Winch Motor Selection

The characteristics desired for the winch drive motors were:

- ability to maintain constant torque, when controlled by appropriate servo valves, over a wide range of motor speeds,
- operate in stalled condition (zero motor speed) over prolonged periods of time without damage,
- must be fully reversible and still maintain constant torque,
- low inertia of moving parts,
- high torque to weight ratio, and
- instantaneous response.

The type of motor found to be best suited for this application was the fixed-displacement piston type commonly used in the aerospace industry. Typical of this motor type are the Vickers, Inc., motors described in Figures 5.8 and 5.9*. The motor characteristics outlined were well within the torque and speed requirements of the chassis and wheel winch systems.

The hydraulic drive motor for the wheel winch was chosen on the basis of a 1:1 drive ratio and the maximum torque corresponding to the heaviest LSV wheel. The MF-3918-25 motor in Figure 5.9 was selected to accomodate the maximum nominal torque of 900 in.-lb. The corresponding motor weight of 22.1 lb was found acceptable, although it was recognized that this may be worthy of further investigation should motor weight become critical.

* Similar motors are available from other vendors.

Selection of the chassis winch motor was based upon a compromise of effective inertia of rotating parts and the hydraulic motor weight. The design torque of 11,000 in.-lb at the winch drum corresponds to the maximum chassis weight for a 10,000 lb (4500 Kg) LSV. Two of the MF-3921-30 motors driving each chassis winch were found to be the best choice. A higher torque winch would have reduced the motor rotating inertia, but the corresponding motor weight penalty was disproportionate for consideration.

VICKERS Fixed Displacement Piston Type Hydraulic Motors

3000 PSI SERIES

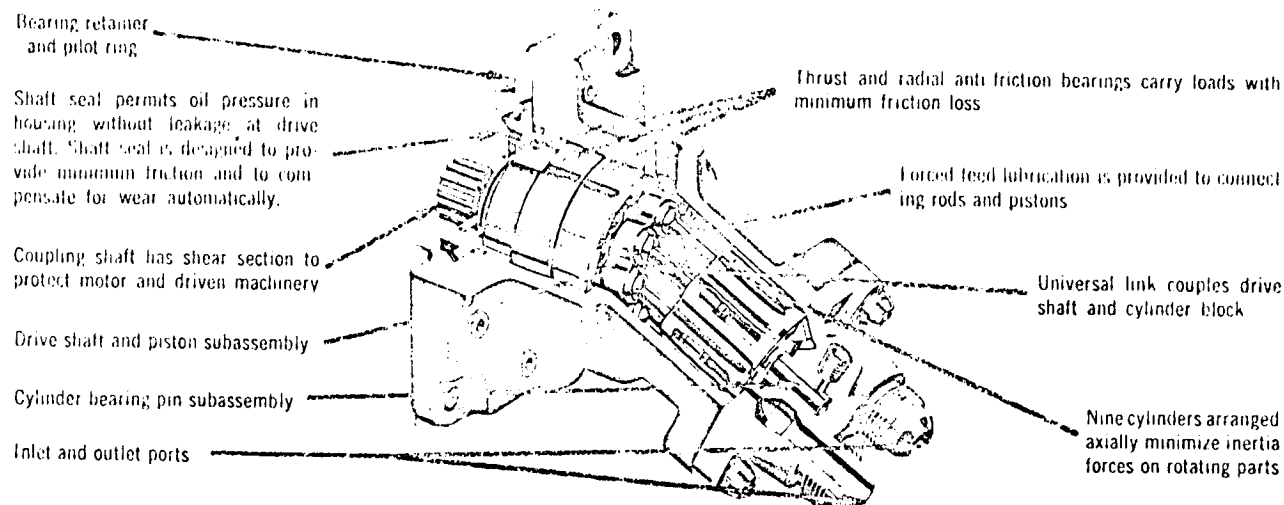


Figure 5.8

GENERAL DESCRIPTION

Vickers 3000 psi fixed displacement hydraulic piston-type motors are used in oil hydraulic circuits to convert hydraulic pressure to rotary mechanical motion. Full torque is instantaneously available. Rotation direction is determined by oil flow path through the motor. Speed control and rotation reversals are very simply and easily accomplished. Hydraulic motors can be used for dynamic braking, as stalling due to overload will not damage them. Operation can be continuous, intermittent, continuously reversing or stalled without damage to the motor when protected by proper system overload relief valve settings.

ACCELERATION

With zero external load, the acceleration for the MF-3906 motor at 3000 psi is 3.4×10^5 (radians/sec²); at 4500 psi it is 5.1×10^5 . The MF-3921 acceleration at 3000 psi is $.43 \times 10^5$ (radians/sec²); at 4500 psi it is $.64 \times 10^5$. These are theoretical maximums.

TIME CONSTANT

The time required to accelerate hydraulic motors from standstill to maximum intermittent speed with

no external load, using the torque available at 4500 psi, varies between .0028 sec for the 3906 size and .0065 sec for the 3921 size.

MINIMUM REVOLUTIONS TO STOP

Minimum number of revolutions to stop from maximum continuous speed is between .116 and .173 for all motor sizes. This is the angular distance the hydraulic motor will rotate before the back torque (assumed produced by 4500 psi) overcomes the kinetic energy of the rotating group. No load on the output shaft is assumed.

MOUNTING POSITION

There is no restriction in mounting position except that the drain line must be connected to the reservoir so the motor case remains filled with hydraulic fluid during all operations. Internal motor parts depend on this fluid for lubrication. Also, at installation, motor housing must be completely filled with hydraulic fluid.

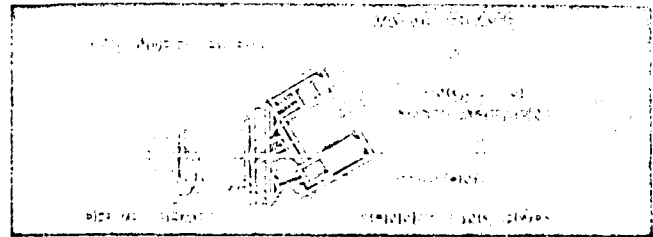
HYDRAULIC FLUID

Use mineral oil conforming to military specifications for aircraft hydraulic systems.

HOW THEY WORK

Vickers fixed displacement motors convert a continuous flow of hydraulic oil under pressure to rotary mechanical motion. Cylinder block is offset relative to the drive shaft causing the pistons to traverse their respective cylinder bores. As a piston moves away from the valve plate under pressure, the opposite bottomed piston moves toward the valve plate exhausting spent hydraulic oil. The nine pistons perform the same operation in succession so that the acceptance of hydraulic oil under pressure is continuous and the conversion to rotary motion is smooth.

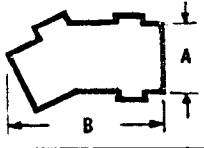
The housing is always full of oil, and during operation, nominal leakage past the pistons and valving surfaces of the cylinder block maintains lubricating oil flow through the housing. This flow returns to the reservoir through the case drain line.



Proper hydrostatic balance between cylinder block and valve plate provides necessary hold-down force for the block. Valving leakage is held to a minimum without producing excessive bearing pressure.

Axial cylinder arrangement minimizes inertia forces on rotating parts and eliminates the need for large bearings, permitting high rotative speeds. This feature, together with others briefly summarized in this bulletin, results in Vickers piston type hydraulic motors having the highest efficiency (both volumetric and overall) in the industry.

Figure 5.9

Series Model Number	Theoretical Displacement (cu in./rev)	Theoretical Flow at 1500 rpm (gpm)	Theoretical Torque at 3000 psi (in.-lb)	Theoretical Maximum Intermittent Power at 3000 psi (hp)	Weight (lb)	Maximum Recommended Speeds at 3000 psi			
						Continuous (rpm)	Intermittent* (rpm)		
MF-3906-15 MF-3906-20 MF-3906-25 MF-3906-30	0.049 0.065 0.080 0.095	0.318 0.422 0.519 0.617	23.5 31.1 38.4 45.4	4.9 6.6 8.1 9.6	2.1	10,000	13,300	2½ Sq.	4¼
MF-3907-15 MF-3907-20 MF-3907-25 MF-3907-30	0.097 0.128 0.159 0.188	0.632 0.835 1.032 1.221	46.4 61.4 75.8 89.7	7.8 10.3 12.8 15.1	4.1	8000	10,600	4¼ Sq.	4¾
MF-3909-15 MF-3909-20 MF-3909-25 MF-3909-30	0.190 0.251 0.310 0.367	1.234 1.630 2.013 2.383	90.7 119.9 148.1 175.2	12.2 16.2 20.0 23.6	4.9	6400	8500	4¼ Sq.	5½
MF-3911-15 MF-3911-20 MF-3911-25 MF-3911-30	0.310 0.409 0.507 0.598	2.013 2.656 3.292 3.883	147.8 195.4 241.4 285.6	16.9 22.3 27.7 32.6	6.8	5400	7200	4¼ Sq.	5¾
MF-3913-15 MF-3913-20 MF-3913-25 MF-3913-30	0.492 0.650 0.803 0.950	3.195 4.221 5.214 6.169	234.8 310.2 383.4 453.6	23.1 30.5 37.7 44.6	10.0	4700	6200	4¼ Sq.	6¾
MF-3915-15 MF-3915-20 MF-3915-25 MF-3915-30	0.786 1.039 1.284 1.519	5.104 6.747 8.338 9.864	375.3 496.0 612.9 725.1	31.6 41.7 51.6 61.0	16.5	4000	5300	6 Dia.	8½
MF-3918-15 MF-3918-20 MF-3918-25 MF-3918-30	1.216 1.607 1.986 2.349	7.896 10.435 12.896 15.253	580.6 767.2 948.0 1122.0	42.4 56.0 69.2 81.9	22.1	3500	4600	6 Dia.	8¾
MF-3921-15 MF-3921-20 MF-3921-25 MF-3921-30	1.900 2.511 3.103 3.671	12.338 16.305 20.149 23.838	907.2 1198.8 1481.3 1752.5	57.6 76.1 94.0 111.3	32.6	3000	4000	6¼ Dia.	10¾
MF-3924-15 MF-3924-20 MF-3924-25 MF-3924-30	3.040 4.017 4.964 5.873	19.730 26.070 32.216 38.116	1452.2 1918.1 2370.1 2804.1	78.3 103.5 127.9 151.3	44.5	2500	3400	9¼ Dia.	11¾

*For higher speed requirements, consult Vickers Application Engineer. Also, see speed range chart on next page.

5.5 TROLLEY DRIVE SYSTEM REQUIREMENTS

The power requirements for the platform drive system is derived from the design guideline which requires the vehicle to be able to travel at a forward speed of 20 kilometers per hour and provide enough reserve power for a 2 g acceleration. Applying this requirement to the simulator platform;

$$HP = FV/550$$

where

$$F = \text{Trolley platform weight} \times \text{acceleration}$$

and

$$V = \text{forward speed, ft/sec}$$

$$V = 18.25 \text{ ft/sec}$$

The nominal weight of the platform is 2500 lbs, thus,

$$HP = \frac{2500(2)(18.25)}{550} = 166 \text{ hp, peak}$$

The nominal horsepower requirement is power required under a 0.1 g acceleration:

$$HP_{(nom)} = \frac{2500(.1)(18.25)}{550} = 8.3 \text{ hp}$$

It is noted that there is a 20 to 1 ratio of peak to nominal horsepower.

The drive system torque requirements are based on other considerations of the system. In order to limit the maximum tension in the suspension cables, a large diameter cable is preferable. However, to keep the bending stresses in the cable low, a large diameter capstan would be required. This in turn causes a large inertial force and reduces the capability of the system to react to sudden changes. Since the largest cable force is

$$F = 1/2 m g_t = 1/2 (2500/g) 2 g = 2500 \text{ lbs,}$$

(assuming two capstan drives for symmetry) a 5/16 inch diameter cable would provide an adequate margin of safety after pretensioning. The diameter of the capstan was taken as 20 times the cable diameter, or 6.25 inches, in order to minimize cable bending stresses.

This combination gives a required capstan torque,

$$T_c = F r = 2500 \times 3.125 = 7820 \text{ in-lb.}$$

Two Vickers fixed displacement motors, Series Model Number MF-3924-20 (see Figure 5.9) provides adequate power and torque for our application. This motor has the capability of producing 151 hp at a continuous speed of 2500 rpm, using an input pressure of 3000 psi. By using a speed reducer or belt drive, the speed required by the capstan (669 rpm) can be achieved. The drive ratio would be 2.78:1 and the corresponding maximum input motor speed would be 1860 rpm.

5.6 HYDRAULIC POWER SUPPLY REQUIREMENTS

Hydraulic motors were chosen to provide power for the chassis winches, wheel winches and the trolley drive motors. The motors which seem most suitable for this application were a series of Vickers fixed displacement piston type hydraulic motors designed to operate at 3000 psi. The chief advantages of these motors are the high acceleration and deceleration rates that are available.

In order to supply the required power, the hydraulic power of each system was estimated as described below.

Chassis Motors

Three pairs of Vickers MF-3921-30 motors were chosen for this application. The required flow is $q_c = QR_c$, where η is the number of motors required, Q is the flow in cubic inches per motor revolution and R_c is the motor to winch drive ratio, or $q_c = 6(3.671)(3.14)/1728 = 40.05 \times 10^{-3}$ cu ft/winch revolution. The flow rate,

$$Q_c = q_c \dot{\theta} = \frac{q_c \dot{Z}_c}{2\pi R_c},$$

where \dot{Z}_c is cable velocity in feet per second and R_c is the winch pitch radius in feet, or

$$Q_c = 25.5 \times 10^{-3} \dot{Z}_c.$$

The steady state values of \dot{Z}_c for the MOLAB vehicle were obtained from Bendix MOLAB data. (See Figure 4 of Reference 5.)

Wheel Motors

A maximum of six winch motors will be required for the six-wheeled version of the MOLAB. A single Vickers MF-3918-25 motor will be required for each wheel winch assembly. For each winch the flow is $q = 6(1.986)(1)/1728 = 6.9 \times 10^{-3}$ ft³/winch revolution and

$$Q_w = \frac{6.9(10^{-3}) \dot{Z}_w}{2\pi R_w} = 4.4 \times 10^{-3} \dot{Z}_w \text{ for } R_w = .25 \text{ ft.}$$

For steady-state cases, \dot{Z}_w and \dot{Z}_c have the same value.

Trolley Drive System

The selection of these motors is discussed in the previous section. Two motors were used to provide for balanced yaw moments. As before, $q = 2(5.873)(2.78)/1728 = 18.9 \times 10^{-3} \text{ ft}^3$, and

$$Q_d = \frac{18.9(10^{-3}) \dot{X}_d}{2\pi \left(\frac{6.25}{2 \times 12} \right)} = 11.6 \times 10^{-3} \dot{X}_d,$$

where \dot{X}_d is the vehicle's horizontal velocity component.

Power Supply Requirements

The total required flow rate, Q_T is the sum of the above systems

$$\begin{aligned} Q_T &= Q_c + Q_w + Q_d \\ &= 25.5(10^{-3}) \dot{Z} + 4.4(10^{-3}) \dot{Z} + 11.6(10^{-3}) \dot{X} \\ Q_T &= 29.9(10^{-3}) \dot{Z} + 11.6(10^{-3}) \dot{X} \end{aligned}$$

From this equation, Figure 5.10 was plotted from the data in Figure 4 in Reference 5, on vertical and horizontal velocities for various terrain slopes. The maximum flow of 78.7 gal/min occurs at a slope of -3.5 degrees; that is, when the vehicle is traveling down a slope of 3.5 degrees.

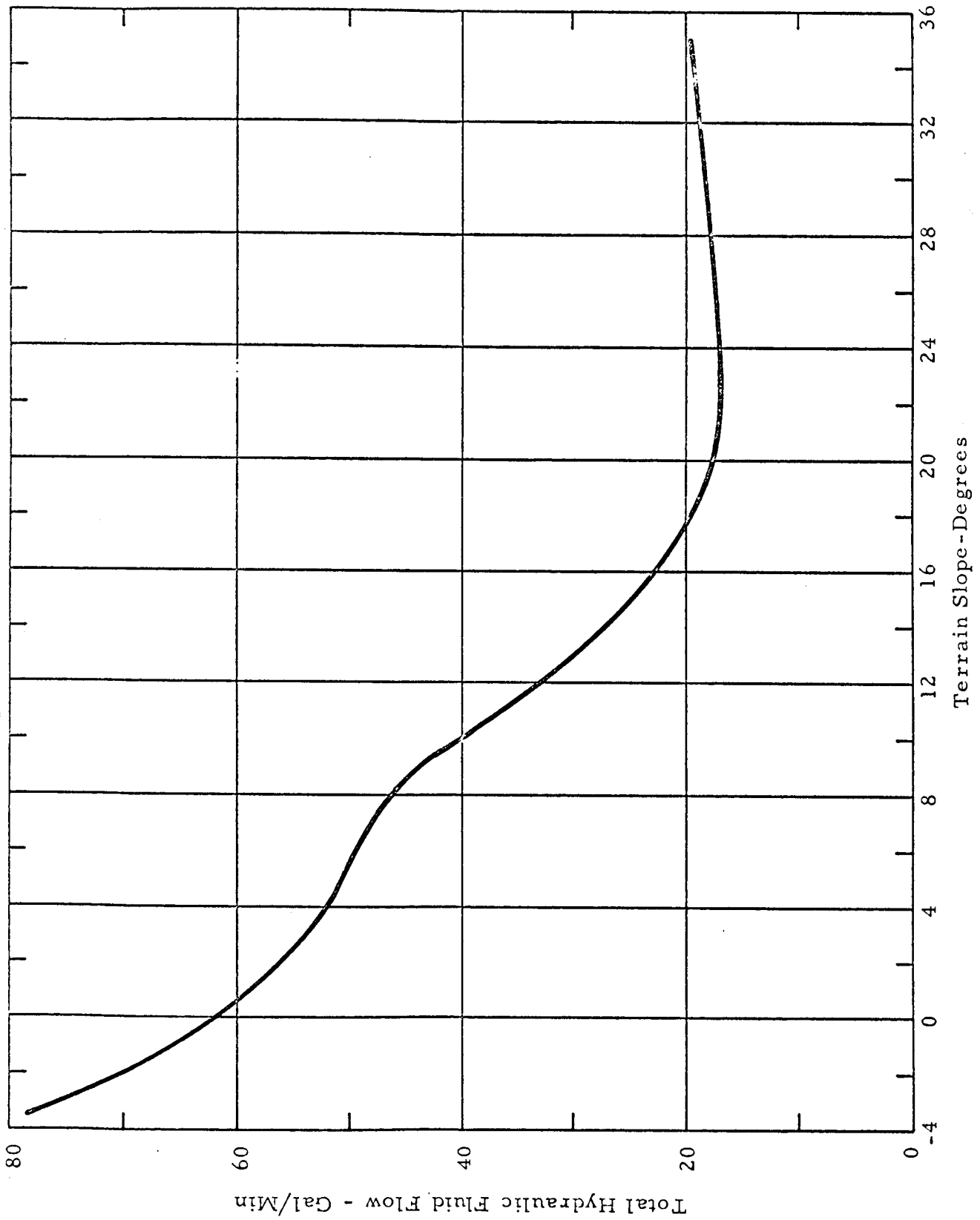


Figure 5.10 - Total Hydraulic Fluid Flow vs Terrain Slope

Since each motor is designed to operate at 3000 psi, the supply pressure must be higher. Therefore, assuming a 3500 psi supply pressure, the motor horsepower must be

$$HP = \frac{PQ}{1715} \quad \text{where } Q \text{ is flow rate in gal/min}$$

P is in psi

$$= \frac{(3500)(78.7)}{1715}$$

$$HP = 179$$

Hydraulic Pump

Comparisons of hydraulic pumps led to the choice of two Vickers PV3044 inline piston pumps because of their high horsepower to weight ratio, rapid response and reasonable cost. Although the pump is only rated at 87.8 hp, while 89.5 hp is required, this pump exceeded the 5650 rpm and 3050 psi rated pressure by 25%, for over half the 750 hour test during a recent MIL-P-19692B specification qualification. This would amount to 50.5 gpm pump flow rate which is 133 horsepower.

Finally, two electric motors are needed. Each must deliver approximately 100 horsepower at approximately 6000 rpm in order to compensate for system efficiency.

Electric Motor

An aircraft type motor designed by Westinghouse was chosen. This motor has an output of 100 hp at 8000 rpm and at 400 Hertz. The high frequency allows the motor to be of very light weight (about 165 pounds). An alternate motor built by TRW and is described in Reference 1 may be even lighter. The Westinghouse motors weigh 330 pounds and will require a reduction gear each, giving a total weight of 400 pounds for 200 hp output, or 1/2 hp per pound of motor. The ironless motors by TRW will produce about

2 hp per pound of motor but additional development would be necessary for these motors.

It must be pointed out that these power requirements were based on steady state conditions. Accumulators in the supply pressure lines will provide the transient hydraulic power for the wheel, chassis and trolley drive system dynamic requirements.

Section 6

2-D LUNAR GRAVITY SIMULATOR COST ANALYSIS

The costs of a two-dimensional LGS are presented in Table 6.1, with a design and fabrication schedule in Figure 6.1. A total cost of \$418,500 is estimated for a 50-week program. A fee of \$31,400 ($7\frac{1}{2}\%$) is estimated for a total of \$449,900. This estimate is based on the following assumptions.

1. A minimum cost straight-line system was assumed as a basis of costing. Other approaches such as an oval track system may approach the cost of a 3-D system.
2. A suitable building will be available for the installation of the rail support structure. A suitable building would give clear dimensions of 250 feet long (probable minimum) by approximately 64 feet high. The costs of the rails and cross members with installation labor is included in this estimate; however, the costs of modification of the building to provide the necessary support structure is not included.
3. Labor costs are based on \$12 per hour for project, research and design specialists; \$10 per hour for analysis, engineering and testing; and \$8 per hour for shop labor and drafting time.
4. The overall schedule is dependent on vendor's quoted long lead time of certain procured items, notably the chassis and wheel winches. Any reduction of this time can reduce the overall schedule as much as 6 weeks.
5. Costs of modification of the LSV are not included in this estimate.
6. Analog and digital computer costs were estimated at \$100 and \$450 per hour, respectively.

Additional design efforts may eliminate some of the custom designed items, resulting in a reduction of cost and schedule time.

Table 6.1
COST ANALYSIS SUMMARY
TWO-DIMENSIONAL LUNAR GRAVITY SIMULATOR

<u>Initial Design Phase</u>	3750 Manhours	11 Weeks	\$ 67,900
Stress Analysis	530 Hours		
Design and Analysis	1700 Hours		
Drafting	1060 Hours		
Programmer	460 Hours		
Analog Computer	220 Hours		
Digital Computer	12 Hours		
<u>Detail Design Phase</u>	5790 Manhours	13 Weeks	\$ 89,200
Stress Analysis	750 Hours		
Design and Analysis	2540 Hours		
Drafting	2220 Hours		
Programmer	280 Hours		
Analog Computer	280 Hours		
Digital Computer	12 Hours		
<u>Hardware Fabrication Phase</u>	7260 Manhours	26 Weeks	\$ 68,400
Fabrication	2950 Hours		
Installation	2090 Hours		
Testing and Qualification	1630 Hours		
Liaison	590 Hours		
<u>Materials Cost</u>			\$193,000
		Cost	\$418,500
Fee (7½%)			31,400
	Total Cost		\$449,900

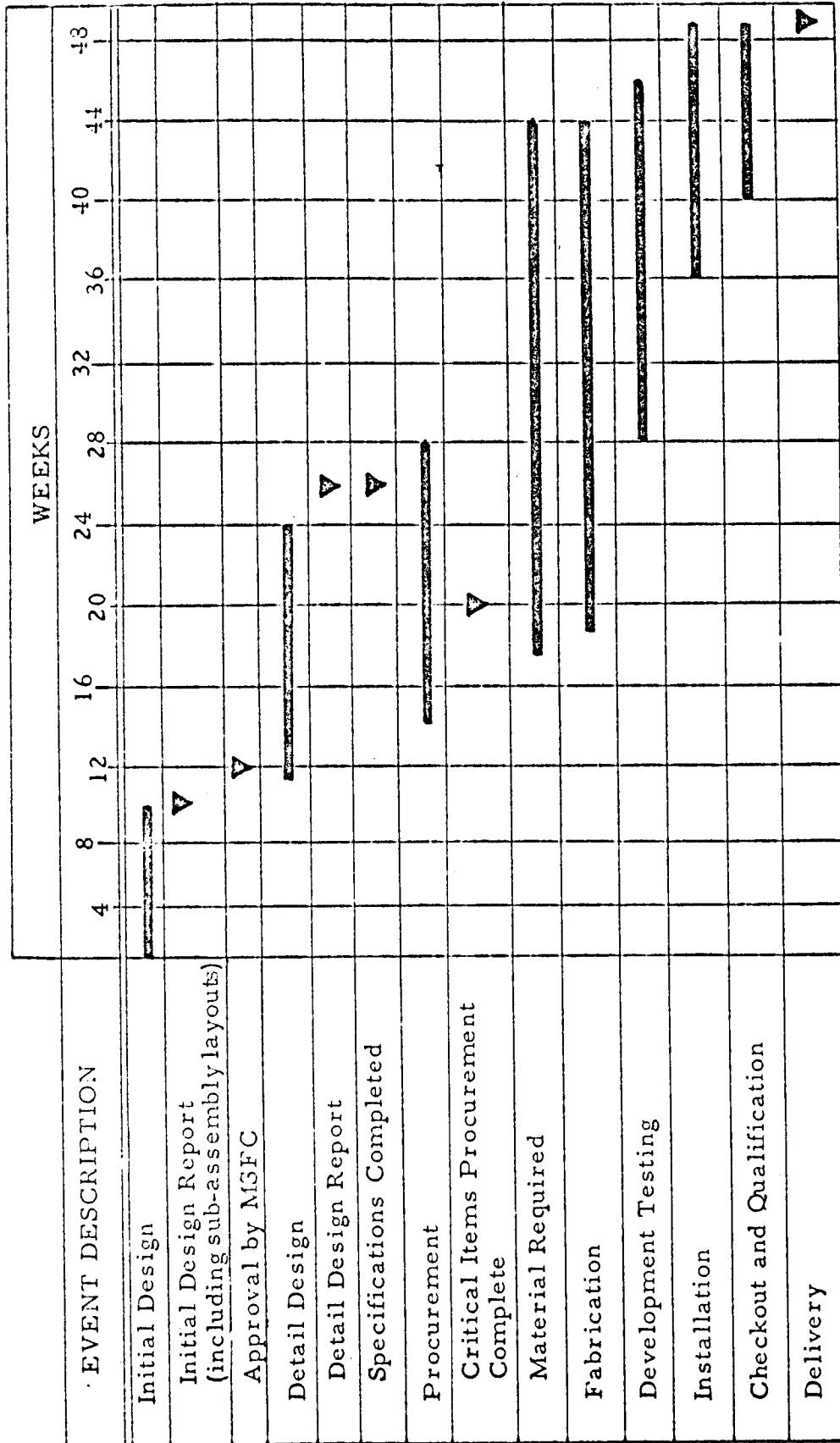


Figure 6.1 - Design and Fabrication Schedule for Two-Dimensional Lunar Gravity Simulator

Section 7

CONCLUSIONS AND RECOMMENDATIONS

The results of the tasks performed during this reporting period suggest the following conclusions and recommendations.

1. Precise control of the forces at each suspension point will require tandem-type compensating networks in the force control system to provide the necessary damping characteristics in each of the force control loops. This compensating network would consist of operational amplifiers and exchangeable (plug-in) RC modules to adapt the filter module to the specific vehicle being tested.
2. A trolley drive system with a displacement optical-type sensor is the recommended concept. The alternative cable angle sensing concept will compromise the system performance. In either case, rate sensing is required.
3. Static longitudinal errors due to large variations in LSV pitch and roll angles may be minimized by maintaining a suspension cable length (\approx rail height) greater than 30 ft.
4. Further studies involving LGS analog simulation should include a comprehensive investigation of the obstacle simulation for the LSV wheel dynamics. Comparison of various obstacle simulation methods with actual test data would be an important part of this study.
5. Recommended design conditions are those commensurate with the vehicle engaging a one foot simulated obstacle at maximum vehicle velocity. The maximum dynamic lunar gravity errors were $\leq 20\%$ for the LSSM and $\leq 30\%$ for the MOLAB. Wheel chassis suspension device errors for the roll condition were approximately equal. For the pitch case chassis suspension device errors were one-third less of the wheel system errors.
6. Peak wheel accelerations were found to vary linearly with obstacle height. Also, the peak lunar gravity errors were found to vary almost linearly with obstacle height in most cases.

7. Lunar gravity error for the force control system is quite sensitive to cable length. Errors of 100% were observed for the LSSM wheels with a 170 ft cable length. Maximum errors for the recommended 30 - 50 ft range are 8 to 20%. LGS rail height should be minimized for reduced lunar gravity error.
8. Horizontal acceleration errors due to trolley drive system dynamics may be reduced considerably with increased cable length (\approx rail height). However, the recommended cable length of 30 - 53 ft results in a maximum error of only .0025 Earth g's or less.
9. The two-dimensional LGS system described is recommended for further design efforts and subsequent development. Generally, the system can be made from currently available state-of-the-art components.
10. Cost for design and development of the 2-D LGS, excluding rail support structure, test terrain, building, etc., is estimated at \$449,900. The corresponding schedule encompasses approximately 50 weeks.

Section 8
FUTURE WORK

Continued study efforts for the remainder of the program are outlined below. These tasks are in accordance with the program plan shown in Figure 1.2. It is recommended that the corresponding schedule in Figure 1.2 be amended to deliver the final report draft and presentation on October 17, 1966.

<u>Task</u>	<u>Continued Study Efforts</u>
2.0	Analyze the requirements and prepare conceptual designs of a three-dimensional LGS system. Analyze the problems associated with expanding the 2-D to a 3-D system.
3.0	Conduct an analysis of a system for suspending the driver in a typical LSV configuration. The LSSM vehicle is suggested as a basis for the design analysis.
4.0	Conduct a cost and schedule analysis for the design, manufacture, assembly and checkout of a LGS system. This study will consider the 2-D cost analysis as a baseline and add the necessary data for a 3-D system.
5.0	Prepare a final report draft for the LGS study. It is recommended that this report be published in four volumes. Volume I will describe the overall LGS study program and Volumes II, III and IV will be updated reports describing the interim study phases.

Section 9
REFERENCES

1. First Interim Report, Preliminary Design Study of a Lunar Gravity Simulator, LMSC/HREC, A783082, 29 July 1966.
2. Graham, D. and R. C. Lathrop, The Synthesis of Optimum Transient Response: Criteria and Standard Forms, Trans. AIEE, November 1953.
3. Rothbart, H. A., Mechanical Design and Systems Handbook, page 6-56, Table 6.8C, McGraw-Hill Book Company, New York, 1964.
4. Timoshenko, S. and G. H. MacCullough, Elements of Strength of Materials, page 242, Third Edition, D. VanNostrand Company, Inc., Princeton, N. J., 1949.
5. Technical Proposal, Lunar Gravity Simulator, LMSC 894320, LMSC/HREC A712116, 17 December 1965.